Rafael Santiago Floriani Pereira

AGING RESISTANCE IMPROVEMENT OF 3Y-TZP: LASER TEXTURIZATION AND COATING (12CE-TZP AND 5Y-PSZ)

Tese submetida ao Programa de Pós-Graduação em Ciência e Engenharia de Materiais da Universidade Federal de Santa Catarina para a obtenção do Grau de doutor em Ciência e Engenharia de Materiais
Orientador: Prof. Dr.-Ing Márcio Celso Fredel
Coorientador: Prof. Dr. Bruno Alexandre Pacheco de Castro Henriques

Florianópolis
2017

Ficha de identificação da obra elaborada pelo autor através do Programa de Geração Automática da Biblioteca Universitária da UFSC.

Pereira, Rafael Santiago Floriani
Aging resistance improvement of 3Y-TZP : Laser texturization and coating (12CE-TZP and 5Y-PSZ) / Rafael Santiago Floriani Pereira ; orientador, Márcio Celso Fredel, coorientador, Bruno Alexandre Pacheco de Castro Henriques, 2017.
149 p.
Tese (doutorado) - Universidade Federal de Santa Catarina, Centro Tecnológico, Programa de Pós Graduação em Ciência e Engenharia de Materiais, Florianópolis, 2017.
Inclui referências.
1. Ciência e Engenharia de Materiais. 2. Zircônia. 3. Envelhecimento. 4. Biocerâmica. 5. Laser. I. Fredel, Márcio Celso . II. Henriques, Bruno Alexandre Pacheco de Castro . III. Universidade Federal de Santa Catarina. Programa de Pós-Graduação em Ciência e Engenharia de Materiais. IV. Título.

Rafael Santiago Floriani Pereira

AGING RESISTANCE IMPROVEMENT OF 3Y-TZP: LASER TEXTURIZATION AND COATING (12CE-TZP AND 5Y-PSZ)

Esta Tese foi julgada adequada para obtenção do Título de doutor, e aprovada em sua forma final pelo Programa de Pós-Graduação em Ciência e Engenharia de Materiais.

Florianópolis, 06 de outubro de 2017.

_____
Prof., Dr. Guilherme Barra
Coordenador do Curso

Banca Examinadora:

Prof. Dr.-Ing. Márcio Celso Fredel Orientador Universidade Federal de Santa Catarina	Prof. Dr. Eng. Filipe Samuel C. P. Silva Universidade do Minho Videoconferência
Prof. Dr. Eng. Adriano Michael Bernardin Universidade do Extremo Sul Catarinense	Prof. Dr. Eng. Antônio Eduardo Martinelli Universidade Federal do Rio Grande do Norte
Prof. Dr. Daniel Enrique Garcia Universidade Federal de Santa Catarina	Prof. Dr. Eng. Sergio Yesid G. González Universidade Federal de Santa Catarina

Este trabalho é dedicado a todos que tiveram paciência comigo durante este período.

AGRADECIMENTOS

Agradeço, primeiramente, a minha família, especialmente minha mãe, Anna Santiago Floriani Pereira e minha irmã Anna Carolina Floriani Pereira, pelo apoio e motivação que têm me dado durante toda a vida e sem as quais jamais seria metade do que sou.
À minha namorada, Mayara Cordeiro, que me motivou e foi minha família durante os momentos mais difíceis vividos no exterior.
Também fica a gratidão aos meus avós, meu pai e familiares por contribuírem e por estarem presentes.
Ao meu orientador e professor, Márcio Celso Fredel, pela orientação, confiança e oportunidade dadas a mim desde a graduação.
Ao meu orientador em Portugal, professor Filipe Samuel Silva, por todo o apoio, auxílio e confiança.
Aos meus amigos vimaranenses, Caroline Gomes, David Araújo, Miguel Sampaio, Flávio Bartolomeu e Driano Rezende, pelo companheirismo e por amenizarem a saudade de casa nos tempos em Portugal.
Aos meus amigos, Ramon Mezari, André Cabral, Ruben Acevedo, Marcelo Barros, Fernando Peixoto, Fernando Machuca, Cesar Stupp, Useche Inchauspe, Henrique Tajiri, Pietra Araujo e Francesca Albino pelo bom convívio, esclarecimentos e amizade durante todo o doutorado.
Aos professores Cláudia Volpato e Bruno Henriques, pelo apoio prestado durante todo o doutorado.
Aos companheiros de laboratório em Portugal, Oscar Carvalho, Paulo Pinto, Paulo Silva, Georgina Miranda, Sara Madeira, Mafalda Costa, Diana Farias, Telma Dantas, Rita Ferreira e José Pires, pelo companheirismo durante o tempo em terras lusitanas.
Aos meus amigos em geral, por me apoiarem e ajudarem em todos os momentos.
Ao CNPQ e CAPES pelo auxílio financeiro no Brasil e no exterior.
À Universidade Federal de Santa Catarina e cidadãos do Brasil, pela oportunidade de crescimento profissional e pessoal.

Se fosse fácil achar o caminho das pedras, tantas pedras no caminho não seria ruim.

(Humberto Gessinger)

ABSTRACT

Zirconia-based ceramics have been successfully used in the dentistry field. However, in the recent past, several HIP implants, containing zirconia pieces, were surgically replaced due to a phenomenon called aging. Because of this, many studies have been performed aiming at avoiding this phenomenon. Some alternatives found were grain size decrease and yttria replaced by cerium oxide in order to stabilize the zirconia tetragonal phase. Notwithstanding, this replacement has a disadvantage on mechanical strength. As an alternative to reduce aging, two approaches were used in this work: the manufacturing of a protective layer, by dip coating, and recrystallization, by laser treatment, of yttria stabilized zirconia. Moreover, adhesion issues and weak biological connection of zirconia-based ceramics have been extensively discussed and laser treatments are reported as an alternative to overcome these problems. In this thesis, in order to evaluate the effect of these surface modifications, a 3 mol% yttria stabilized zirconia commercial powder was used as bulk material. This powder was uniaxially pressed (200 MPa) into discs and the green bodies were dip coated using suspensions containing 12 mol% ceria stabilized zirconia or 5 mol% yttria stabilized zirconia. After sintering, samples showed a good coating-bulk homogeneity and aging protection for about 36 years *in-vivo*. Regarding mechanical properties, coating quality seems to play a more significant role than the material used, decreasing the resistance from ~1600 MPa to ~700 MPa. Laser treatments were performed in the same bulk material described, pressed and sintered. This approach was effective in aging kinetics reducing due to zirconia grains recrystallization, decreasing the monoclinic content from ~20% to ~10 after 18 h of accelerated aging. Samples mechanical strength was reduced regarding parameters used. The highest bending strength was measured as ~1400 MPa and the worst ~600 MPa.

Keywords: Zirconia, aging, laser texturing, dip coating, B3B.

RESUMO

Cerâmicas à base de zircônia têm sido usadas com sucesso na área odontológica. Entretanto, em um passado recente, diversas próteses coxofemorais, com componentes fabricados em zircônia, necessitaram ser reimplantadas devido a um fenômeno chamado envelhecimento. Por conta disto, muitos estudos têm sido realizados em busca de minimizar este fenômeno. Algumas alternativas encontradas foram a redução do tamanho de grão deste material ou a substituição da ítria por óxido de cério para a estabilização da fase tetragonal da zircônia. Todavia, esta substituição traz consigo a desvantagem da redução da resistência à flexão deste material. Como alternativa para minimizar os efeitos do envelhecimento duas abordagens foram utilizadas neste trabalho: a criação de uma camada resistente ao envelhecimento, via *dip coating* e a recristalização, via tratamento a laser, da zircônia estabilizada com ítria. Além disso, problemas de adesão e fraca conexão biológica das cerâmicas à base de zircônia já são amplamente discutidos, podendo os tratamentos a laser serem também aplicados visando contornar esta lacuna. Para o estudo do efeito destas modificações superficiais, foi utilizado como material base um pó comercial de zircônia estabilizada com ítria a 3 mol%. Este pó foi compactado via prensagem uniaxial (200 MPa) e nestas amostras a verde foram realizados recobrimentos, via *dip coating*, utilizando suspensões contendo pós de zircônia estabilizada com céria a 12 mol% ou zircônia estabilizada com ítria a 5 mol%. Após sinterizadas, as amostras mostram boa coesão recobrimento-substrato e capacidade de proteção ao envelhecimento por, pelo menos, 36 anos *in vivo*. Em relação às propriedades mecânicas, a qualidade do revestimento parece desempenhar um papel mais significativo do que o material utilizado, diminuindo a resistência de ~ 1600 MPa para ~ 700 MPa. Os tratamentos com laser foram realizados no mesmo substrato descrito, prensado e sinterizado. Esta abordagem foi eficaz na redução do envelhecimento devido à recristalização dos grãos de zircônia, diminuindo o conteúdo monoclínico de ~ 20% para ~ 10% após 18 h de autoclave. A maior resistência à flexão foi medida em ~ 1400 MPa e a menor ~ 600 MPa, de acordo com os parâmetros utilizados no laser.

Palavras-chave: Zircônia, envelhecimento, texturização a laser, dip coating, B3B.

LIST OF FIGURES

LIST OF TABLES

LIST OF ABREVIATIONS AND NOTATIONS

12Ce-TZP	12 mol% ceria tetragonal zirconia polycrystals
3Y-TZP	3 mol% yttria tetragonal zirconia polycrystals
5Y-PSZ	5 mol% yttria partially stabilized zirconia
CIELAB	International commission on illumination L*a*b* color space
FIB	Focused Ion Beam
LTD	Low temperaure degradation
Ra	Average roughness
Rq	Root mean square roughness
Rt	Total height roughness
Rsk	Skewness roughness
YSZ	Yttria stabilized zirconia

TABLE OF CONTENTS

CHAPTER 1 - GENERAL INTRODUCTION

Since Garvie [1] first publication on zirconia martensitic transformation, a lot of studies lead to knowledge improvement about this material. Bending strength, for example, was mentioned for him to be in the order of 650 MPa, while nowadays this number is easily found above 1 GPa [2,3]. Much of this increase was obtained by improving microstructures and the mechanism responsible for zirconia mechanical strength, which involves a phase transformation from a metastable structure to a more stable one, i.e. tetragonal to monoclinic respectively [4]. In this way, it is possible to find pure zirconium oxide in three different crystalline structures depending on temperature: monoclinic, tetragonal and cubic. However, only the former is stable at room temperatures and to stabilize the others it is necessary to use dopants (other oxides) in accurate quantities. Garvie [1], for example, have used calcium oxide to create a microstructure composed by tetragonal grains dispersed in a cubic matrix, called partially stabilized zirconia (PSZ) that can be also achieved using alternative oxides, such as yttria, magnesia and ceria. This material was the first observed presenting martensitic transformation, once stabilizers used at that time (MgO and CaO) are only capable to stabilize tetragonal phase in the presence of cubic phase [5].

In addition to the referred microstructure, another one has special interest when mechanical properties are considered: tetragonal zirconia polycrystal (TZP), which almost completely formed by tetragonal metastable grains, the phase related to toughness mechanism. This microstructure is achieved mainly by Yttria and Ceria stabilization (Y-TZP and Ce-TZP) and the oxide contents must be carefully controlled to obtain no cubic grains, as well to keep tetragonal grains metastable enough to the required application [5,6].

Due to the lower stabilizer quantities necessary to obtain metastable tetragonal zirconia grains, the higher bending strength achieved and the good aesthetical properties (whiteness), yttria stabilized zirconia was introduced as biomaterial, especially for applications where mechanical properties are the main requirement. In this sense, two biomedical fields can be highlighted in the use of this material: Dentistry (as prosthesis) and orthopedics (as hip implants). For the former, the market still growing and success rates are close to gold-standard materials. However, hip

implants didn't follow the same way and the initial good perspectives were not confirmed. In this sense, one event was responsible for the zirconia downgrade in orthopedics used: the reported failure of several implants, leading patients to replacing them [7,8].

The question about zirconia failure was created and the behavior behind the answer was published in 1981. In his work, Kobayashi [9] showed that zirconia may change crystalline structure even without mechanical or thermal stress. He called this phenomenon aging and it has been since then extensively studied, receiving also the name of low temperature degradation (LTD) [10–13]. Different reasons were given for this transformation, but nowadays there is almost a consensus that it is caused by oxygen vacancies filling [14]. In this way, oxygen vacancies are strongly created when zirconia is stabilized by yttria, once the first have valence +4 while the second +3, which creates difference in oxygen balance and, consequently, atomic voids [15].

Aiming at avoiding the spontaneous phase transformation in zirconia, researchers have developed different strategies to handle this issue. Camposilvan [3], for instance, used infiltration of cerium salt to create a layer capable to inhibit oxygen diffusion to a Y-TZP bulk. Using the same metal, cerium, but with a different approach, Palmero [16] increased zirconia LTD resistance by replacing yttria for ceria to obtain a Ce-TZP, which mechanical strength was increased using other ceramics as reinforcement. Another way to avoid aging is preventing grains growth during sintering step of Y-TZPs. In this way, alumina nano-scaled have been used to keep grains small, maintaining the compromise of low porosity and reducing aging kinetics [17,18]. Recrystallization of sintered material is also an alternative to design microstructures with small grains, being possible to achieve that through melting, promoted by laser irradiation [19,20].

Based on that, this work aims at overcoming aging problems and in verify the influence of zirconia-based coatings and laser treatments on aging and mechanical properties of YSZ samples.

1.1 - HYPOTHESIS AND OBJECTIVES

1.1.1 - Hypothesis

The thermal and chemical surface modifications performed on zirconia-based ceramics for aging phenomena avoidance does not significantly influence the biomechanical performance.

1.1.2 - General Objective

Decrease zirconia aging kinetics by means of surface modification, with no significant impact on the mechanical strength.

1.1.3 - Specific Objectives

- Processing of thin zirconia aging-protective zirconia coatings.
- Aging behavior assessment of zirconia coated samples.
- Flexural resistance assessment of zirconia coated samples.
- To promote grain size decrease by means of laser irradiation.
- Aging behavior assessment of laser irradiated samples.
- Flexural resistance assessment of laser irradiated samples.

1.2 - THESIS STRUCTURE

The present work is structured as a compilation of research tasks. Previous to this compilation, two chapters are included: Chapter 1 (current) with a problem overview and objectives of this thesis and Chapter 2 that presents the literature review.

In order to contextualize the aspects discussed in the following chapters, as well to give to the readers the fundamental knowledge about topics exposed during this work, Chapter 2 expose some fundamentals about ceramics & properties, zirconia, zirconia aging and laser treatment.

Research papers are presented from Chapter 3 to Chapter 6. The papers are exposed as submitted, containing: Abstract, Introduction, Material and Methods and Conclusions. References are all put together at the end of the document.

Chapter 3 is an overview about zirconia as implant material and strategies that can be used to avoid aging behavior. It makes

an introduction of the strategies used during Chapters 4 and 5 and is presented as published.

Chapter 4 make practical some ideas exposed in Chapter 3, with Tetragonal Zirconia Polycrystals coated by other zirconia-based ceramics and aging behavior of these pieces.

Chapter 5 is the continuation of studies presented in Chapter 4, focusing on the mechanical response of coated materials.

Chapter 6 deals with the influence, on aging, of sintered zirconia surface preparation by means of laser patterning.

Chapter 7 shows the mechanical response of samples treated in Chapter 6 and the influence of strategies developed in that publication.

Chapter 8 presents general conclusions from this work, suggestions to future works and additional studies performed during the doctoral period.

CHAPTER 2 - LITERATURE REVIEW

2.1 - MECHANICAL RESISTANCE OF CERAMICS

Components' failure process starts in a region where the stress level is higher than the materials' resistance. For ceramics, this resistance is normally related to chemical bonds breaking, once failure commonly happens during elastic strength. In this way, is possible to calculate a theoretical resistance using solid binding energy. However, this account doesn't match with experimental data. This behavior is explained due to the existence of defects into the materials.

Due to the fragile behavior, without macro plastic deformation, the mechanical resistance of ceramics is explained through linear elastic fracture mechanics, which was firstly researched by Inglis [21]. Through the first concept proposed by Inglis, a theory of materials resistance was made taking account the size of the flaw, "a", responsible for the failure. When this defect is under a cleavage load, the critical stress concentration caused by him is called K_{Ic}, which is the maximum stress that the material support before the failure. Then the material resistance can be calculated as a function of the defect critical size by the equation:

$$\sigma_f = \frac{K_{IC}}{\sqrt{a}} \tag{1}$$

In addition to mechanical resistance decreasing, defects have a bigger effect in ceramics, when compared to metals. The absence of plastic flow (dislocation movement) cause catastrophic failure in this material, with no deformation, and no uniform ultimate strength value, being this property related to the size and geometry of the defect that leads to the failure [22].

The failure of a brittle piece can be satisfactorily explained by an analogy used by Weibull, which says that the survival probability of a chain, composed of various links, will be given by the weakest link. In the case of brittle materials, the weakest link will be the larger defect [23].

From a global view, defects that cause ceramics failure comes from the process and can be satisfactorily described by Weibull equation [22–24]:

$$F = 1 - \exp\left(-\frac{\sigma}{\sigma_0}\right)^m \tag{2}$$

where F is the failure probability, σ is the ultimate stress according to this probability, σ_0 is the stress that 63.2% of the samples have failed and “m” is the Weibull modulus, which describes the resistance values dispersion. Materials with high “m” shows smaller strength data dispersion or, in other words, have homogeneous defects.

Using this equation, ceramics resistance can be obtained as a statistical data, which each stress level related to a failure percentage.

Summarizing, ceramic pieces have two more important parameters to be considered, in terms of static mechanical behavior, when compared to metals: K_{Ic}, which is an intrinsic material property and Weibull modulus, which is a statistic parameter related to defects that come, usually, from the manufacturing process.

2.1.1 - Ceramic toughening mechanisms

The absence of plastic deformation makes brittle materials sensitive to defects. These defects can be suppressed during processing. Notwithstanding, process costs increase as defects size decrease. Moreover, internal stresses or superficial defects can appear in use, raising ceramic weakness: low K_{Ic}.

As the process costs are too high to obtain a defect-free ceramic, some strategies are used to improve this material in terms of fracture toughness, i.e. to be capable to resist to larger defects. This improvement is achieved by toughening mechanisms. During this work, three mechanisms needs special attention:

- Pre-stressing: This mechanism can be achieved by mechanical, thermal or chemical stresses. The thermal approach is commonly used for glasses, where the surface is cooled much faster than the bulk, making the second to create a compressive layer in the surface, increasing the stress necessary to growth defects.
- Crack shielding (microcracking): Microcracks, formed by thermal stress, for example, reduce the material elastic modulus in a specific zone. If another, bigger, crack growth to this zone, microcracks acts by spreading the energy of the growing flaw.
- Transformation toughening: Since a crack is formed and starts to grow, stress concentration related to this flaw (K_I)

also increase, till a moment when achieving K_{Ic} and the material breaks. This is a ceramic normal behavior. However, when a crack starts to grow in some zirconia based materials, or special SiO_2, the stress field in the crack tip is able to promote a martensitic transformation, i.e. a phase transformation without temperature and diffusion. In zirconia's this phase transition is from tetragonal to monoclinic, followed by a volume expansion of about 4%. This expansion creates a compressive field in the crack tip, suppressing the original stress and even increasing the load necessary to continue flaw propagation. Notwithstanding, to show this behavior zirconium oxide needs a metastable phase able to change by means of a stress field. To achieve it is necessary to know zirconia and its phases in the presence of other oxides.

2.1.2 - R Curve behavior

As discussed before, K_{Ic} is the maximum stress concentration that a ceramic material resists before an unstable crack propagation, which leads to its failure. In other words, this property measures the size of the largest flaw that a material can survive with.

However, after the development of toughened ceramics, it is possible to have a crack growing in a ceramic material without its failure, i.e. K_{Ic} that is supposed to be a unique number, changing according to the crack length.

This toughness changing is described by a curve, called R-curve, and is only observed in toughened ceramics. In these materials, the energy necessary to crack propagation is increased as the flaw increases (until a threshold) [25]. Figure 1 shows the R-curves of three different materials; stishovite (SiO_2), silicon nitride (Si_3N_4) and 3 mol% yttria stabilized zirconia (3Y-TZP). The first and last materials show the same toughening mechanism, transformation toughening, while the second takes advantage of crack deflection.

Figure 1 - R-curve for three different toughened materials: Stishovite, silicon nitride and 3Y-TZP [26].

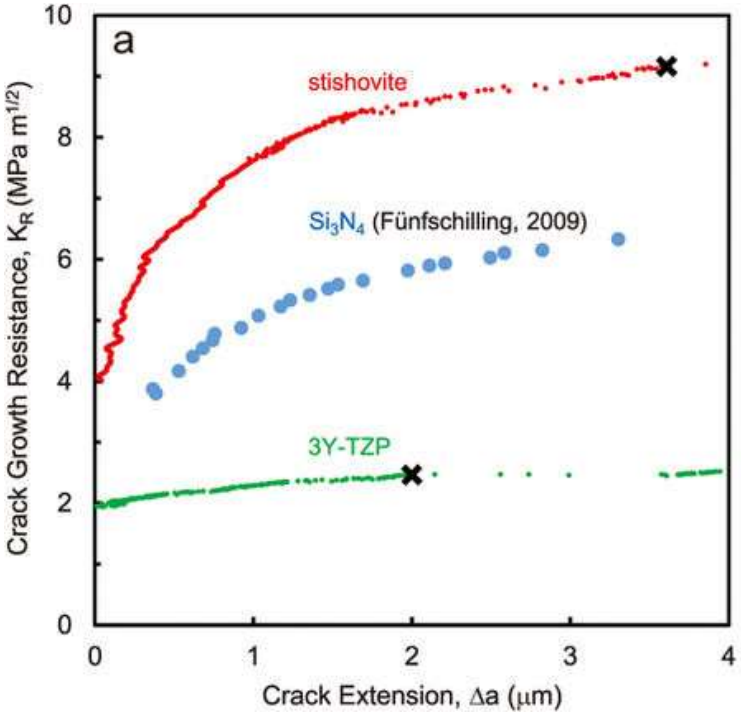

By analyzing this chart, is possible to observe the huge effect of toughening mechanisms in ceramics. In addition, these curves may give the idea that silicon nitride and stishovite have higher mechanical strength compared to zirconia. Nevertheless, even having the lowest fracture toughness among the materials showed in Figure 1, zirconia shows the higher mechanical strength, when compared to all ceramic materials, as shown in Figure 2.

Figure 2 - Ceramics flexural strength comparison (adapted from [27]).

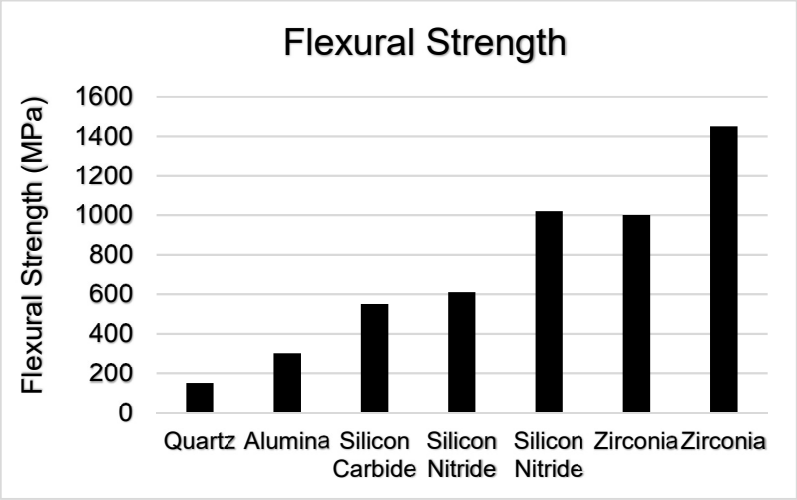

2.2 - ZIRCONIUM OXIDE

Zirconium oxide, or zirconia, can be found at atmospheric pressure in three polymorphic structures: cubic (above 2370 ºC), tetragonal (between 1200 and 2300 ºC) and monoclinic (under 1200 ºC), i.e. the last one is the most stable at room temperature, as observed in Figure 3 [28].

Figure 3 – Zirconium oxide structures [29].

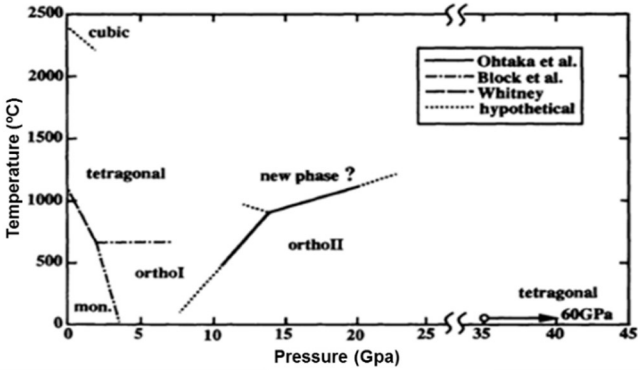

Due to cubic and tetragonal low thermodynamic stability and no mechanical stability of monoclinic pieces (actually is not

possible to obtain components made by monoclinic zirconia), pure zirconium oxide have no applicability as engineering material [6,28].

However, it is possible to stabilize other two phases using specific oxides, cubic ceramics, which change completely the material properties as, for example, mechanical resistance, optical permeability and ionic conduction [28,30–32].

Generally, it is possible to say that greatest mechanical properties are obtained by means of tetragonal stabilization, due to the transformation toughening mechanism, while physical properties (electrical and optical) are obtained in the cubic structure.

The discovery of the zirconia potential to structural applications was reported by Garvie [1] , who published the paper describing the zirconia transformation toughening. As previous discussed, to obtain transformation toughening is necessary to have a metastable phase, tetragonal, with a strict controlled composition, formed by zirconia and some stabilizer as, for instance, yttrium oxide, cerium oxide or magnesium oxide. The stabilization of tetragonal phase creates a category of zirconia materials called zirconia toughened ceramics, which can be found in different microstructures [6,28,30].

In the same way that phases are created by adding stabilizers, microstructures follow the same rule, being possible to create composites, between monoclinic, tetragonal and cubic, and monophasic material with these structures. The quantity of stabilizer added will define the microstructure obtained, which can be separated into four main groups [5,6]:

- Fully Stabilized Zirconia (FSZ) – A monophasic material composed only by cubic grains.
- Zirconia Toughened Composite (ZTC) – Zirconia tetragonal grains embedded in a rigid matrix as, for instance, alumina.
- Partially Stabilized Zirconia (PSZ) – Tetragonal grains embedded in a cubic zirconia matrix.
- Tetragonal Zirconia Polycrystal (TZP) – Fully tetragonal microstructure.

To illustrate the influence of the amount of stabilizer added in the zirconia microstructure, Figure 4 shows a zirconia-yttria phase diagram and respective phases obtained.

Figure 4 - Microstructures obtained by yttrium oxide add [6].

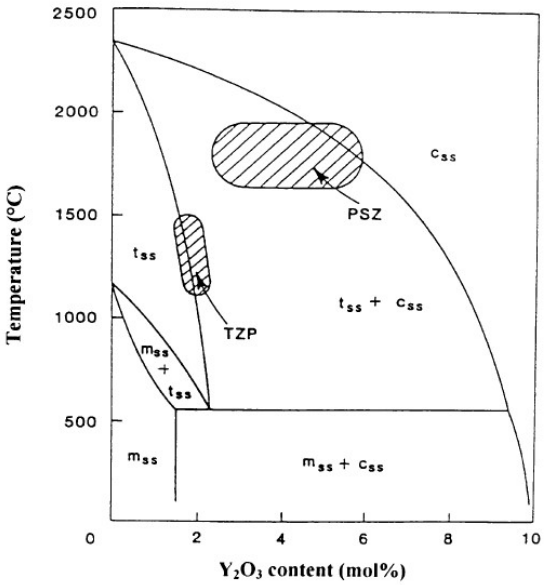

After discovery of cubic and tetragonal phase stabilization by metallic oxides [1], a lot of studies were performed in order to discover the influence of each oxide in zirconia phases [32].

2.2.1 - Stabilizers

In nowadays, publications show that is possible to stabilize tetragonal phase with: CaO, MgO, Y_2O_3, CeO_2, Er_2O_3, Gd_2O_3, La_2O_3, Sc_2O_3 and Yb_2O_3. However, most studied oxides, and most applicable, are CaO, MgO, Y_2O_3 and CeO_2 [33].

In this work, only the last two will be studied, once best mechanical resistance results are obtained with them. Moreover, two different microstructures will be tested: TZP and PSZ. Each condition, regarding microstructure and stabilizer, gives to zirconia different mechanical properties, as showed in Table 1.

Table 1 - Zirconia properties according stabilizer and composition [34–37].

Property	Youngs´ Modulus (GPa)	Flexural Strength (GPa)	Hardness (HV)
3Y-TZP	215 – 240	1200	170
12Ce-TZP	210	600	120
5Y-PSZ	210	485	130

2.2.1.1 - Yttrium oxide

When fully oxidized, yttrium is a trivalent metal that has, with oxygen, a cubic lattice [28,33]. One of the great advantages of this oxide is that is possible to stabilize tetragonal and cubic zirconia microstructures even using low stabilizer quantities, as can be observed in Figure 5 [15].

Figure 5 - Phase diagram ZrO_2-Y_2O_3 [28].

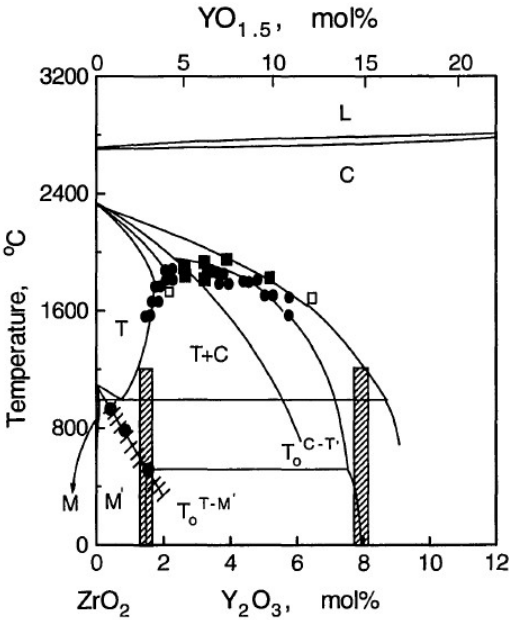

Yttrium ion takes a part in zirconia lattice as a substitutive atom, replacing zirconium. Notwithstanding, there is an electronic difference between these two metals in the lattice: zirconium is tetravalent while yttrium is trivalent. This mismatching creates oxygens vacancies into the material, Figure 6, which is accepted by many authors as the mechanism responsible for tetragonal phase stabilization [15,28].

Figure 6 - Unit cell of yttria stabilized zirconia and the vacancy formed by the presence of yttrium atom (yellow) [34].

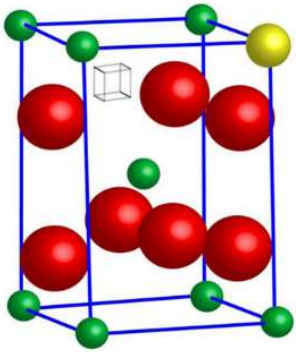

2.2.1.2 - Cerium oxide

In the same way as yttria, and all zirconia stabilizers, cerium oxide also have cubic a structure. However, when fully oxidized, cerium is a tetravalent ion, which makes the substitution in zirconia lattice neutral electrically. Because of this, high stabilizer quantities must to be used to stabilize cubic and tetragonal structures, as can be seen in Figure 7 [28].

Figure 7 - Phase diagram ZrO_2-CeO_2 [28].

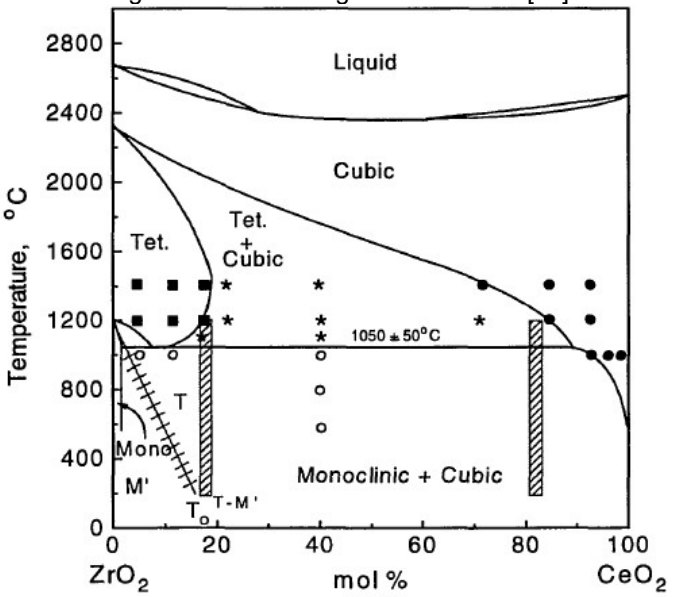

2.2.1.3 - Other oxides

Two other oxides should be highlighted in use as zirconia stabilizers: MgO and CaO. Both are alkaline earth metal and have a valence of +2, creating balancing oxygen with zirconium.

2.2.2 - Zirconia as biomaterial

Zirconia as biomaterial research and development has started in the last 50 years. The first publication in the biomedical application is from Helmer and Driskell, apud Maccauro [6], in 1969, while the first publication in zirconia to produce hip implants was made by Christel in 1988 [38].

Nowadays, there are more than 600.000 implanted femur heads in worldwide. Moreover, zirconia based ceramics have been also increasing in applicability in dentistry [30].

In the dental field, as in hip implants, the metal-ceramic prosthesis is the gold standard product. However, the pursuit of high level aesthetic and natural appearance, in addition to the controversy about metal side effects into the human body, lead to a development of whole ceramic pieces [39,40].

Although new materials and process development, ceramics still brittle and this low toughness, allied to low flexural resistance, comes up when the industry is pushed to replace metals for ceramics. The need for better mechanical properties in ceramics, subjected to high masticatory loads, leads to the introduction of zirconia in dentistry [13,41]. Table 2 shows a comparison between mechanical properties of some biomaterials.

Table 2 - Properties of some materials for biomedical applications [6,42].

Property	Youngs' Modulus (GPa)	Mechanical Strength (MPa)	Hardness (HV)
Y-TZP	210	>1000	1200
316 SS	200	650	190
CoCr	230	700	300
Ti6Al4V	110	800	100
Alumina	380	>500	2200
Lithium disilicate	95	346	590

Table 2 shows that zirconia mechanical strength is higher than all biomaterials. Comparing with metals, the great disadvantage of zirconia is the brittleness. On the other hand, bioceramics, as alumina and lithium disilicate, also have the same behavior, having also much lower mechanical strength than zirconia. In addition to the strength, biomaterials used as implants also must have Youngs' modulus (YM) closer as possible to the tissues around them. In Table 3 is possible to observe some properties of human tissues, including YM. In this sense, titanium alloys have huge vantage over all referred materials, once they exhibit one of the lower YM and one of the higher mechanical strength. Because of YM mismatch, alumina has been replaced by zirconia in applications that requires bone contact.

Table 3 – Mechanical properties of some human tissues [43–46].

Tissue	Density (g/cm^3)	Tensile Strength (MPa)	Youngs' Modulus (GPa)
Cancellous bone	1.0 – 1.4	1.5 – 38	0.01 – 1.57
Cortical bone	1.8 – 2.0	35 (transversal) 283 (longitudinal)	5 – 23
Tooth enamel	3.0	16.7	80.4
Tooth dentin	2.1 – 2.4	103	21.6

Zirconia mechanical strength and bio-inertness, made this material the most promising material in the attempt to replace metals for bio-applications. However, despite these initial good perspectives, with thousands of products implanted, several hip prostheses were recalled, leading patients to the operating table [8,47]. These prostheses were metal-ceramic pieces, but the problem reported was the zirconia failure during the application. Due to this problem, zirconia has been avoided in hip prosthesis manufacturing. Investigations were also performed and the phenomenon behind the failure was called Low Temperature Degradation (LTD), which was, in part, described in 1981, reported at 250 ºC, revealing that zirconia should be more investigated when applied in vivo [9].

2.2.3 - Low temperature degradation

The issue reported in 1981, by Kobayashi [9], was identified as a spontaneous phase changing (without mechanical or thermal stresses) in a presence of water molecules, followed by microcracking and mechanical resistance loss. This behavior was called aging. After this publication, a lot of researches were performed in order to try to explain the phenomenon behind this phase changing, observing the transformation at lower temperatures. Because of this, the behavior also receives the name of low-temperature degradation (LTD) [30,48,49].

Trying to describe the aging behavior, Yoshimura [50], made some important discoveries, in 1987. Even without the

understanding of the phenomenon behind the transformation, these discoveries still being applied nowadays.

- Transformation happens faster between 200 ºC and 300 ºC and is time dependent.
- Water, or steam, increases transformation.
- Transformation starts from surface to the bulk.
- Higher stabilizers content and small grain sizes increase transformation resistance.

In one important publication about the topic, Lawson [51] describes that the aging happens between 65 and 500 ºC. Maybe due to the belief in this low-temperature limit, zirconia was introduced in bio-applications without the necessary investigation about LTD. This concern changed only after hip prostheses failure, when researches about why these products have failed were performed.

Even before the hip prosthesis failure, theories about the phenomenon behind the aging were created. Hannink, apud Zhao [28], suggested that the phenomenon could be compared to metal stress corrosion, where an external environment reacts with a lattice solute (yttria, for example), leading to bonds' break. In metals, this break is responsible for brittle fracture, in tetragonal zirconia it should cause phase changing. This model proposes that LTD is related to the water molecules chemisorption [49,50], which breaks Y-O bonds, what is also known as subcritical crack growth.

Nowadays, the most accepted model is that OH^- diffuses in zirconia lattice, what is explained by oxygen vacancies discussed in 2.2.1.1 - [7,30,52]. Due to valence difference, yttria creates a huge vacancies amount in zirconia lattice. These vacancies are responsible for tetragonal phase stabilization. In other words, tetragonal structure is created mainly because this electronic stress. When zirconia is exposed to a wet environment, water molecules are adsorbed in its surface and, because of chemical potential, they are broken in H^+ and OH^- As zirconia lattice is electronic unbalanced, missing O^-, the negative ions of the water have the potential to diffuses into the material. This atom diffusion fills the vacancies created due to yttria stabilization, tending to balance electronic charges and, consequently, being responsible for tetragonal destabilization, Figure 8. This explanation fits with the fact that only tetragonal zirconia stabilized by yttria suffer LTD [14,15,30].

Figure 8 - Scheme of zirconia aging [33].

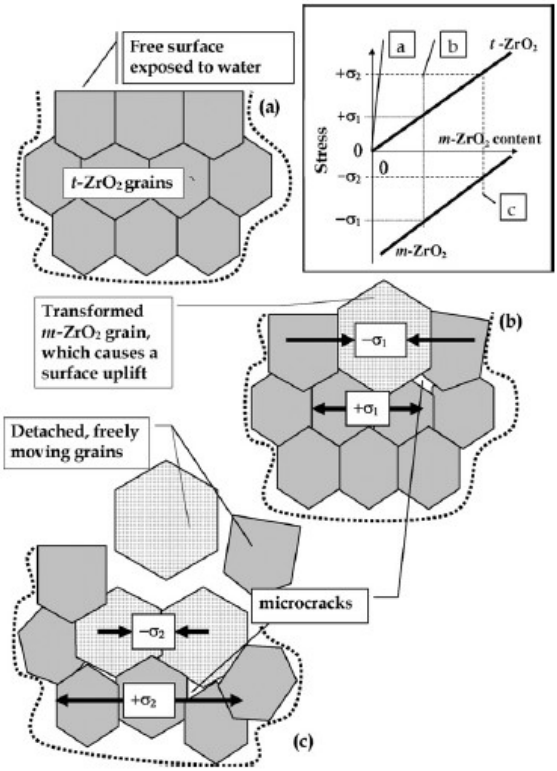

As previously discussed, zirconia tetragonal phase is metastable and needs some energy to transform to monoclinic. There are two paths to this transformation: toughening or LTD. The first increases zirconia mechanical strength, while the second is assumed to be deleterious for this property. LTD starts on the surface in contact with water molecules and growth to the bulk. Materials features as porosity, grain size, stabilizer content and residual stresses can change aging kinetics.

2.2.3.1 - Accelerated aging

In order to accelerate the LTD phenomenon and measure, in acceptable times, the mechanisms involved, researches have been using autoclave in different pressure and temperatures [7,30,49,53,54].

Tsubakino [55], has shown that transformation follows a nucleation and growth mechanism that can be described by Johnson-Mehl equation:

$$f = 1 - exp[-(b.t)^n] \quad (3)$$

where “f” is the transformation fraction, “t” the time and “n” and “b” constants, being the second ruled by Arrhenius law:

$$b = b_0 \exp\left[-\frac{Q}{RT}\right] \quad (4)$$

where “b_0” is a constant, “Q” is an activation energy, “R” the gas constant and “T” the temperature.

After hip implants failure, the low temperature limit for aging occurrence had no more value and in one of this studies, Chevalier [7], correlated these equations, through thermodynamic and material response, to create a relation between autoclave tests and material during application. Using activation energy and b_0, found experimentally, he proposed a standardized test performed in steam at 134 ºC, where one hour of test corresponds to two years in the human body.

Nowadays this test is a part of ISO13356 [56] and allow to measure aging evolution during a human-life implantation.

2.3 - SURFACE FUNCTIONALIZATION

In addition to mechanical properties, other zirconia behaviors make zirconia an interesting material to in-vivo applications. Whiteness and bio-inertness, allied to high strength and toughness, are probably the most attractive features of this material in the pursuit to replace metals in humans.

However, despite of the bio-inertness benefits, this behavior also makes zirconia inert enough to doesn’t interact with bio-media. Because of that, osseointegration of titanium and zirconia are similar, once the second has a surface formed by titanium dioxide [57,58].

Aiming to increase cellular response and promote mechanical anchoring between bone and implant, several studies have been done in ceramics and metals functionalization[59].

Surface roughness is one of the parameters used to enhance cell growth and increase mechanical stabilization of implants [60]. In this way, sand blasting and acid etching (SLA) is the commercial gold standard treatment in titanium implant surfaces [61]. Combined, these finishing processes create micro

and sub-micro roughness, which is reported to implant-bone anchoring, called primary stability, and bone growth in implant surface, called secondary stability [62].

Because of the success achieved in titanium implants, the same treatment was applied to zirconia pieces. Notwithstanding, crack nucleation can be addressed to both techniques and mechanical results are controversial [63,64], needing deeply studies to set acceptable processing parameters, as for example: blasting particle size and composition, pressure and distances, as well acid concentration, temperature and times [59].

As an alternative to surface modification, laser patterning is also being studied. The main difficulty about this technique is crack formation due to the thermal gradients developed. On the other hand, this process allows a better control of roughness profile, in addition to be a contamination free treatment, which reinforces the potential to a biological application. [65].

2.3.1 - Laser

Materials' laser treatment is used in different application, due to its versatility and simplicity. Lasers are often used to metals treatment [66], coatings [67], surface cleaning [68], biological tissue treatments [69] and biomaterials patterning [70].

Lasers work with a certain wavelength, which depends on its construction, and can concentrate a huge amount of energy in a single point [60]. The phenomenon behind laser functioning was predicted by Einstein in 1917, called stimulated emission [71]. It is related to another phenomenon, photoelectric effect, where light excites and emits electrons from the material surface.

Taking advantage of stimulated emission is possible to confine the photons between two mirrors, increasing energy density. If one of the mirrors has some transparency to wavelength generated, is possible to create a monophasic light beam, which is the laser [72].

Wavelength produced by laser depends on the material to be excited, since different materials have different fundamental electron energy states. Based on power capability, the main choice for material processing are: CO_2, CO, Nd-YAG, Nd-Glass and Excimer [71]:

Moreover, when a laser beam, with specific intensity and wavelength, interacts with a solid, some energy will be absorbed, some reflected and some transmitted, depending on laser

wavelength, intensity and material that laser interacts. For materials heating, photons must to be absorbed and interact with material's electrons, exciting them. Electrons, in turn, can interact with phonons that cause lattice vibrations, which are responsible for solids temperature, for example [71,72].

Because of that, is important to select a wavelength that is absorbed by the material of interest, since reflected photons have no interest in solids heating. In Figure 9 is possible to see the relation between reflectivity (1 - absorptivity) and wavelength for different metals. In the same figure is also possible to observe three different lasers and their wavelength: Excimer, Nd-YAG and CO_2.

Figure 9 - Reflectivity of solids according to wavelength [71].

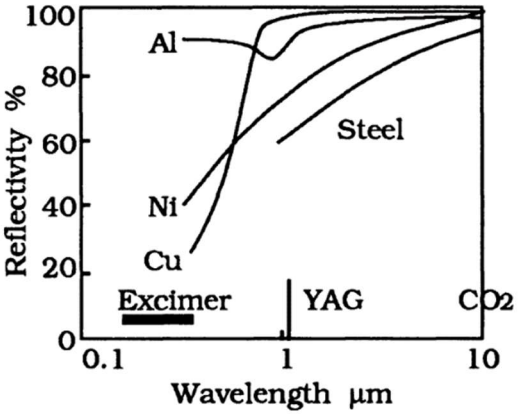

Due to fundamental wavelength obtained and, therefore, photon energy, Nd-YAG has been one of the first choices to heat solid materials. In this equipment, photons are generated in neodymium in an yttrium aluminum garnet rod.

2.4 - PROCESSING

The manufacturing process of ceramics has the same names as metals and polymers as, for example: casting, injection, forming, pressing. The difference is while plastic materials can flow even in low temperatures, brittle materials must be "plasticized" by a plasticizer or a binder. This adding is so important that each process needs a specific viscosity. Viscosity, in turn, is strongly

affected by plasticizer or/and binder addition. For the processes used in this thesis, pressing and dip coating, binder and plasticizer content are completely different from each technique to another.

Due to very low intrinsic plasticity and plasticizer removing process, manufacturing of defects-free ceramics is an expensive and difficult task, as mentioned before. In this sense, processes must be studied for each material to obtain acceptable samples quality.

2.4.1 - Pressing

Pressing is accomplished by placing the powder into a die and applying pressure to achieve compaction. Powders are, most of the cases, agglomerates, formed by spray dried slurries.

Depending on load direction, the process can be classified in: uniaxial, biaxial and isostatic pressing. Uniaxial pressing can be divided in single or double action, according to piston movement. In addition to load, temperature also divides the process, which can be classified in cold or hot [73].

The absence of plastic flow in ceramics makes sintering step responsible for most of the density increasing. Because of that, hot pressing processes have their space in ceramics fabrication, once fewer defects are created when forming and temperature are applied together [74]. However, these kinds of processes are expensive in terms of equipment and processing time, which makes their use only applicable in pieces that have high requirements and value.

Pressing followed by sintering, in two steps, is the most used manufacturing process for ceramic components. The great advantage of this technique, compared to hot pressing, is processing costs and times. Comparing to other ceramic processes, pressing is also easier in terms of density control, once green densities are higher than obtained in castings, for example. Because of that, shrinkage is commonly lower, reducing chances of crack and pores formation.

Different parameters can affect green body densities, as mean particle size, particle size distribution, plasticizer content, the load applied during the pressing process, etc. In this thesis, only one load was tested per material, once all powders used were commercial ones [75].

Moreover, some defects created during pressing process are not possible to eliminate during sintering. Porosity is the most

common and depends of powder features and process parameters. Delamination is another common pressing defect, which can be avoided decreasing pressing load, reducing friction forces between the green body and the die, and elastic recovery of the green body, with the disadvantage of porosity increase [76].

2.4.2 - Dip coating

In addition to pressing, dip coating process was also used to manufacture ceramic samples in this thesis.

As the name suggests, dip coating consists in dipping a sample in a suspension, coating it. This process is known for simple operation, low cost and the use of harmless raw materials [77].

Despite simple operation, dip coating has much more parameters to be set when compared to the pressing process. Suspension rheology, for example, is hard to control and have a huge influence in the final process. Shear strains, controlled by dip velocities, also play a significant role during layer fabrication. Holding time and sample porosity are also important, and all of them are related to each other [78,79].

The capillarity of the porous substrate creates a wet layer from the accumulation of particles [80]. This process can produce a coating layer/thickness in the range of 100 nm to 100 μm [81]. The immersion of the substrate in the coating suspension ensures that most of the material surface is completely coated. Layers are easily obtained by liquid evaporation of solutions, which can contain metal oxide precursors, organic matters, monomers, polymers, ceramics, or various kinds of nanoparticles [80,82]. Any aqueous solution can be easily deposited when proper processing conditions are applied [79,80].

Moreover, to have a solid deposition in the sample's surface, it is necessary to have a stable suspension, i.e. particles must be a colloid into a liquid media. To obtain this kind of suspension two ways are possible: to have viscous media or small particles, commonly nano-sized. Notwithstanding, nano-particles tend to agglomerate due to superficial forces. Because of that, two precautions shall be done: the using of deflocculant and particles deagglomeration.

When a nano-powder is bought, or synthetized, particles have a huge superficial energy, creating agglomerates, even without binders. To ensure that particles will be in suspension as

particles, not agglomerates, is important to neutralize the effect of surface energy. This task is achieved by an addition of a deflocculant in the liquid media, which will keep each particle separated [83,84].

However, agglomerations of nano-powders are formed when they are put in contact, during synthesis, transport, processing, etc. Due to this affirmation, is reasonable to think that the powder used to produce a suspension will not have free particles, but agglomerates. Because of that, even having a liquid with deflocculant, is important to give energy to the suspension to break agglomerations. It can be done by ultrasound, milling or mixing, depending of the size of the particles and the force of agglomeration [85,86].

CHAPTER 3 - NOVEL STRATEGIES FOR THE ENHANCEMENT OF ZIRCONIA AGING BEHAVIOR

3.1 - ABSTRACT

Zirconia is widely used as ceramic material, mainly because of its high bending strength (up to 1,5 GPa), accounted by a martensitic phase transformation. However, a behavior called low temperature degradation can affect zirconia properties, reducing and making hard to predict its lifetime under wet environments. To prevent this behavior some strategies have been developed, as using new materials and new processing techniques. This document will give a brief explanation about zirconia-based materials and the future of this oxide ceramic as material for dental applications.

3.2 - INTRODUCTION

The need for metals substitution in human body has led to an increase in zirconia interest, encouraging new strategies to develop products using this material.

As well described in literature, zirconia based biomaterials have some advantages when compared with titanium alloys, such as: high tensile strength (up to 1500 MPa), whiteness and high biocompatibility. Even compared with other bioceramics, like alumina, its relatively low Young's modulus (~200 GPa) and high fracture toughness (up to 15MPa$\sqrt{m}$), make zirconia a good choice to human body applications [5,16,47,87].

Fracture toughness and tensile strength are both related to the same toughening mechanism, which is responsible to inhibit crack propagation, called trans-formation toughening. In this phenomenon, a meta-stable phase (tetragonal) is exposed to a mechanical stress concentration. This stress is enough to causes a phase change from tetragonal to monoclinic, leading to a volume expansion, about 4%, which causes compression stress on the tip of the crack, stopping it.

However, even exhibiting great mechanical properties, in-service catastrophic failure events of zirconia hip prostheses have been reported in late 1990's [7,47]. This event was addressed to an unexpected behavior at human-body temperatures, able to decrease mechanical properties of the material [7]. For this reason,

Published in Proceedings of the IV International Conference on Biodental Engineering, 2017, ISBN 9781138057371

the phenomenon is known as Low Temperature Degradation (LTD) or also referred as aging.

Because of the danger related to LTD of zirconia based ceramics, a lot of studies were performed showing that the key for this phenomenon is water, which causes oxygen diffusion into the material [14,30,52]. This oxygen causes stresses in the zirconia lattice, promoting a phase transformation without an external mechanical load.

However, notwithstanding the concern with failures in orthopedic applications, the use of zirconia-based materials is substantially growing in the dentistry field [88], mainly in the production of all ceramic restorations using yttria stabilized tetragonal zirconia polycrystals (Y-TZP) [89].

3.3 - STRATEGIES TO AVOID AGING

Yttrium is a trivalent metal when bonded with oxygen while zirconium is tetravalent. When the oxide of the former is used to stabilize the tetragonal phase of zirconia, an oxygen unbalancing is caused, and vacancies are generated. This difference in valences allied to the metastability of tetragonal phase, makes only yttria stabilized zirconia to show unsettling aging behavior [16,88].

Alternatively, other oxides such as magnesia, calcia and ceria, can also be used to stabilize tetragonal phase with the advantage of not generating significant amount of oxygen vacancies thus, showing al-most no aging [47,88].

Nevertheless, the mechanical strength exhibited by zirconia stabilized by higher contents of yttria (> 3mol.%) or by other stabilizers might be significantly reduced. Ceria, for instance, can stabilize the tetragonal phase of zirconia with appreciated fracture toughness (12 MPa$\sqrt{m}$) and without aging sensitivity, Figure 10 [16,47,88].

Figure 10 Different ceria stabilized zirconia materials in comparison with classical 3mol.% yttria stabilized zirconia (Adapted from [16])

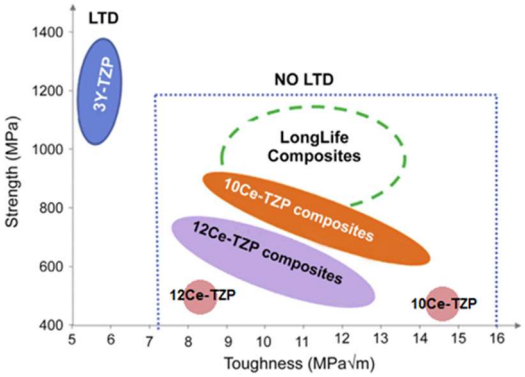

Hence, there are nowadays three main ways to avoid zirconia aging:

1 - Yttria fully stabilized microstructure modification, using precipitates as alumina, to obtain small microstructural grains and, as a consequence, ceramic-ceramic composite materials, Figure 11. This approach was mainly used to improve mechanical properties of hip implants, with the drawback, for oral applications, of increasing the Young's Modulus of the composite [90–92].

Figure 11 - Composite of 3 mol% yttria stabilized zirconia and alumina [37].

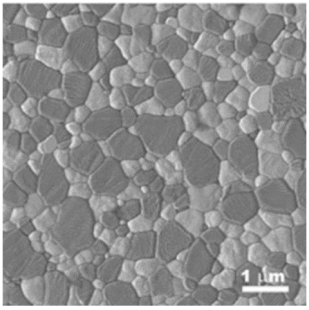

2 - Dopant changing, where the mainly challenge is to obtain acceptable mechanical properties without using yttrium oxide (yttria). Here two oxides have been shown good potential: Cerium oxide (ceria), Figure 12, with studies coming from hip materials designs; and magnesium oxide (magnesia), where a partially stabilized microstructure gives interesting aesthetics along with suitable mechanical properties to use as crowns

Figure 12 - Ceria stabilized zirconia composite: A) $SrAl_{12}O_{19}$ B) Al_2O_3 and C) Ce-TZP [30].

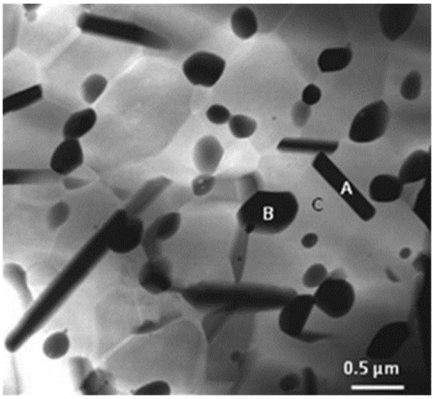

3 - Avoid the Y-TZP contact with water, or moisture, by a surface protection layer, using glass or a co-dopant, for example, in the surface of the piece, Figure 13, [3,93]. The challenge in this approach is to create a homogeneous layer with good mechanical properties, considering that cracks start to propagate from the surface and that it may dramatically impact the mechanical strength of the materials.

Figure 13 - Layer of ceria-stabilized zirconia upon a 3 mol.% yttria stabilized zirconia framework.

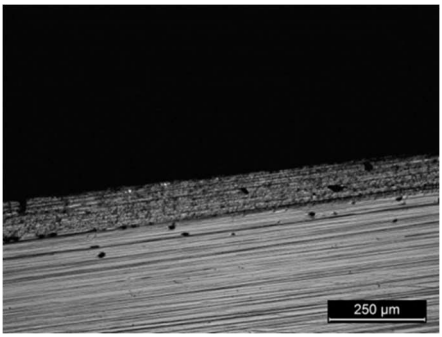

3.4 - FUTURE TRENDS

As zirconia is still being one of the most reliable ceramics, in terms of fracture toughness (K_{IC}), and its properties are also really appreciated, one may foresee further improvements based on the

strategies previously described, with more studies being conducted.

In the context of dental applications, is possible to split the material requirements in two different categories: the ones with aesthetical demands and the others that do not.

In the first category, where dental prosthesis is the main example, the challenge is how to obtain a trans-lucent zirconia without losing in mechanical proper-ties and aging resistance. Moreover, because of such aesthetical requirements, is not possible to use ceria as stabilizer, once it has a yellowish color.

In these aesthetical applications (dental restorations) is also usual to apply a porcelain veneer, which masks the white color of zirconia. The future in this application is go for monolithic zirconia restorations without a surface layer of glass or feldspathic porcelain, once most of failures in this prosthesis are regarded to fracture and exfoliation of the veneering material [89] Monolithic zirconia restorations, exhibiting a gradient in translucency given by the presence of different stabilizers over the volume of the zirconia part is also being attempted.

The second category gives more freedom to work with different zirconia based materials, once no teeth–like color or translucency are required. In this way, ceria stabilized zirconia is one of the most promising materials, especially as a ceramic-ceramic compound. Nevertheless, yttria stabilized zirconia will be continuously investigated, specially to produce ceramic-ceramic composites, which can have the highest strength for ceramic materials.

As a component with higher mechanical requirements than dental crowns, and also because of their traumatic replacement, dental implants need to be tested under compatible in-service conditions, namely those where zirconia have shown special problems: the LTD and subcritical crack growth, which is like stress corrosion for some oxides ceramics.

For both categories, it is likely that zirconia will be, in few years, the gold standard material, replacing titanium alloys and disilicates. However, to make it possible, researchers and scientists have to handle some of the challenges previously discussed, developing new materials and processing techniques.

Published in Proceedings of the IV International Conference on Biodental Engineering, 2017, ISBN 9781138057371

CHAPTER 4 - IMPROVEMENT OF 3Y-TZP AGING BEHAVIOR RESISTANCE BY MEANS OF DIP COATED ZIRCONIA-BASED PROTECTIVE LAYERS

4.1 - ABSTRACT

In this work protective coatings were produced to avoid 3Y-TZP low-temperature degradation (LTD). Two different routes were used to manufacture layers of 5Y-PSZ and 12Ce-TZP: pressing and dip coating. In order to decrease the layer thickness of dip coated samples, suspensions were prepared without plasticizer. Coatings thickness of around 7 μm were obtained using 5Y-PSZ or 12Ce-TZP. This thickness is enough to prevent LTD for about 32 years *in vivo*.

4.2 - INTRODUCTION

Zirconia aging sensitivity is a function of several parameters, from material and environment. Materials grain size, porosity, stabilizer amount and element, water saturation in air and temperature are some examples that can change the material resistance to this behavior [11,51]. In this sense, researchers are trying to decrease grain sizes and replace yttrium oxide as the stabilizer to decrease LTD kinetics.

Aiming at avoiding the spontaneous phase transformation in zirconia, researchers have developed different strategies to handle this issue. Camposilvan [3], for instance, used infiltration of cerium salt to create a layer capable to inhibit oxygen diffusion to a yttria tetragonal zirconia polycrystals (Y-TZP) bulk. Using the same metal, cerium, but with a different approach, Palmero [16] increased zirconia LTD resistance by replacing yttria for ceria to obtain a ceria tetragonal zirconia polycrystal (Ce-TZP), which mechanical strength was increased using other ceramics as reinforcement. Another way to avoid aging is preventing grains growth during sintering step of Y-TZPs. In this way, alumina nano-scaled have been used to keep grains small, maintaining the compromise of low porosity [18,94].

However, these approaches are not sufficient to ensure the final requirements of the materials. Grain size decreasing reduces aging kinetics, but there is no evidence that is possible to completely avoid the phenomenon using this strategy. The ISO for yttria-stabilized zirconia for implant applications says that this

material must be tested in terms of aging [56]. On the other side, stabilizer changing may be a good strategy to avoid LTD, since only yttria seems to stabilize tetragonal zirconia by vacancies, which are responsible for aging [7,14,30,95]. The disadvantage of this approach is the low flexural resistance of other stabilizers (commonly ceria, magnesia, and lime) when compared to 3Y-TZP, which are the zirconia gold standard in terms of bending strength [5,11,16,88].

Y-TZP coating processes may be good alternatives in the attempt to combining both requirements: aging resistance and mechanical strength. The disadvantage of this strategy is that coating materials will not have mechanical strength similar to the 3Y-TZP bulk. Moreover, coatings could change the white Y-TZPs surface, what can be a problem for applications that require aesthetic, as in dentistry.

Aiming at overcoming these challenges, in this work two different approaches based on the production of thin Ce-TZP and Y-PSZ protective coatings were explored aiming at avoiding the action of the low-temperature degradation in 3Y-TZP structures. The Ce-TZP was used to create a coating that is insensible to the aging phenomenon, and therefore, to avoid oxygen diffusion. At the same time, as this oxide has a yellow color that is undesired in some of the zirconia applications (e.g. prosthetic dentistry), another approach was to study thin layers of Y-PSZ over Y-TZP substrates, which have the advantage of being translucence, due to their mainly cubic grains.

4.3 - MATERIALS AND METHODS

4.3.1 - Layer thickness calculation

As reported by Chevalier [7], aging happens following an Arrhenius equation, from the surface to de bulk and by oxygen ions diffusion. Based on this knowledge, 3Y-TZP life-time can be evaluated trough accelerated aging, i.e. rising temperature to increase oxygen diffusion and decreasing experimental time. As the purpose of this work is to avoid aging and the success of this will be measured by standardized autoclave tests, ISO 13356, the minimum layer thickness was calculated to ensure protective behavior for ceramic applications, particularly to human body applications.

Moreover, the commercial powder selected to be one of 3Y-TZP coatings (Zpex Smile) is formed mainly by cubic phase (5Y-PSZ) and has Yttria content of ~5 mol%, which increases oxygen diffusivity when compared to 3Y-TZP [96–98]. Therefore, layer minimum thickness was calculated using cubic diffusion velocities, the most severe ones, for test temperature (134 ºC) to ensure that 3Y-TZP would not to be affected by OH^- during the higher time exposed to moisture, 18h.

Using Arrhenius equation and oxygen diffusion data obtained in literature, activation energy of 1eV and pre-exponential coefficient 0.0034 [97], the maximum diffusion depth calculated for cubic structures was ~1 μm, which means that the minimum coating thickness of 5Y-PSZ must be equal or greater to this value so the 3Y-TZP bulk is not affected by aging problems..

4.3.2 - Samples fabrication

Two types of coated samples were fabricated using different processes: double action pressing and dip coating. Double action pressed discs were produced using as follows: commercial 3Y-TZP powder (TZ-3YSB-E, Tosoh, Japan) was double action pressed in a stainless-steel die with a diameter of 18 mm under 200 MPa, resulting in discs with around 1.8 mm thickness. Afterwards, a thin layer of commercial 12 mol% ceria stabilized zirconia powders, 12Ce-TZP, (Hitachi, Japan) was uniaxially, double action, pressed under 200 MPa over the green 3Y-TZP disks were then sintered in air, for 2h, at 1500 ºC using a heating rate of 8 ºC/min. Samples fabricated using this technique will be referred as Ce-TZPp.

Dip coated discs were alternatively produced in order to decrease layer thickness and to improve the coatings fabrication control. In this way, disks of 18 mm diameter were uniaxially, double action, pressed using a commercial 3Y-TZP powder (TZ-3YSB-E, Tosoh, Japan) under 200 MPa. After pressed, green samples were dip coated, using two different commercial powders: 12Ce-TZP and 5Y-PSZ. 12Ce-TZP coatings were manufactured by using commercial 12 mol% ceria stabilized zirconia powders (Hitachi, Japan). The 5Y-PSZ powder (Zpex Smile, Tosoh, Japan) was first debinded by a pyrolysis process at 600 ºC during 1 hour, before suspensions preparation. During suspensions preparation, ultra sound deagglomeration was used for both materials.

During 3Y-TZP green bodies coatings, a spindle apparatus was used to obtain a constant speed of 12 mm/s, with a total dip time of about 6 seconds. In order to improve layers' density, some samples were submitted to more than 1 dip, with a homogenization time of 10 minutes between each dip. Table 4 shows different process parameters and the respective sample name used in this work. Final drying was performed at room temperature for 18 hours. Sintering temperature was defined according coated material, being 1450 ºC for the 12Ce-TZP layers and 1500 ºC for 5Y-PSZ ones.

Table 4 - Coatings suspensions according to the material and solid content.

Name	Liquid / Percentage	Powder / Percentage	Dispersant	Number of dips
Ce-TZP23x1	Water / 76%	12Ce-TZP/ 23%	Dolapix CE64	1
Ce-TZP23x2				2
Ce-TZP23x3				3
Ce-TZP28x1	Water / 71%	12Ce-TZP/ 28%		1
Ce-TZP28x2				2
Ce-TZP33x1	Water / 66%	12Ce-TZP/ 33%		1
Y-PSZ23x1	Water / 76%	ZpexSmile/ 23%		1
Y-PSZ23x2				2
Y-PSZ23x3				3

Figure 14 shows different processing routes used to produce three groups of coated materials.

Figure 14 - Different process used to produce coated samples.

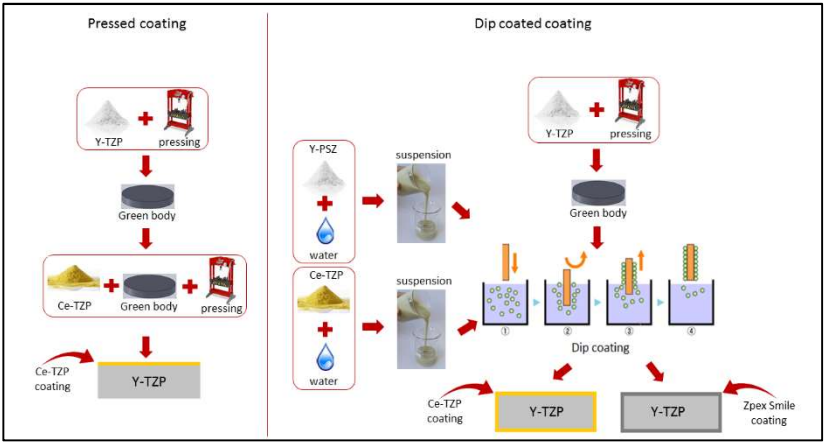

Suspensions were characterized regarding to powder size distributions and rheology, while sintered samples were analyzed in terms of microstructure, color and aging behavior.

To evaluate aging, autoclave tests were performed following ISO 13356, in steam at 134 ºC under 2 bar and for different times. Monoclinic content was measured by XRD, Copper K-α, technique using Toraya modification of Garvie & Nicholson equation, considering the maximum intensities of peaks.

Considering the possibility of oxygen diffusion across coatings, as previously described, XRD analysis might not be enough to measure aging in sub-superficial layers, especially to assess 3Y-TZP bulk [13]. On the other hand, sample cutting, to assess underlayer material from a cross-section, induces phase transformation because of stresses generated, which can be confused to aged grains. In order to remove mechanical stressed material, from cutting process, and keep only aged grains, a subsequently mechanical polishing could be performed. However, this step hides grain boundaries and a final thermal etching, used to reveal grain boundary, must to be used. Nevertheless, the temperature reached, 1200 ºC, is the same used to recovery transformed grains, which makes this procedure unfeasible.

As an alternative to overcome these difficulties, focused ion beam (FIB) was used to carefully polish samples cross section,

with the advantage of revealing grains [99]. After that, low temperaure degraded regions could be observed as rough grains, similar to transformed grains reported elsewhere [30]. The underlayer material could then be qualitatively evaluated in terms of aging [53].

The color of specimens was measured using the CIE L*a*b* system without specular reflectance, once dip coating creates rough surfaces, which changes completely material glossiness.

4.4 - RESULTS AND DISCUSSION

4.4.1 - Suspensions characterization

In order to understand suspensions and coatings behavior, mean particle size (MPS) of powders was analyzed in suspension, as shown by Figure 15, where dashed lines mean particle size of suspension (d50). MPS was measured as 227 nm for Y-PSZ, after debinding and deagglomeration, and 752 nm for Ce-TZP after deagglomeration.

Figure 15 - Mean particle size in suspension after dispersing.

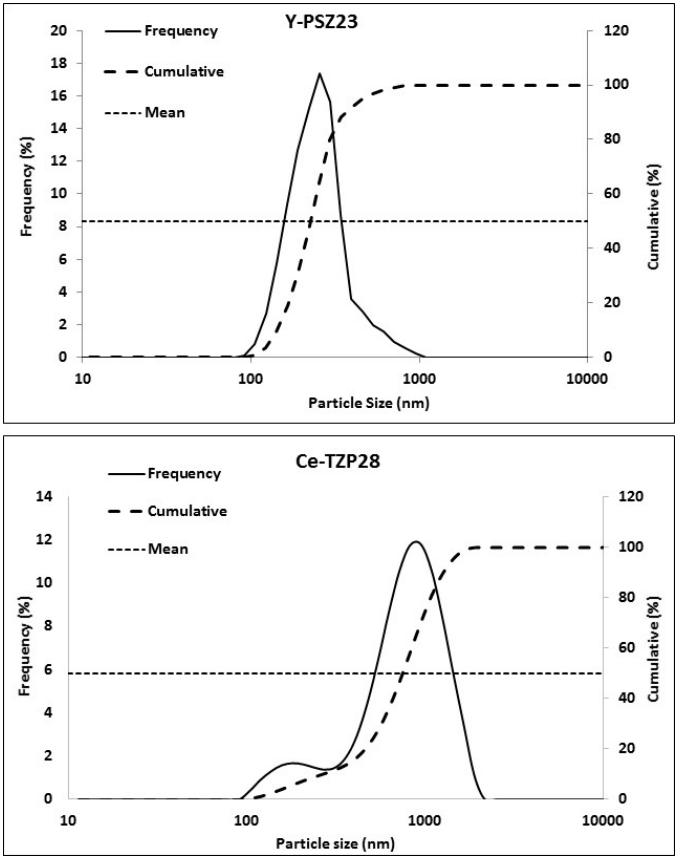

Rheological behavior of suspensions containing 28 and 33 wt% of 12Ce-TZP were analyzed, as well as for 23 wt% 5Y-PSZ, Figure 16. As expected, all suspensions follow a Newtonian behavior, once no binder were added, solid loading are low and powders are nano scaled, maintaining suspension stability, i.e. without agglomerating and decanting.

An increasing from 28 wt% to 33 wt% of solid loading in 12Ce-TZP suspensions showed a weak influence on viscosity of suspensions, due same reasons explained before, growing from 1.7 mPa*s to 1.8 mPa*s. Y-PSZ showed 1.6 mPa*s for this property.

Figure 16 - Viscosity for different suspensions and solid loading.

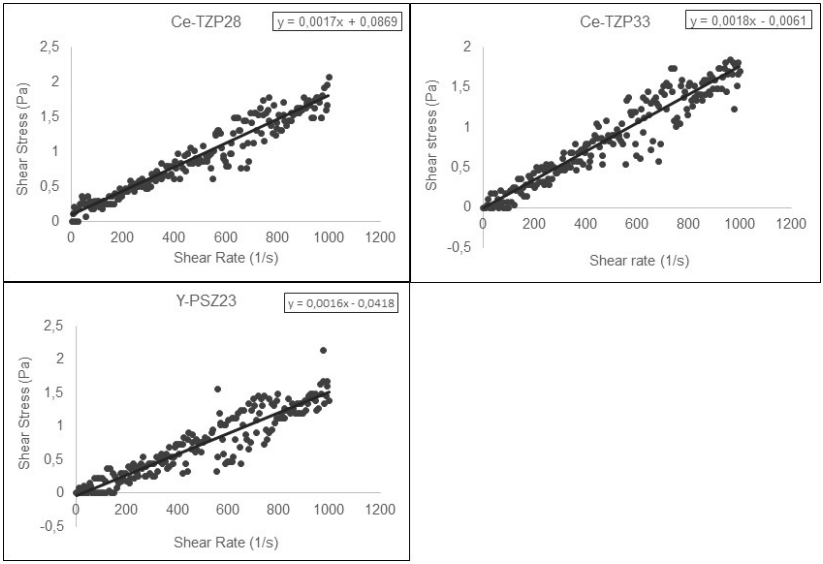

4.4.2 - Color results

As an important property for aesthetical materials, dip coated samples were characterized in terms of color. Figure 17 shows this property changing according to different coating processes.

Figure 17 - CIELAB color coordinates obtained for each dip coating condition. Dashed (- - -) lines refers to 3Y-TZP sintered samples, used as standard value.

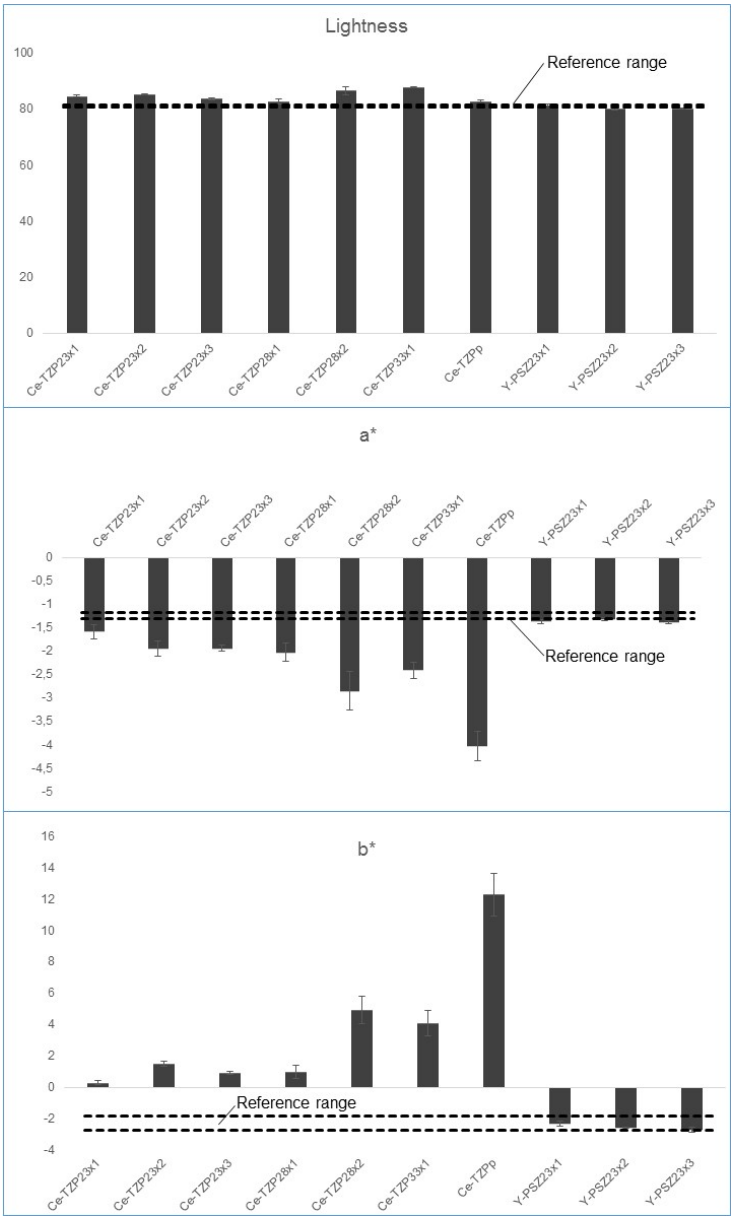

As whiteness is determined by a correlation between L*a*b*, as higher is the lightness and as closer to zero are a* and b*, whiter will be the material. Dashed lines, in Figure 17, are measurements of 3Y-TZP parameters after sintered, considered as standard values in this study.

For samples coated with 5Y-PSZ, values are similar to 3Y-TZP, which is expected once both materials are white and the layer material have some translucence. 12Ce-TZP, in turn, when fully oxidized, shows a high yellowness (high values in b* axis), leading to changes in whiteness due to process parameters, namely the increase in the layer thickness.

In fact, increasing the number of dips for each sample, the yellowness and greenness also tend to increase, while lightness didn't change too much. The best results, as regard to whiteness of the specimens, were obtained using one dip of Ce-TZP23 suspension, which could be somehow anticipated and is explained by the fact that this suspension had the lowest solid content among the others. When coated three times, Ce-TZP23 has decreased yellowness and maintained greenness, comparing with Ce-TZP23x2, probably because all dips were performed before sintering process, leading to a coating removal during third dip.

4.4.3 - Microstructure

The first feature about aging protective coating is the capacity to avoid moisture and OH^- contact, which requires a dense coating. Figure 18 shows the micrographs of the microstructure and morphology of the different coatings produced either by pressing or by dip coating.

Figure 18 - General view of layers' surface and porosities for different coatings: Ce-TZPp (a), Ce-TZP23x1 (b), Ce-TZP23x2 (c), Ce-TZP28x1 (d), Y-PSZ23x1 (e) and Y-PSZx2 (f).

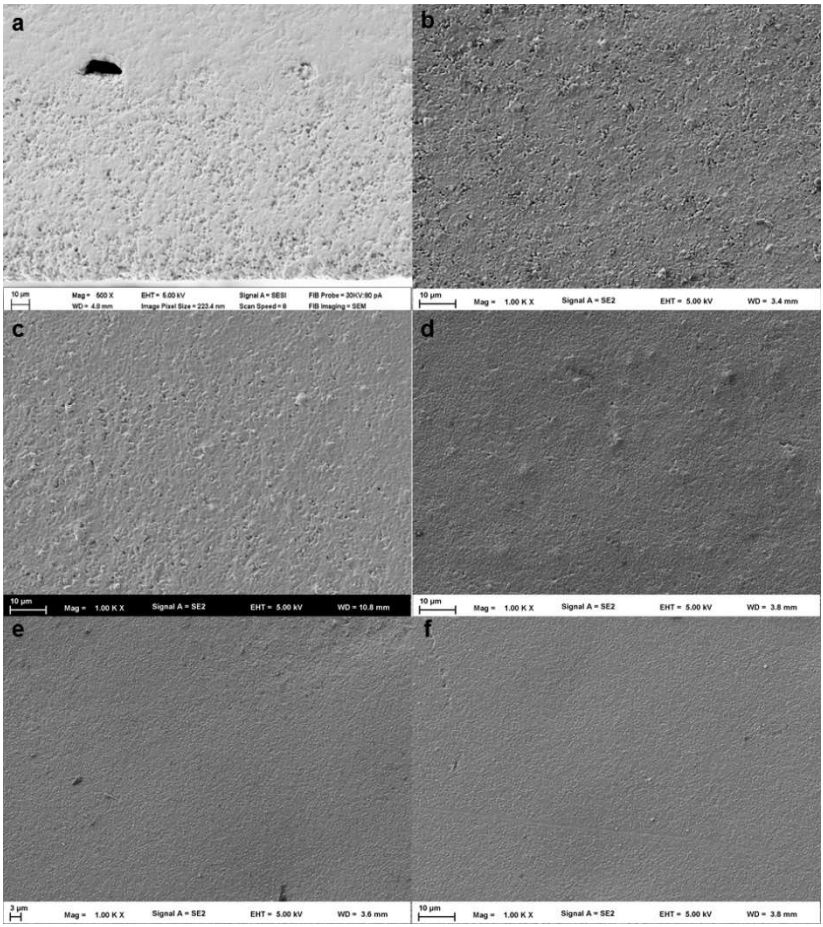

Pressing was used to produce a layer of about 100 μm, Figure 18a. Using this process is possible to easily control the protective coating thickness, once this parameter is ruled by the weight of powder that is poured into the die. On other hand, decreasing layer thickness, the powder dispersion over the 3Y-TZP disc also decreases. Because of this, the best acceptable layer, in terms of uniformity and thickness, was obtained using the technique showed before. Regarding porosity, Figure 18a shows

an apparent porosity, even when pressed under 200 MPa and sintered at 1500 ºC. In fact, porosity arising from process is much lower than observed in this micrograph, where voids can be related to material pullout during polishing process, as will be seen ahead in this text where FIB polished micrographs are shown and analyzed, Figure 22.

Microstructures obtained by 12Ce-TZP dip coating are showed in Figure 18b-d corresponding to Ce-TZP23 one dip, Ce-TZP23 two dips and Ce-TZP28 one dip, respectively. As porous layers are considered undesired, processing using one dip and lowest solid content suspension was discarded, once superficial layer porosity is around 2.0%. However, when another dip was performed, porosity decreases to ~1.2%. Increasing the solid content in the suspension also produces more uniform surfaces, with around 0.5% of porosity with the advantages to have only one dip, which reduces the number of operations, and shows better results in terms of color, as reported before. For samples coated with 5Y-PSZ, Figure 18e-f, there are no significant differences between surfaces and open porosities (~99,9%).

Taking into account these results, Ce-TZP28 and Y-PSZ23 were selected to create protective layers to be evaluated in accelerated aging tests. As this phenomenon is strongly related to grains size, measurements of this parameter were made and a microstructural overview can be also seen in Figure 19.

Figure 19 - Grain size of the protective coatings selected for aging tests: (a) Ce-TZP and (b) Y-PSZ.

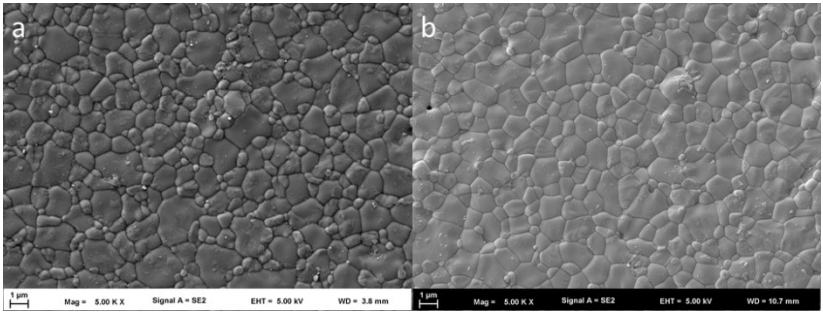

5Y-PSZ is formed mainly by cubic phase [35], having a grain size much bigger than for Y-TZPs sintered in the same condition (~400 nm), which is in accordance to the behavior reported in literature [100,101]. In fact, the measured mean grain size was

0.90 ±0.13 µm, showing, combined with the XRD analyses, Figure 20, that microstructure obtained is manly cubic.

Figure 20 - X-Ray diffractogram of commercial 5Y-PSZx1 and 3Y-TZP.

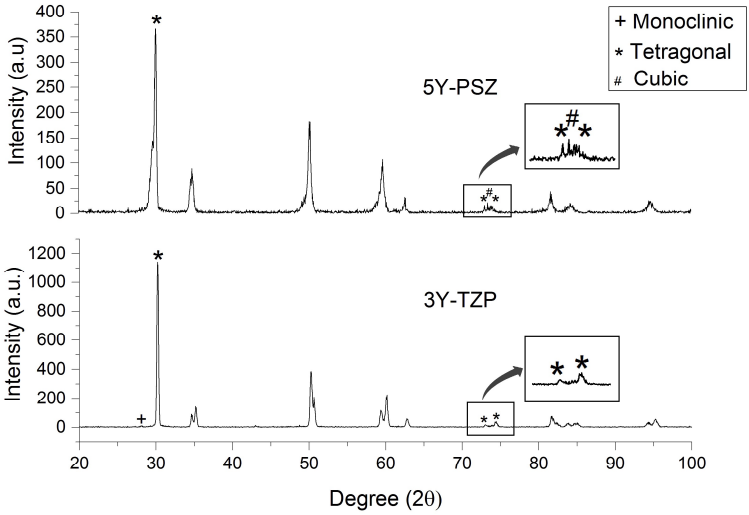

As all samples were co-sintered, 12Ce-TZP coatings have a trend to have an increasing in grain size, once this ceramic increases its density in lower temperatures when compared to yttria stabilized zirconia, as can be observed elsewhere [3]. However, temperature and time used must be higher to avoid porosity in the bulk (3Y-TZP). For this reason, Figure 19b shows a superficial coating grain size of 0.92 ±0.11 µm.

4.4.4 - Aging

Because of challenges reported in materials and methods, aging results were divided in two sections: XRD Results and Microstructure results.

4.4.4.1 - XRD Results

Both coating materials used, were supposed to be inert to aging effect, at least for the times and temperatures used. As XRD maximum depth analysis is around five micrometers [13] and coating thicknesses were intentionally fabricated above this value,

the aging curves were plotted in order to validate the initial assumption that coatings did not underwent low temperature degradation, Figure 21.

Figure 21 - Monoclinic content after aging in different coatings.

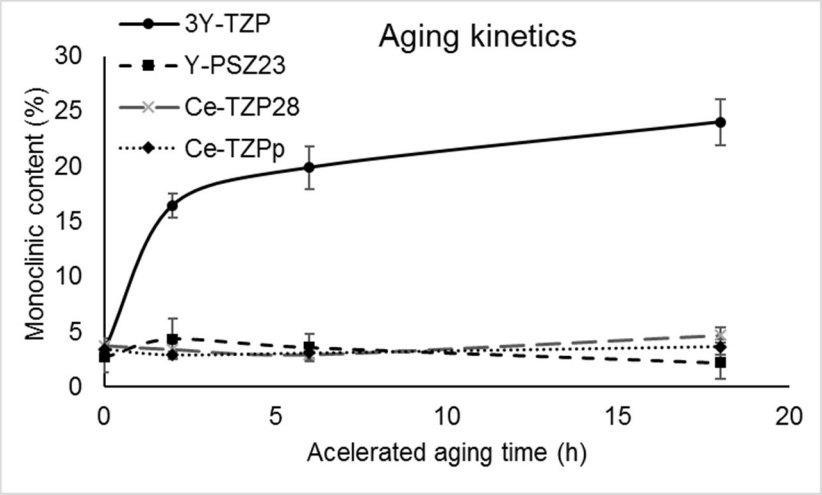

As shown in Figure 21, almost no degradation is observed in both coatings (12Ce-TZP and 5Y-PSZ), which contrasts to the behavior of the uncoated 3Y-TZP substrate. Monoclinic content observed in coatings, can be related to sample measurement errors.

4.4.4.2 - Microstructure results

As explained before, the existence of monoclinic phase under the protective coating was evaluated using SEM analysis, to verify if there are no OH^- diffusion across protective coatings after accelerated aging, Figure 22.

Figure 22 - SEM of coatings' cross sections after Focused Ion Beam polishing: Ce-TZPp (a), Ce-TZP28x1 (b) and Y-PSZ23x1 (c).

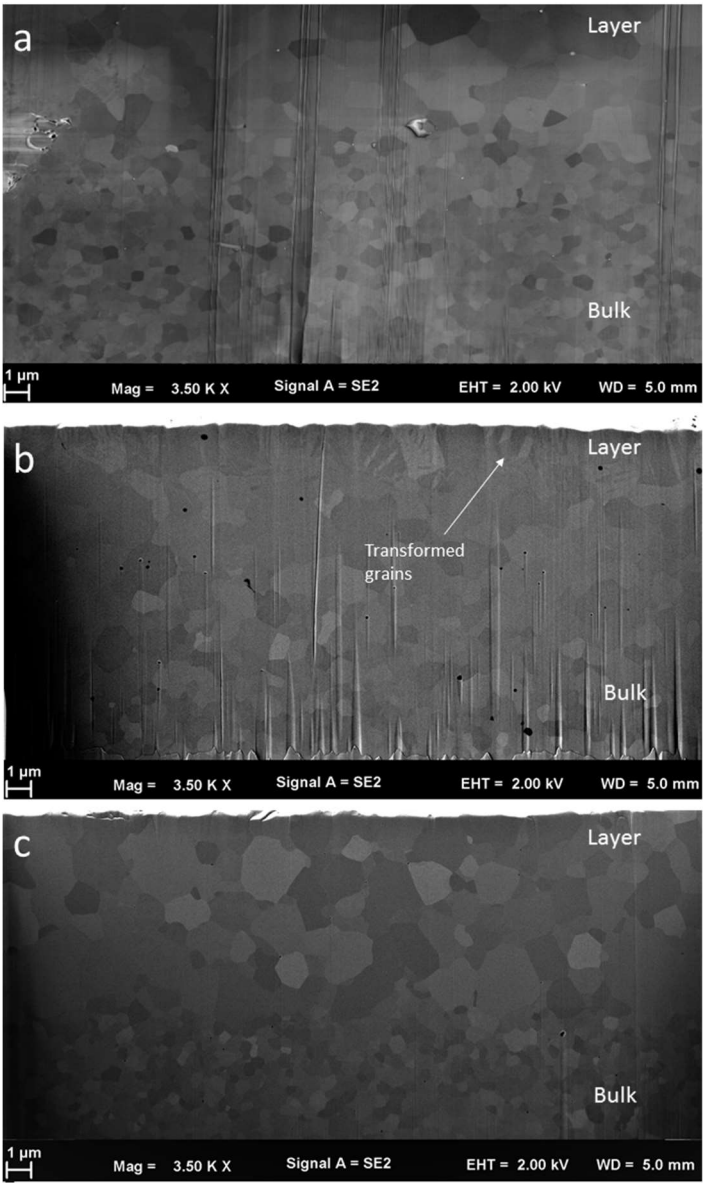

Additionally to the Ce-TZP28x1 and Y-PSZ23x1 specimens that were selected for the aging study, the Ce-TZP coated specimens produced by the double action pressing technique, and which the coating thickness was overestimated as regard to the avoidance of OH^- diffusion to the bulk, were also evaluated in terms of protective behavior, Figure 22a.

Besides LTD resistance, another important interlayer feature to evaluate is thermal coupling, which can also create residual stresses, leading to phase transformation. This way, because of similar composition of materials (they are mainly zirconia) thermal expansion coefficient should be very close, thus avoiding thermal stresses, as reported for Fischer [102]. Notwithstanding, powders have different behavior during pressing and sintering, which may create density gradients, causing different shrinkage in the samples and, consequently, martensitic transformation. In addition, pressed layers, showed in Figure 18a, suggest the presence of some porosity, which could be detrimental when trying to avoid OH^- diffusion. However, after FIB polishing few pores were observed and many of them related to interlayer area, coming most probably from pressing stage, Figure 22a.

Because of a quite dense and uniform layer about 100 μm, no LTD was observed in 3Y-TZP bulk. Contact area and high temperatures, provide conditions to interdiffusion, as observed comparing grain sizes transition in Figure 22a, which shows absence of monoclinic grains that could be generated during process.

Figure 22b shows the cross section of Ce-TZP28x1 coated samples. In this image is possible to observe ceria stabilized zirconia grains, 0.92±0.11 μm, on the surface and smaller yttria ones in the bulk, 0.31±0.28 μm. Because of the nature of the process, dip coating, and higher cerium diffusivity into zirconia lattice, a smooth transition in grain size is possible to see between the coating and the bulk materials, which makes difficult to accurately measure the coating thickness (measured here to stay between 5 and 10 μm). The first layer of grains shows the rough aspect referred before, which means a superficial phase transformation. Taking into account the grains length, (~1 μm) is possible to confirm the coating thickness calculations presented before, once no degradation in deeper distances, evidencing the protective behavior of the layer. Furthermore, no micro-cracks were observed in transformed zone. This crack-free

microstructure, makes the transformed zone able to increase material fatigue resistance and flexural resistance [64], by creating a compressive layer in the surface material. Grain size is also related to phase transformation observed in this first layer of grains, once big grains reduce tetragonal stability of zirconia, as reported elsewhere [103]. This superficial behavior explains why monoclinic content evolution is not strongly observed with XRD, once this technique analyses about 5 micrometers of the material thickness. Black points observed in the micrograph can be addressed to residual porosity.

Coatings produced with Y-PSZ23x1 suspension, Figure 22c, showed the best density when compared to the above discussed coatings, as showed in Figure 18. The transition between 5Y-PSZ and 3Y-TZP is clearly observed, once grains of the former are much bigger, 0.90 ±0.13 μm than those of the latter 0.46 ±0.14 μm. Coatings with ~7 μm thickness were obtained and LTD was not observed. Bulk 3Y-TZP grains were also unaged, evidencing that for the thickness used OH^- diffusion was not enough to affect this material.

The difference between 3Y-TZP grain sizes achieved for each coating can be related to the temperature during sintering process, once ceria-based coatings were sintered at 1450 ºC, while 5Y-PSZ was sintered at 1500 ºC.

4.5 - CONCLUSIONS

Protective coatings were successfully produced over 3Y-TZP substrates either by double action pressing or by dip coating techniques. The former technique produced uniform layers of ~100 μm while in the latter thicknesses of 5-10 μm could be obtained.

Suspensions having solid contents of 23 wt% and 28 wt% of 5Y-PSZ and 12Ce-TZP, respectively, showed best results regarding density (99.9 % and 99.5 %) and yellowness.

Grains sizes obtained for both coatings (Ce-TZP28x1 and Y-PSZ23x1) were much bigger (around 0.9 μm) than for bulk material (~0.4), being further observed a smooth transition between 12Ce-TZP and 3Y-TZP. Difference between 5Y-PSZ and 3Y-TZP were attributed to the different phases present, mainly cubic in the first case and mainly tetragonal in the second case.

Accelerated aging tests showed almost no LTD in the coatings, after XRD analysis. SEM analyses showed signs of

transformation at the outmost layer of grains in 12Ce-TZP coating, which can be addressed to the big size of the grains.

Finally, the pre-designed coating thicknesses, around 7 μm for 5Y-PSZ coatings and 5-10 μm for 12Ce-TZP coatings, proved to cope successfully in the protection of 3Y-TZP bulk structures from low temperature degradation.

CHAPTER 5 - MECHANICAL PROPERTIES OF DIP COATED ZIRCONIA-BASED PROTECTIVE LAYERS

5.1 - ABSTRACT

This work aimed at evaluating the mechanical properties of 3Y-TZP with different aging resistant zirconia based-coatings. Layers of 12Ce-TZP and 5Y-PSZ were manufactured, over 3Y-TZP discs, by means of dip coating process. Roughness and biaxial bending strength were correlated, showing that the second property was not affected by the material used as coating. In addition, crack resistance was evaluated by Vickers indentation, showing that 3Y-TZP substrate is responsible for mechanical resistance of coated samples.

5.2 - INTRODUCTION

As demonstrated by Garvie [1], zirconia is a unique ceramic material, which can combine high bending strength (up to 2 GPa), high fracture toughness, K_{Ic}, (higher than 10 MPa$\sqrt{m}$) and steel-like Young's modulus (around 200 GPa) [6,95]. Specially for ceramics, the first two properties are somehow related and higher K_{Ic} means less failure probability, once ceramics processing defects accounts for the majority of components failure.

Nevertheless, the failure of several hip prostheses highlighted one unexpected behavior, called low-temperature degradation (LTD), which may compromise zirconia structural applications. The main features about LTD are: it is thermal dependent; it happens in the presence of water; large grain size enhances its occurrence; only yttria stabilized zirconia is greatly influenced by LTD [14,40,51].

In order to overcome this issue, the development of coatings to avoid zirconia contact with water is under investigation [3]. The great challenge in this approach is to match thermal coefficients, and Young's modulus (YM), of coatings and zirconia. Another point to be considered is the lower fracture toughness of ceramics used as coatings, which often display lower YM than Y-TZP [104].

Even when a good match in thermal coefficients are achieved, chemical bonding between ceramic and other layers might be weak, causing delamination when a crack grows from surface into the material and propagates through the materials interface [105,106]. On the other hand, if a strong bonding exists,

a crack grows from the surface directly to the bulk, which can be made of 3Y-TZP. This situation is better than the first, once zirconia bulk (3Y-TZP) might be able to arrest the crack propagation. Additionally, thinner coatings are preferred to thicker ones as the thinner the coating the faster is the triggering of toughness mechanism towards the arrest of crack propagation.

In ceramic, most of stress concentration, i.e. crack initiators, comes from manufacturing process. Because of that, bending strength, for example, is measured as a statistic data using Weibull distribution, which gives a failure probability and can also give a clue on how homogeneous are the defects arising from the manufacturing process. Moreover, as ceramics are brittle and have low tolerance to tensile stresses, surface quality of components strongly determines final strength of these materials and roughness parameters are useful to predict it [107].

However, as mentioned by Shen [108], most of papers published in ceramic strength are not related to those that are actually measured in real components. They rather focus on the analysis of well-polished and carefully processed specimens, providing answers about materials behavior instead of real products behavior. It is well known that for intrinsic properties, such as fracture toughness, the sample preparation is of extreme importance for the obtained results. This way, for a more realistic estimation of the real strength of a material (considering that manufacturing defects strongly impacts the final strength) the materials should be tested in the as-manufactured state, every time real components do not undergo post processing surface treatments.

Based on these proposals, the present work aims to evaluate the mechanical response of aging protective coatings (12Ce-TZP and 5Y-PZS) over 3Y-TZP substrates. These materials were selected to avoid the above reported thermal and chemical mismatch problems, aiming at improving both the LTD resistance of components and the chemical bonding between layers.

5.3 - MATERIALS AND METHODS

5.3.1 - Samples fabrication

Discs with 1.8 mm of thickness were fabricated, by double action pressing, using a tetragonal zirconia polycrystals commercial powder (TZ-3YSB-E, Tosoh, Japan) in a stainless-

steel die (Ø18 mm) under 200 MPa of pressure. After pressing, samples were divided in two groups: uncoated (control group) and coated. The former was sintered in air, at 1500 ºC for 2h using a heating rate of 8 ºC/min. Specimens from the control group will be referred hereafter as 3Y-TZP. In order to evaluate roughness influence in flexural strength, ten samples from the control group were polished using a diamond suspension of 3 µm, resulting in two different groups: Polished and as-sintered. These specimens were used to flexural tests and roughness control only. For the remaining tests, due to the low coating thickness (~10 µm), all samples were polished using diamond suspensions of 15 and 3 µm, only.

The second group of green discs was divided in two new groups. Each new group was dip coated using suspensions made by one of two commercial powders: 12 mol% ceria stabilized tetragonal zirconia polycrystals, 12Ce-TZP, (Hitachi, Japan) and 5 mol% yttria partially stabilized zirconia or 5Y-PSZ, (Zpex Smile, Tosoh, Japan). Table 5 shows the composition of the suspensions used in this study. Prior to suspension preparation, 5Y-PSZ powder was debinded by a pyrolysis process at 600 ºC during 1 hour. Suspensions were sonicated for 60 seconds (UP200St, Hielscher, Teltow) for particles deagglomeration.

3Y-TZP green bodies were dipped in the suspension at constant speed of 12 mm/s and the holding time was ~3 seconds. Before sintering a drying process was performed for 18 hours at room temperature. Regarding sintering conditions, the same dwell time and heating rate were used for all groups, 2h and 8 ºC/min, respectively. The sintering temperature was defined according to optimized sintering condition previously defined by the authors for these materials, i.e. 1450 ºC and 1500 ºC for 12Ce-TZP and 5Y-PSZ powders, respectively, considering density and grain size achieved. Suspensions' compositions, Table 5, and coating parameters were defined according previous studies, which took account aging protective behavior of them.

Table 5 - Coatings suspensions according to the material and solid content.

Name	Liquid / Percentage	Powder / Percentage	Dispersant
Ce-TZP28	Water / 71%	12Ce-TZP / 28%	Dolapix CE64
Y-PSZ23	Water / 76%	Zpex Smile / 23%	

Figure 23 shows a summarization of samples processing.

Figure 23 - Coated and control samples fabrication.

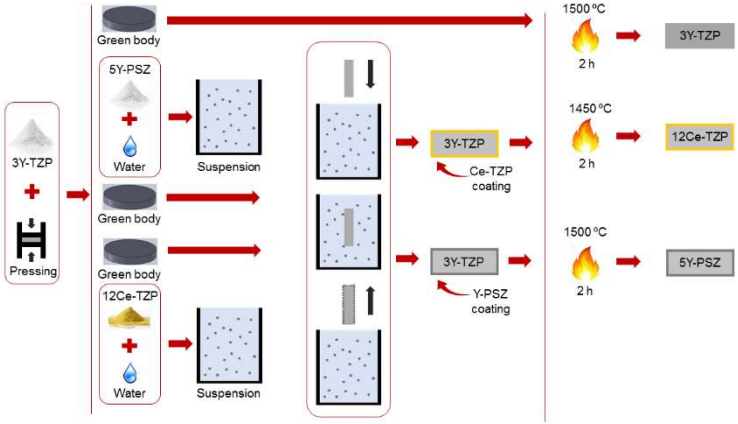

In order to understand materials behavior during indentation tests, some discs of 12Ce-TZP and 5Y-PSZ were also manufactured by double action pressing. The only difference, during the pressing process, between them and 3Y-TZP samples was the pressure applied, which was 100 MPa for both. The sintering parameters were the same as those used for sintering the coatings (described above).

Uncoated samples composed by pressed monolithic powders will receive the name of the composing powders, as follows: 3Y-TZP, 12Ce-TZP and 5Y-PSZ. Coated samples will receive suspension's nomenclature: Ce-TZP28 and Y-PSZ23.

5.3.2 - Mechanical tests

Roughness was measured using a contact profilometer (SJ-210, Mitutoyo, Kawasaki) and three measurements were made per

sample. In addition, three discs of each condition, 3Y-TZP, 3Y-TZP polished, Ce-TZP28 and Y-PSZ23, were analyzed, resulting in nine measurements for each condition. The following roughness parameters were obtained for all samples: Ra, Rt, Rq and Rsk.

Young's modulus and hardness were both analyzed by instrumented indentation, using a Berkovich indenter, with 2 N of maximum load and 30 seconds of holding time. In this test three samples of each condition (3Y-TZP, 12Ce-TZP, 5Y-PSZ, Ce-TZP28 and Y-PSZ23) were tested. Elastic and plastic depth were provided by the equipment software. Young's modulus was calculated using reduced modulus, measured by the equipment, following equation 10:

$$\frac{1}{E_r} = \frac{(1-\upsilon_s^2)}{E_S} + \frac{\left(1-\upsilon_i^2\right)}{E_i} \quad (5)$$

where, E_r is the reduced modulus, E_s the sample Young's modulus, E_i the indenter modulus, υ_s sample's Poisson and υ_i indenter Poisson.

Vickers hardness was also measured. The indentations were made in the monolithic discs of different materials (3Y-TZP, 5Y-PSZ and 12Ce-TZP) and also in 3Y-TZP coated discs (Y-PSZ23 and Ce-TZP28). Three indentations were performed in each disc using loads of 2, 15, 30, 45 and 60 N, with 30 seconds of holding time. Surface damage resistance (SDR) was also measured using data collected in this test, following equation 11. Because of the errors associated to the technique [109,110], results were used only as an comparison of crack propagation in this study.

$$SDR = \frac{0.035 H_V \sqrt{a}}{3\sqrt{\frac{l}{a}}\sqrt[5]{\left(\frac{H_V}{3E}\right)^2}} \quad (6)$$

where, Hv is the Vickers hardness of the material, "a" is the half diagonal of the Vickers indent, "l" is the crack length measured from indent corner and "E" is the material Young's modulus.

Biaxial flexural tests were performed in a ball on three balls (B3B) apparatus, where the radius formed by three balls is 5 mm, and a load rate is 0.1 mm/s. Ten samples of each condition (3Y-TZP, 3Y-TZP polished, Ce-TZP28 and Y-PSZ23) were tested.

5.4 - RESULTS AND DISCUSSION

5.4.1 - Layer thickness and grain size

Previous studies showed that using the methodology described is possible to produce samples with around 7 μm of coatings thickness, for both suspensions, which was enough to avoid aging behavior of 3Y-TZP bulk, Figure 22. Grain sizes were measured, by intercept method, for Ce-TZP28 and Y-PSZ23 as 0.92 ±0.11 and 0.9 ±0.13 μm, respectively and 0.31 ±0.28 for 3Y-TZP samples.

5.4.2 - Roughness

Because of defects commonly developed by coating processes, roughness was used in this study to characterize mainly the open porosity and topography of the coatings, as well as the differences obtained for pressed substrates, Table 6.

Table 6 - Roughness parameters of the different 3Y-TZP uncoated (Polished and as sintered) and coated (Ce-TZP28; Y-PSZ23) samples.

Sample	Ra (μm)	Rq (μm)	Rt (μm)	Rsk (μm)
3Y-TZP Polished	0.06 (±0.07)	0.15 (±0.29)	-0.58 (±0.08)	-0.58 (±0.21)
3Y-TZP	0.14 (±0.02)	0.19 (±0.05)	0.34 (±1.65)	-0.70 (±0.78)
Ce-TZP28	0.51 (±0.28)	0.69 (±0.45)	4.76 (±3.57)	-0.31 (±0.76)
Y-PSZ23	0.48 (±0.12)	0.67 (±0.25)	5.15 (±3.31)	-1.05 (±1.55)

Both groups of coated samples, Ce-TZP28 and Y-PSZ23, showed similar values of average roughness (Ra), root mean square roughness (Rq) and maximum distance between valleys and peaks (Rt). These two groups presented significant differences in skewness (Rsk) parameter, though, which shows a trend of Y-PSZ23 samples having more valleys than peaks on the surface.

A comparison of polished 3Y-TZP and as sintered 3Y-TZP shows an expected reduction in Ra, to values reported elsewhere [111]. However, during polishing process one sample kept Ra similar to the as sintered condition, making the standard deviation much higher than expected, as well all other parameters

measured. Rt, for instance, has shown similar results for both conditions, but in fact, lower values were expected after polishing (around 0.3 for well-polished samples), once this process tends to soften the scratches. Skewness is also strongly affected because of that, since polishing balance peaks and valleys quantities [112].

5.4.3 - Instrumented indentation

Figure 24, shows the penetration depth for a Vickers indenter and 2N load over the different specimens. These measurements might give initial insights on materials properties such as hardness and micro-plasticity, as well as on the layers' interaction with bulk.

Hence, monolithic 12Ce-TZP shows more plasticity than the other samples, as expected for ceria stabilized zirconia [11]. For penetration depth achieved, around 3.2 micrometers for Ce-TZP28, coated discs seem to have an average behavior about plasticity. This behavior can be explained by low layers' thickness achieved, around 7 micrometers. 5Y-PSZ, in turn, shows a similar penetration when compared to 3Y-TZP, making difficult to correlate coating and bulk behavior.

Figure 24 - Maximum penetration depth achieved using a 2N load on uncoated 3Y-TZP, coating materials in the form of bulk discs (12Ce-TZP and 5Y-PSZ) and 3Y-TZP discs coated with 12Ce-TZP (Ce-TZP28) and 5Y-PSZ (Y-PSZ23).

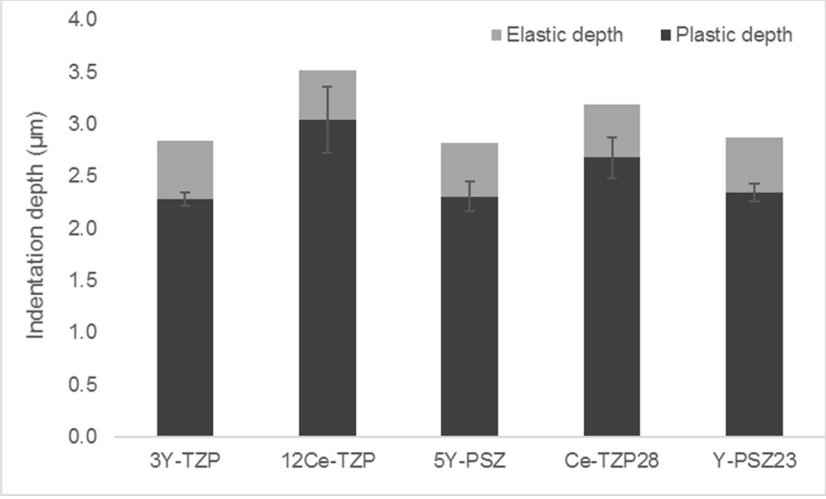

Because Young's modulus is a property ruled by chemical bonds, great variations were not expected, as can be seen in Figure 25, which shows the Young's modulus calculated from the experiment.

Figure 25 - Calculated Young's modulus of uncoated 3Y-TZP discs, coating materials in the form of bulk discs (12Ce-TZP and 5Y-PSZ) and 3Y-TZP discs coated with Ce-TZP (Ce-TZP28) and Y-PSZ (Y-PSZ23).

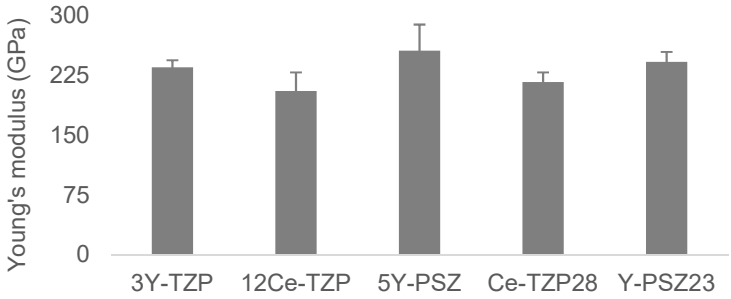

Another result obtained in this test was the hardness values, calculated by means of the penetration depth. As reported by other authors, 12Ce-TZP exhibits greater plasticity than 3Y-TZP [11]. Therefore, lower hardness values are expected to be obtained for this material as well as for samples coated with it, as can be observed in Figure 26. In addition to instrumented (Berkovich) indentation, Vickers micro-hardness was also measured by imprinting measurements, showing lower values along with lower results variability than the former.

Figure 26 - Berkovich (instrumented) and Vickers (imprint measument) micro-hardness values of uncoated 3Y-TZP discs, coating materials in the form of bulk discs (Ce-TZP and Y-PSZ) and 3Y-TZP discs coated with Ce-TZP (Ce-TZP28) and Y-PSZ (Y-PSZ23).

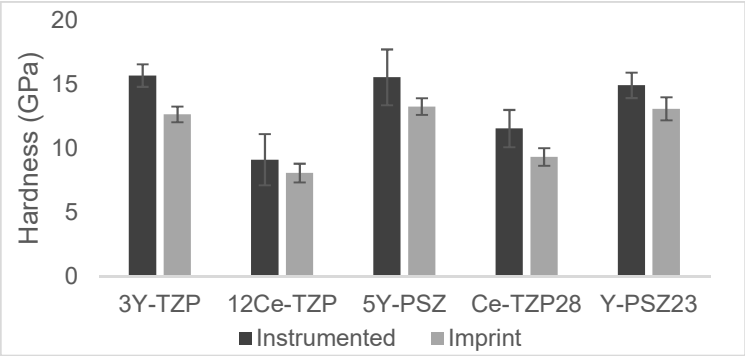

Due to the nature of this measurement, based on micro-plasticity, it is possible to observe a clear interaction between 12Ce-TZP coatings and 3Y-TZP bulk in samples formed by these materials. In fact, as observed before, for penetration depth achieved, around 3.2 μm, the stress fields created by the indentation overcome the 7 μm layers thickness, which makes that the hardness values obtained for these samples are influenced by the stiffness of the 3Y-TZP bulk material. Y-PSZ23, in turn, presented hardness values similar to those of the coating and bulk materials, 5Y-PSZ and 3Y-TZP, respectively. This is explained by the fact that both materials present similar Young's moduli and micro-plasticity.

5.4.4 - Ball on three balls flexure

In order to assess the influence of coatings on the mechanical properties of 3Y-TZP discs, ball on three balls tests were performed. As the objective of this work is to produce a reliable process easily applicable in industry, dip coated samples were tested "as coated", i.e. without polishing, revealing the resistance of components rather than of materials. Therefore, mechanical strength data is presented in two different statistical approaches, Weibull and Gaussian distribution, Table 7.

Table 7 - Mechanical properties of coated and control groups.

Sample	m	σ_0 (MPa)	Average (MPa)	S.D.
Polished 3Y-TZP	5.7	1602	1481	302
3Y-TZP	5.4	1154	1064	238
Y-PSZ23	8.5	726	685	89
Ce-TZP28	5.2	673	620	133

As observed in Table 7, coating process decreases flexural resistance of the samples. This behavior can be explained by surface defects, which affect mechanical properties of ceramics [111,113,114]. On the other hand, Weibull coefficient is similar for three conditions, revealing that defect distribution is also similar for polished 3Y-TZP, as sintered 3Y-TZP and as sintered Ce-TZP28. Y-PSZ23 samples displayed an increase in Weibull modulus, which might be related to a uniformity in pore size distribution created during the coating process relative to that occurred in the production of Ce-TZP28 discs.

Figure 27 shows a correlation between the flexural strength and the surface roughness of the specimens. The data of the polished 3Y-TZP specimens was also included in this graph.

Figure 27 - Relationship between flexural strength and roughness of coated samples and control groups.

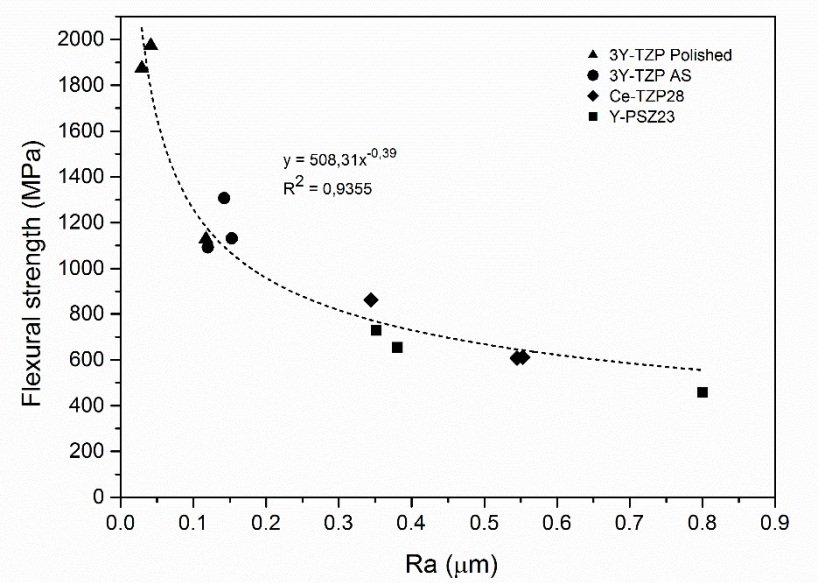

The result of Figure 27 shows that resistance of coated material is strongly dependent of roughness created during the process. This behavior is in accordance with monolithic ceramics in flexure, where a crack nucleates from a surface defect and grows to the bulk [115]. This mechanism is only observed for layered materials that have a strong bonding between layers and bulk, as showed in Figure 22, where no interlayers were observed. Otherwise, cracks start in surface defects and grows along the interface.

From the above results, it can be concluded that the flexural strength of the coated discs was not affected by the strength of the coating materials, as the thickness was low (~7um) compared to that of the 3Y-TZP bulk (1800um). This behavior is supported by the high correlation factor (R2=0,9) between the surface roughness and the fracture strength of the coated discs shown in Figure 27. The lower flexural strength exhibited by the coated discs were then caused by the flaws generated at the surface (pores, surface irregularities) during the dip coating process rather than coating the disc with a material of lower strength.

5.4.5 - Vickers indentations

The previous analyses have shown that the different base materials (3Y-TZP, 12Ce-TZP and 5Y-PSZ) presented different surface mechanical behaviors (hardness, plasticity). The surface mechanical properties of the coated specimens (Ce-TZP28 and Y-PSZ23) seems to be different from those of the coating materials, which seems to be affected by the mechanical properties of the bulk material (3Y-TZP). Hence, micro-indentation tests were performed to assess the influence of the load applied to the hardness measurements, as well as the relationship between surface damage resistance (SDR) and hardness for coated samples.

Figure 28 shows the Vickers hardness as a function of applied loads (2 to 60N) for uncoated and coated specimens.

Figure 28 - Vickers hardness as a function of applied loads.

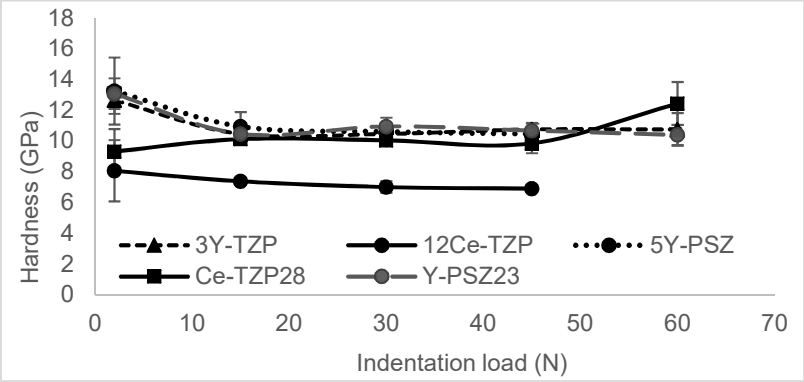

Because of the difference in first loads, 2N to 15N, hardness shows a deviation in values between samples in the same group. Regarding to coated samples, 2N, hardness measurement takes account both materials stiffness (coating and bulk). On the other hand, when higher loads are used, penetration depth increases in a way that is mainly the bulk material (3Y-TZP) hardness that is measured, as can be seem in Figure 28.

Hardness decreases for three samples, 3Y-TZP, 5Y-PSZ and Y-PSZ23, from 2N to 15N. This load influence on the measured hardness has been already reported elsewhere [116–118]. The difference in hardness behavior of Y- based to Ce- based zirconia, may be addressed to micro-plastic deformations, showed

in Figure 24, since Y-TZP and Y-PSZ have more elastic recovery when compared to the Ce-TZP.

Through the SEM images depicted in Figure 29, it is possible to observe that for 2N of load, only 5Y-PSZ surfaces showed micro-cracking. On the other hand, for higher loads (15, 30 and 45N) 3Y-TZP start also presenting crack formation as shown in Figure 31.

Figure 29 - Imprints of Vickers indentations using 2 N for uncoated materials a) 3Y-TZP, b) 12Ce-TZP, c) 5Y-PSZ and coated samples: d) Ce-TZP28 and e) Y-PSZ23

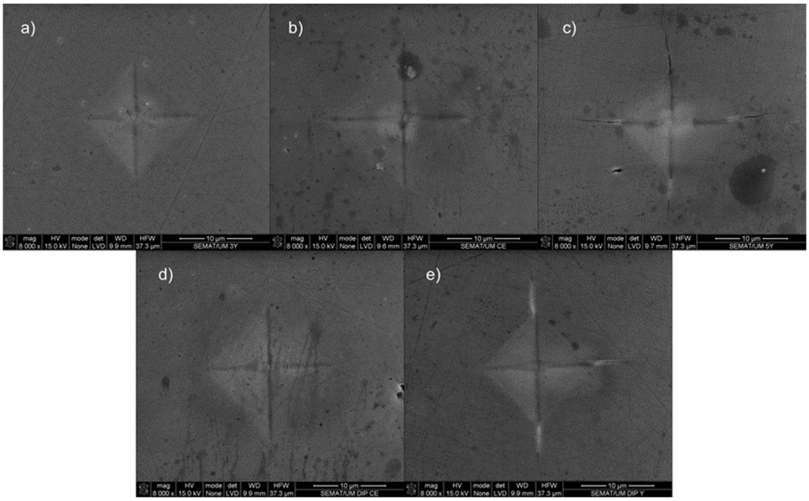

Based on this observation, authors suggest a standardization of zirconia hardness measurements, since this material have some resistance to crack propagation and because of crack presence, or absence, results can't be completely correlated. During this study was possible to observe that HV maintained a quite constant value after crack propagation, while the behavior for uncracked samples cannot be accessed. For this reason, we believe that a kind of R-curve should be plotted also for zirconia hardness, once comparison between cracked and uncracked materials could be inaccurate, as Petit [118] results suggest.

Even with the problems reported, it is possible to conclude that for Ce-TZP28 the load used in instrumented indentation, 2N, measured a combined hardness between coating and bulk, while loads above 15N measured mainly 3Y-TZP. The same rationale

cannot be applied to Y-PSZ23 coated samples, once materials have similar harness between each other.

Another important property evaluated for ceramics is the surface damage resistance (SDR). As this work is about coatings and a crack has more probability to start from the surface, the more resistant is the coating material to crack propagation the higher will be the damage tolerance of the component.

However, as already seen, biaxial flexure strength is lower for coated materials and it can be explained by the defects created during coating process. Moreover, 5Y-PSZ has lower flexural resistance and SDR when compared to 3Y-TZP. Because of that, surface damage resistance was analyzed for all base materials used in this work, as well as for coated samples, Figure 30.

Figure 30 - Surface damage resistance of the uncoated (3Y-TPZ and 5Y-PSZ) and coated (Y-PSZ23) samples as a function of Vickers indentation load.

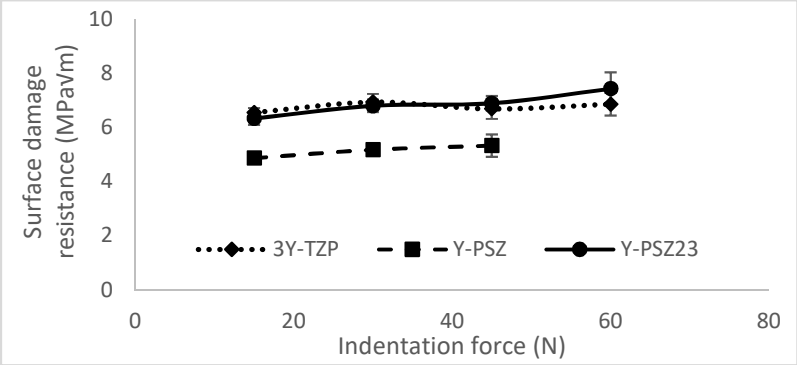

12Ce-TZP and Ce-TZP28 SDR values could not be obtained by the micro-indentation technique as no cracks were formed in the range of loads tested in this study. Vickers indentations using 100N were also tested, but all samples have broken in this condition. The observation made for the 12Ce-TZP specimens, which displayed a high damage tolerance (crack propagation resistance) but has lower flexural strength [16,88] highlights the importance of the manufacturing process in achieving high quality surfaces of coated products.

5Y-PSZ shows a lower SDR when compared to 3Y-TZP, as displayed in Figure 30 and further illustrated in Figure 31 where crack sizes can be compared. The behavior observed in Y-PSZ23,

also reinforces the hypothesis created for flexural resistance test, once coatings have less than 10 micrometers and cracks generated by indentations interacts with both materials (5Y-PSZ and 3Y-TZP), showing a trend to follow bulk SDR and, as a consequence, bending strength. These results show that layers are strongly bonded to each other, once cracks nucleate in the surface and as the load increases crack depth also increases, until the moment that stress field created in 3Y-TZP play a significant role to phase transformation and SDR enhancement.

Figure 31 - Cracking of indented samples in 15N: a) 3Y-TZP; b) 5Y-PSZ and c) Y-PSZ23.

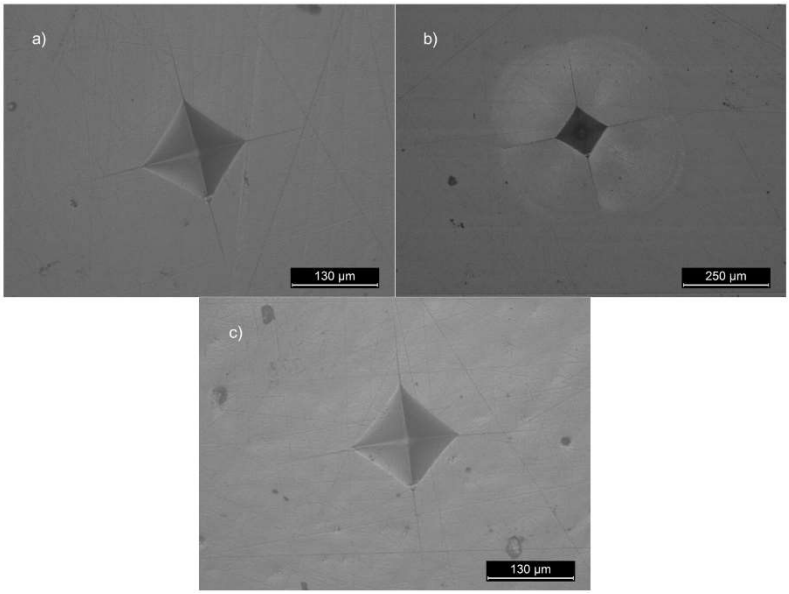

Using a semi-circle, starting at the impress and going to the crack tip, to represent the stress field around crack sublayers, and considering Palmqvist cracks ($0.25 < l/a < 2.5$) [119], a stress field of around 80 µm depth can be estimated for Y-PSZ23 samples. This is much deeper than the coating thickness (~7 µm), which explains why SDR follows 3Y-TZP bulk behavior instead of that of 5Y-PSZ.

Figure 31b shows a deformation field around indentation cracks. Deville [54], reported the same kind of deformation around indentations. In his work, this modification was addressed to phase

transformation and occurred due to a Young's modulus, hardness and load combination. However, as showed in the present work, 3Y-TZP and 5Y-PSZ exhibit similar behavior regarding elastic-plastic properties. The main difference between these materials is the resistance to crack propagation. Because of that, we believe that transformation observed is probably due to median crack formation, once the relation between crack length and indentation diagonal is much higher in 5Y-PSZ when compared to 3Y-TZP and Y-PSZ23 samples.

5.5 - CONCLUSIONS

The average roughness of coated samples (12Ce-TZP and Ce-TZP28) was higher than that of uncoated 3Y-TZP substrates, displaying similar values for both types of coatings and being caused by the dip coating process. Rsk values show more valleys than peaks for both coated samples, reinforcing that roughness increasing is due to pore formation.

Ce-TZP28 coated specimens showed load-dependent hardness and Young's modulus. For 2N, the behavior observed was between that of the 12Ce-TZP and that of the 3Y-TZP, while for 15 N, or higher loads, these properties seem to follow bulk material properties, 3Y-TZP.

Biaxial flexural strengths of coated samples, Ce-TZP28 and Y-PSZ23, were lower (>30%) than those of the uncoated 3Y-TZP specimens. This was attributed to the worse surface quality, traduced in higher coatings roughness.

A relationship between roughness and biaxial strength was found, showing that the surface quality resulting from the manufacturing process determines the final resistance of coated samples, and not the type of materials used for the coatings.

CHAPTER 6 - AGING BEHAVIOR OF LASER TEXTURED YTTRIA STABILIZED ZIRCONIA SURFACES

6.1 - ABSTRACT

In this work different 3Y-TZP surfaces were produced by Nd:YAG laser irradiation, aiming to study the influence of laser irradiation on aging behavior of this material. Molten-like microstructures were obtained, as well a color change on the laser textured samples. The increasing of 3Y-TZP aging resistance was observed for samples treated at 1200 ºC, after the laser texturization. Moreover, color changing was observed, by XPS, as a consequence of zirconium dioxide chemical reduction.

6.2 - INTRODUCTION

Since zirconia based materials are used to replace titanium alloys and other ceramics as a biomaterial, its mechanical properties and biocompatibility have been extensively investigated [5,17,57,94]. Although zirconia and titanium show similar biocompatibility and osseointegration, zirconium oxide bioinertness shields it from the attack of several fermentation systems of the organisms and also from oxidation, which avoids greater ion release, when compared to metals [57,58]. However, notwithstanding this great advantage, combining biocompatibility and mechanical properties, zirconium oxide is inert enough to have almost no interaction with the bio-media around it, leading to a poor chemical connection between these parts, mainly to bone [57].

As an alternative to overcome this, laser irradiation has been applied to the surface modification of zirconia, becoming highly beneficial to make it bioactive [120]. Laser irradiation can promote considerable changes in surfaces that can lead to improved osseointegration, cell-surface interactions and biological responses [121,122]. These processes have a significant role on the efficiency and lifetime of implants, becoming an important tool for biomedical engineering. The laser irradiation process, besides being versatile in modifying the surface of biomaterials, provides contamination-free surface, which may not be ensured by others techniques, for instance blasting and etching treatment [123]. Laser irradiation also offers higher control and precision when compared to these current applied treatments. The control on the surface characteristics can be achieved by changing lasers

operating parameters, including laser power, laser fluence, beam diameter, energy distribution, energy absorptivity of the treated surface and thermal properties of target [120,121,124,125].

Numerous studies have reported the use of laser treatments on zirconia surface and their consequences on some important properties of this ceramic, especially regarding to biomedical applications [20,65,126–128]. Yasuno et al. [123] studied zirconia implants whose surfaces were modified by fiber laser irradiation and verified that osseointegration was significantly enhanced. Roitero et al. [121] studied the effects of laser parameters on zirconia surfaces and verified that the roughness parameters are dependent on laser fluence and number of pulses. Yilbas [19], increased hydrophobicity using laser gas assisted ablation to create textures in zirconia samples.

No consensus is reached about all the effects of laser treatment on the surface properties of zirconia ceramics, since different results can be obtained according to the laser parameters. In laser treatment, different surface morphologies can be produced according to applied laser fluence in material surface, promoting local melting, vaporization or ablation processes. During laser ablation process, the surface exposure to high temperatures and high cooling rates, gives rise, in a small layer, to material losing of oxygen and, as a consequence, surface becomes dark [65,129,130]. This color change is an undesired modification regarding to aesthetical applications, but researchers demonstrated that is possible to recovery zirconia whiteness by providing temperature and oxygen to the material [65]. Moreover, thermal gradients are created, which may result in formation of residual stresses and cracks, which is harmful for ceramic materials, since they do not present enough plastic deformation, capable to inhibit crack propagation [21,131].

Despite exhibiting excellent mechanical properties, yttria stabilized zirconia exhibits a low-temperature degradation (LTD, or aging), which is a progressive phase transformation from tetragonal to monoclinic at the surface in the presence of water, without external mechanical stresses [5,30,132]. This phenomenon is quite well related to material features such as grain size, porosity and cracks. While cracks and large grains are able to increase LTD rate due to enhanced OH^- diffusion in material, the compressive stresses at the surface, caused by tetragonal to

monoclinic transformation, should decrease this phenomenon [17,54,133].

As already stated by Deville 2006 [54], thermal treatments performed at 1200 ºC are able to reduce residual stresses, both tensile and compressive. This result is in agreement with previous studies [134], where cracks and stresses created by Vickers indentation were suppressed using thermal treatment at this temperature. In the same study, other temperatures were evaluated aiming at stress relaxation, but this was only observed for temperatures above 800 ºC. Below 400 ºC, only tetragonal – monoclinic phase transformation happened, leading to compressive stresses that inhibit crack propagation. However, it is also known that aging proceeds more rapidly between 200 and 400 ºC [51,54] and, as reported in yttria-zirconia phase diagram, tetragonal field is located around 600 ºC.

In summary, heat treatments can be classified (when performed in air) in temperature ranges, as represented in Figure 32:

Figure 32 - Heat treatments temperatures and consequences.

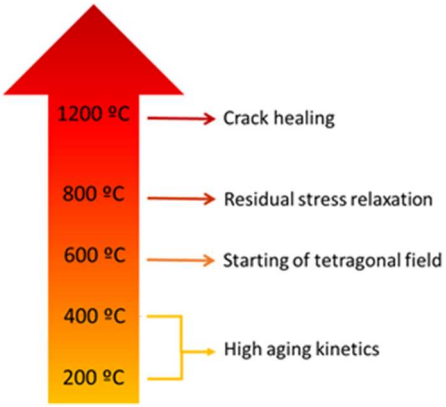

Using these thermal treatment data, it is possible to evaluate the influence of laser residual stresses on LTD.

Correlation between laser texturing, involving melting and ablation, and zirconia aging and heat treatments, as performed in this paper, has not yet been sufficiently explored by researchers. Additionally, color analysis was performed in order to evaluate lightness recovery of aged and thermal treated samples.

In this work, laser irradiation was used to modify zirconia based materials surface, aiming at evaluating aging response in terms of the resulting microstructures. Heat treatments were performed to promote residual stress relaxation and oxygen recovery of samples.

6.3 - MATERIALS AND METHODS

Disks with 14.5 mm diameter were manufactured using a commercial 3% mol yttria stabilized zirconia (TZ-3YB-E Tosoh, Japan). Samples were biaxially pressed under 200 MPa and sintered in air for 2h at 1500 ºC, with heating and cooling rates of 8 ºC/min, giving a grain size of 0.42 ± 0.031 μm (average intercept method). A total of 21 disks were prepared, with three samples for each tested condition.

A Nd:YAG laser (OEM Plus) with a fundamental wavelength of 1064 nm, 3 μm spot size and 6 W of power was employed to irradiate the surface of zirconia disks. Repetition rate and pulse duration were 20 KHz and 35 ns, respectively. In order to compare the effects of laser energy on zirconia surface modifications, two values of laser fluence were performed, according to laser power, being 10% of 6 watts, corresponding to 212.23 J/cm² and 20% of 6 watts corresponding to 424.45 J/cm². Feed rate used was 15.0 mm/s and samples were irradiated on the whole surface.

Roughness analysis was performed, three measurements per sample, using a contact profilometer (Mitutoyo SJ-210). For each condition of treatment three samples were measured. Usual parameters (Ra, Rt and Rq) were measured, besides Rsk.

Skewness, Rsk, describes the curve asymmetry in terms of frequency of valley and peaks along the surface profile, that is, an indicative of the proportion between the number of peaks and valleys. Zero values of skewness mean that peaks and valleys have the same proportion. For higher results, there are more peaks than valleys, while for values below zero, valleys are predominant [112].

Autoclave tests were performed following ISO 13356, in steam, at 134 ºC, under 2 bars pressure, for 2, 6 and 18h. Monoclinic content was measured by XRD technique, Copper K-α, with an incidence angle held in 2º, using Toraya modification of Garvie & Nicholson equation, considering the maximum intensities

of peaks [135,136]. For each condition three samples were measured.

To evaluate aging behavior, samples processed as described in Table 8 were then tested by XRD technique. As the aim of this work is to evaluate laser textured surface resistance to aging, small incidence angle was used, 1º, in order to have a small depth penetration [30].

Table 8 - Compilation of the experimental groups used in this study with the description and objectives of each thermal treatment undergone by the zirconia surfaces.

Sample name	**Description**	**Objective**
Sintered	Sample as sintered	Standard value of aging behavior. Control group.
L10	Laser texture in 0.6 W (424.45 J/cm²)	Verify the influence of laser irradiation on the aging behavior
L20	Laser texture in 1.2 W (848.90 J/cm²)	
T500L10	Thermal treatment in 500 ºC after laser treatment in 0.6 W (424.45 J/cm²)	Recovery of the material lighteness after laser irradiation (oxygen content recovered) without tetragonal recovery and stress relaxation after laser irradiation
T500L20	Thermal treatment in 500 ºC after laser treatment in 1.2 W (848.90 J/cm²)	
T1200L10	Thermal treatment in 1200 ºC after laser treatment in 0.6 W (424.45 J/cm²)	Recovery tetragonal phase, oxygen and stress relaxation after laser irradiation
T1200L20	Thermal treatment in 1200 ºC after laser treatment in 1.2 W (424.45 J/cm²)	

Each thermal treatment was performed in air, using heating rate of 5 ºC/min and during 1 hour at maximum temperature.

Lightness of specimens was measured using the CIE L*a*b* system without specular reflectance, once laser texturing creates rough surfaces, which changes completely material glossiness.

This measurement was used to verify oxygen recovery, assuming that white color is related to zirconium oxidation state.

In order to understand samples color changing, X-ray photoelectron spectroscopy (XPS) was performed. Spectra of as sintered and laser textured samples were analyzed to understand zirconium oxidation state for each condition, using a Kratos Axis-Supra instrument with Monochromatic X-ray source Al Kα (1486.6 eV).

6.4 - RESULTS AND DISCUSSIONS

6.4.1 - Microstructure

Comparing surfaces obtained with different laser fluence, samples produced with 424.45 J/cm² (20% of 6 W) resulted in deeper cavities and more defined grooves than the samples treated with lower laser fluence, 212.23 J/cm² (10% of 6 W), as observed in Figure 33.

Laser irradiation promotes superficial material removal due to local action of ablation, resulting in the formation of cavities/grooves, and melting of most of the superficial outmost layer of the material, being afterwards followed by solidification [20,137]. However, for samples tested at 10% of 6 W, the laser energy absorbed by zirconia surface was not enough to result in well-defined grooves as happened in samples where 20% of 6 W was used. The ablation and vaporization result in a loss of material, as measured by loss of sample weight. For example, L20 samples exhibited a measured weight loss of 6.06± 0.70 mg in an area of approximately 160 mm^2.

Figure 33 - Surface micrographs of the zirconia laser textured samples at powers of 0.6 W (a - d) and 1.2 W (e - h).

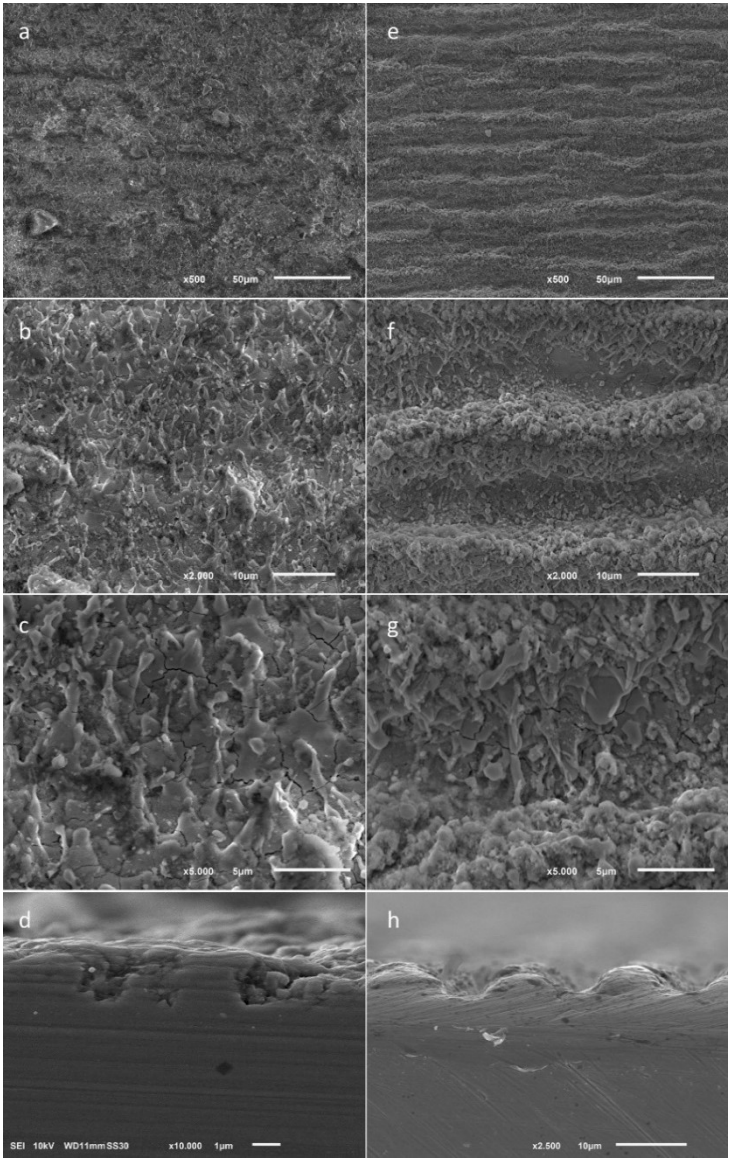

Micrographs also show a large quantity of small cracks formed in the laser treated area, for both samples. As already stated [125], in laser texture of ceramics, and mainly in a refractory material as zirconia, which presents very low thermal conductivity (~15 times lower than that of alumina) thus avoiding heat transfer, thermal gradients created during rapid cooling are able to develop high residual stresses, with creation of different contraction areas (strain), leading to thermal cracks formation.

However, as laser texturing only acts in few micrometers depth, cracks are shallow, as observed in Figure 33d-h, with no subsurface micrometric crack growth. The presence of surface shallow cracks only, seems to be interesting and anticipates a possible low detrimental effect of these cracks on mechanical properties. However, a detailed study of the effect of these textures in specimen's mechanical properties is necessary to validate the previous assumption.

6.4.2 - Roughness

Figure 33 and Table 9 show an increase of roughness parameters values (Ra, Rz and Rt) for higher laser fluence. The roughness data is in good agreement with the morphology of the surfaces depicted in Figure 33. The skewness data for 212.23 J/cm² revealed positive values, indicating that more peaks than valleys are present in the sample. On other hand, for 424.45 J/cm² the value becomes negative, showing a higher prevalence of valleys than peaks for this condition.

Roughness values achieved, allied to microstructures obtained, shows a potential application in terms of implant surface modification, once Ra values are in accordance with most popular techniques applied, specially sandblasting and acid etching[138–141].

Table 9 - Roughness values for different zirconia surface treatments.

Treatment	Ra (µm)	Rq (µm)	Rt (µm)	Rsk (µm)
L10	0.55 (±0.15)	0.70 (±0.18)	4.99 (±1.31)	0.11 (±0.12)
L20	1.25 (±0.12)	1.55 (±0.15)	10.30 (±2.28)	-0.15 (±0.33)
T500L20	1.20 (±0.16)	1.63 (±0.35)	11.22 (±3.30)	-0.26 (±0.70)
T1200L20	1.37 (±0.15)	1.71 (±0.21)	11.35 (±2.89)	-0.38 (±0.40)

Thermal treatments, in other hand, showed no appreciable influence in roughness parameters, as could eventually be expected due to stresses relaxation. In addition to roughness parameters, SEM images also show similar surface morphologies between thermal treated and untreated samples, Figure 34.

Figure 34 - Surface morphology of zirconia samples with different surface textures: L20 (a, d); T500L20 (b, e); and T1200L20 (c, f).

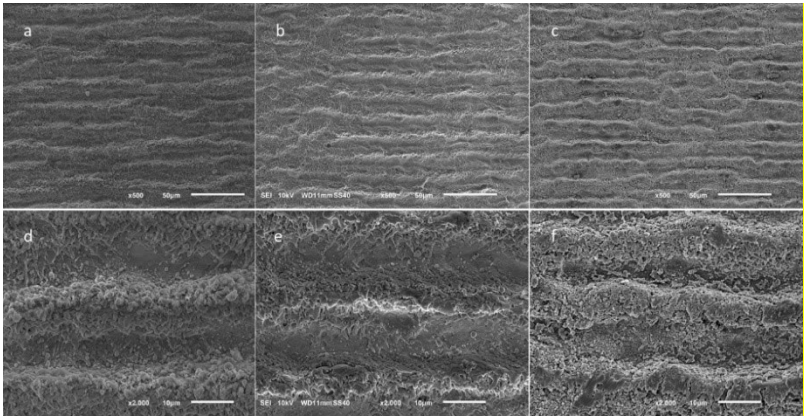

6.4.3 - Color

The very first feature observed after laser irradiation was a change in color of the samples, which became dark, as shown is Figure 35. The spectrophotometry analysis quantifies this darkness in the lightness axis. After heat treatments samples became white again, showing difference only in brightness, which can be explained by roughness, discussed before.

Figure 35 - Visual assessment of zirconia samples subjected to laser irradiation: L10 (a), L20 (b), as sintered (c), T500L10 (d), T500L20 (e), T1200L10 (f) and T1200L20 (g).

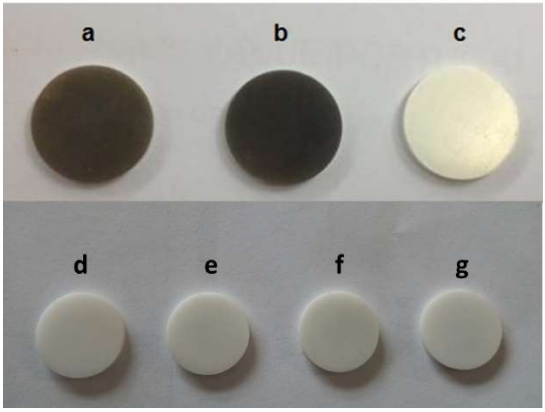

A qualitative assessment of oxygen recovery, after furnace treatments, was proposed using the lightness parameter (L*). Based on this, it is possible to see in Figure 36 that a furnace treatment at 500 ºC was able to restore the zirconia lightness of the initial color (as sintered condition), or, as supposed in this study and based on mechanisms proposed, to restore the oxygen levels in the material to the starting condition [65,142].

Thermal treatments performed at 1200 ºC have not further increased the lightness values relative to those obtained at 500 ºC that already matched the as sintered specimens.

Figure 36 - CIELAB lightness parameter obtained for the different zirconia surface treatments: as sintered (control group); Laser textured (L10 and L20); Laser textured (L10 and L20) followed by a thermal treatment of 500 ºC or 1200 ºC.

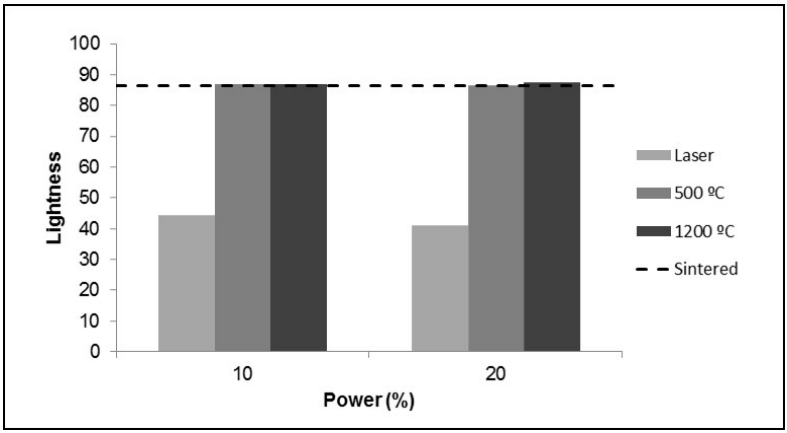

Considered, in this work, as a qualitative measurement of oxygen recovery, color changing was also observed during accelerated aging of laser-textured samples (L10 and L20), once aging promotes OH^- diffusion into zirconia and filling of oxygen vacancies [30]. The color coordinates are plotted in Figure 37 as a function of the aging time. Results show a variation of color coordinates with the aging treatment. Moreover, the color coordinates of the laser-textured samples (L10 and L20) tend to shift to the as sintered lightness values as the aging time increases. These results evidence the fact that zirconia can recover the missing oxygen at the surface under the steam aging conditions, therefore restoring, fully or partially, the original lightness of the material.

Figure 37 - CIELAB lightness coordinates of the as sintered and laser textured (L10 and L20) zirconia as a function of the aging time.

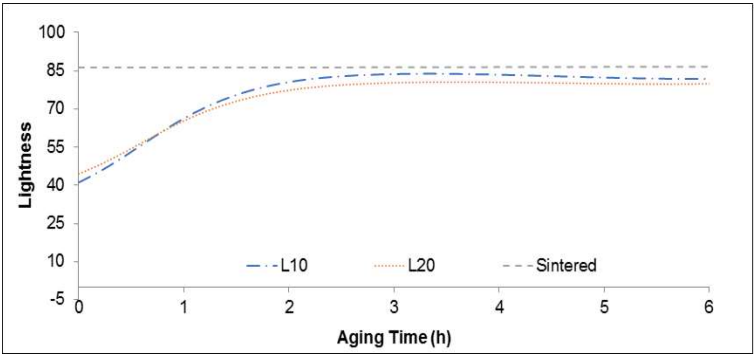

6.4.4 - XPS

Based on Sinhamahapatra [129] study, X-ray photoelectron spectroscopy was performed in order to verify the presence of zirconium sub-oxides ($Zr^{(4-X)+}$), Figure 38. Zirconia white sample, shows a well-defined spectrum, with two peaks in 182.1 and 184.5 eV, corresponding to 3d electrons of ZrO_2. Dark sample, laser textured, in turn, shows a spectrum composed by two more peaks, comparing to the previous, corresponding to zirconium sub-oxides.

Figure 38 - XPS analysis of as sintered (white) and laser textured (dark) ZrO_2.

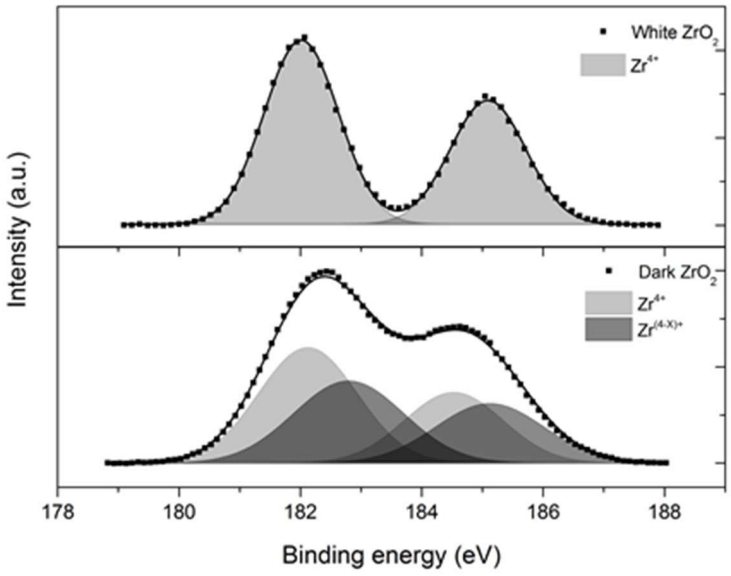

6.4.5 - Aging

As mentioned by Lughi and Sergo [33], grain size and residual stresses affect aging in a complex and linked way, being hard to separate the effects of each other. However, there is consensus about both separately: Small grain sizes decrease Low Temperature Degradation (LTD) kinetics [14], whereas tensile stresses induce the opposite.

In fact, as shown in Figure 39, melting promoted by laser irradiation can recrystallize zirconia, reducing grain size, mean size of about 300 nm (as sintered grain size = 420 nm), which is close to critical size as observed experimentally by researchers (~300 nm) [33].

Figure 39 - Micrograph showing the zirconia grains after the laser irradiation.

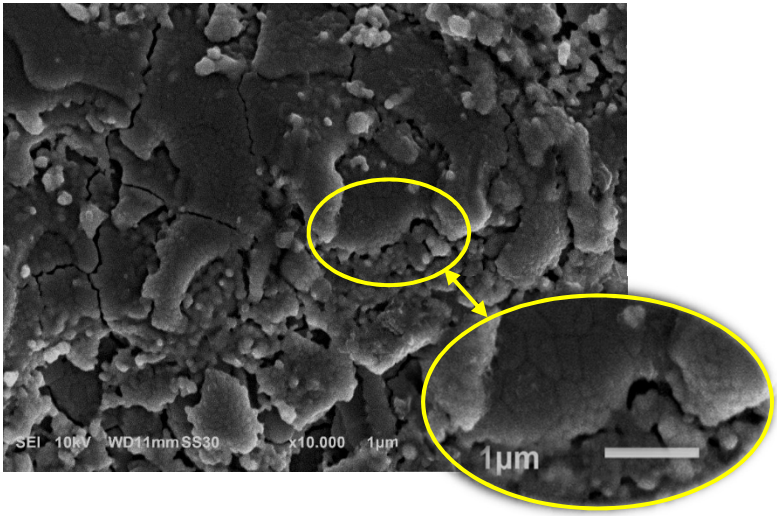

Together with the beneficial changes promoted on the zirconia surface, regarding grain size, laser irradiation also brings undesired microcracks (Figure 39), associated with tensile fields, thus decreasing the LTD resistance [133]. Thermal treatments performed at 500 ºC are able to recovery oxygen, as shown before by color changes, but are not able to release residual tensile stresses, which are responsible for keeping high aging kinetics, as depicted in Figure 40. This figure shows a high presence of monoclinic phase, after 2 hours of aging treatment, in the laser textured zirconia samples and also in the laser textured samples subjected to a thermal treatment at 500°C. In fact, the reduction of oxygen amount does not play a significant role during LTD behavior, once degradation seen for laser textured samples subjected to TT at 500°C (T500L10 and T500L20) that has recovered the oxygen levels, was the same as observed for samples without heat treatment.

Figure 40 - Aging kinetics given by the monoclinic phase content (%) plotted as a function of the aging time for zirconia samples with different surface treatments.

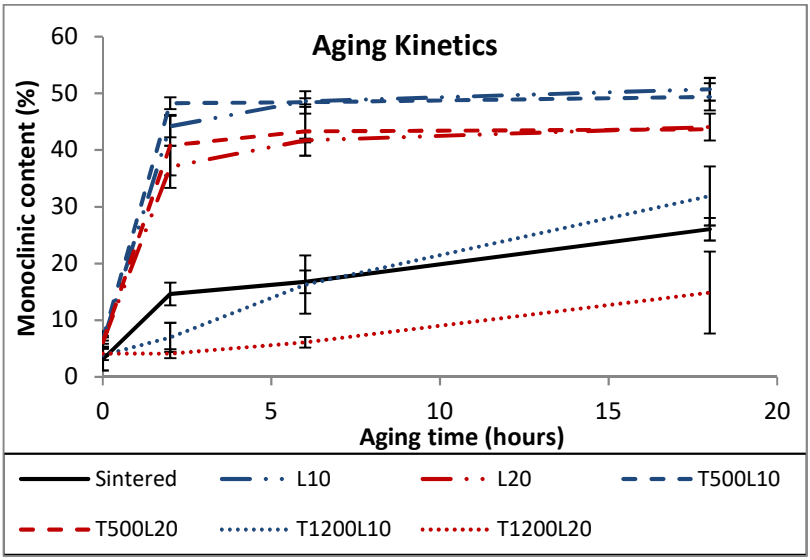

On the other hand, samples treated at 1200 ºC have been able to recover oxygen, relax residual stresses, as reported by Chevalier [134], while keeping low grain size. The combination of these mechanisms leads to enhance aging resistance of these samples as compared to the samples subjected to the other laser and thermal treatments.

The aging kinetics of samples thermal treated at 1200 ºC show a different behavior as compared to the as sintered ones. Additionally, the laser fluence also seemed to influence differently the samples heat-treated at 1200°C. Hence, among these samples, T1200L20 sample is the condition that yields the best aging resistance along the time, followed by the sample T1200L10 and finally the as sintered sample. Such behavior can be explained as follows: in the beginning of the aging process, finest grains should decrease the transformation ratio, while in the final stage of the process, cracks and superficial area could enhance martensitic changing, giving more area and atomics defects (crack tips). Results also highlight the beneficial effects of coupling higher laser fluence in laser with a heat treatment at high temperature (1200°C) in the aging behavior of zirconia.

In fact, as described by Chevalier [7] and Lughi [33], zirconia low temperature degradation is a thermodynamic phenomenon that exhibit a nucleation and growth behavior. Finer grains and absence of residual stresses leads to a changing in OH^- diffusion speeds on zirconia. However, grains are not small enough to stop nucleation process and after process starts there are more area to create first monoclinic points. In the end, growth process has more nuclei to follow, causing bigger transformed area and microcracks. Combining microcracks caused by martensitic transformation with thermal stress released cracks, tensile field is enhanced, giving more condition to LTD.

The influence of different laser fluence (212.23 J/cm² and 424.45 J/cm²) on the aging behavior, can be addressed to the heat input of the samples, once as high the energy employed, the heated area will be also bigger, decreasing the cooling rates during the process, which in turn decreases thermal gradients formed and, consequently, the residual stresses and cracks. As previously discussed, the presence of residual stresses and cracks are particularly relevant as they offer more superficial area for oxygen diffusion, thus increasing the undesirable LTD activity.

6.5 - CONCLUSIONS

This study aimed at evaluation the influence of different laser surface textures on the morphology, color and aging behavior of yttria tetragonal zirconia policrystals. The following conclusions can be drawn:

Different laser fluences resulted in melt surfaces with recrystallized grains having smaller grain sizes than the as sintered zirconia samples.

Structures produced by laser fluence of 212.23 J/cm² show a smoother surface when compared to samples obtained by 424.45 J/cm². The latter samples presented marked grooves with increased Ra and Rsk values.

Heat treatments performed at 500ºC were able to restore the lightness of samples (in lightness, yellowness and greenness), which is assumed to be related to oxidation state of zirconia, meaning oxygen recovery. Treatments performed at 1200 ºC increased the lightness of zirconia. Changes were seen in yellow and green axis but no changes were registered in the lightness.

Aging behavior was improved with a heat treatment at 1200 ºC, once stresses created by laser irradiating were relaxed and mean grain size of zirconia was kept low, when compared to as sintered samples.

Laser textured samples heat treated at 500 ºC showed an increase of LTD kinetics, mostly because of cracks and residual stresses developed during fast cooling of the zirconia melt. The lack of oxygen on the laser textured zirconia surfaces does not seem to play a role in aging behavior, once samples treated at 500 ºC have recovered the missing oxygen and still showed poor aging resistance.

Summarizing the influence of each competing mechanism, namely grain size and residual tensile stresses, it is possible to conclude that the presence of residual tensile stresses seems to be more critical than grain size and the lack of oxygen at zirconia surface during aging. For this reason, heat treatments must be used in laser textured zirconia structures in order to decrease/relief the thermal residual stresses.

CHAPTER 7 - MECHANICAL PROPERTIES OF LASER TEXTURED TETRAGONAL ZIRCONIA POLYCRYSTALS

7.1 - ABSTRACT

A Nd:Yag laser was used to produce three different texture patterns in 3Y-TZP sintered discs. Some of these discs were subsequently submitted to thermal treatments at 500 ºC and 1200 ºC, in order to evaluate the influence of laser and thermal treatments on the mechanical properties of the samples. Monoclinic content in the material surface is affected by laser irradiation. The tetragonal structure is recovered through thermal treatments at 1200 ºC, enhancing the bending resistance of textured 3Y-TZP. Treatments at 500 ºC increase monoclinic content, increasing also the flexural resistance of the samples when compared to higher temperature treatment.

7.2 - INTRODUCTION

Zirconia is widely used as a biomaterial due to its combination of biocompatibility and high flexural strength (> 1GPa) [6,47]. In terms of osseointegration and biocompatibility, several studies have shown that zirconia implants exhibit comparable results to titanium implants [57,58]. Furthermore, zirconia have shown enhanced features over titanium, such as high affinity to bone tissue, aesthetical and non-carcinogenic properties [54,143]. When compared to alumina, zirconia grain has been shown to serve as a nucleation site for the development of calcium-based minerals, which is particularly important for implant material design, thus making zirconia a good choice in many implants applications [143].

Even with calcium affinity, zirconia-based ceramics have still a poor chemical connection with bone, being chemically inert when introduced in human body [144]. To enhance zirconia surface properties, several surface modification techniques have been studied, as sand blasting, acid etching and laser pattering [145]. The purpose of surface modification is to enhance biological performance without compromising material bulk properties. In the surface properties are included the surface energy, the surface charge, wettability as well as the surface topography [146]. The conventional approach for titanium, named SLA, is performed by a

sandblasting followed by an acid-etching treatment, which is considered to be the gold standard surface treatment for bone growth [61]. However, recent studies have shown that laser surface treatment enhances osseointegration by increasing the hardness, corrosion resistance and surface properties, without bulk material contamination [147].

In order to enhance mechanical properties and tetragonal phase stability, zirconia grains should be smaller as possible [14]. In this way, laser treatments seem to be a good alternative, since they are able to melt a thin layer of the material, promoting a surface recrystallization in zirconia [121]. However, cracks are also formed and process parameters should be precisely controlled to avoid excessive mechanical losses [149].

Cotič [150] reported the influence on mechanical properties of sandblasting treatment, showing an increase in flexural strength for treated samples. Other researchers have performed laser treatments in zirconia-based materials, aiming to improve biological response [20,123,151]. However, damages created by laser irradiation on zirconia surface, were not evaluated in these studies.

Although several authors have suggested that laser treatments could be used to improve the surface properties of zirconia, the fact is that thermal gradients created during the laser treatment can damage the surface, thus affecting the mechanical strength.

Furthermore, it must be noticed that few studies are available on the use of Nd:YAG laser to treat zirconia surfaces and there is no consensus on the best processing parameters to use, which underlines the need for complementary studies [20,152]. The challenge still needing an appropriate answer lies on how to produce laser modifications on zirconia surfaces without significantly compromising the mechanical properties.

In this study, 3Y-TZP surfaces were modified by laser and SLA treatments in order to evaluate the influence of each processing condition on the mechanical properties. Moreover, surfaces were also evaluated in terms of energy to a better understanding of chemical modifications arising from the applied processes.

7.3 - MATERIALS AND METHODS

7.3.1 - Samples fabrication

Discs with 1.8 mm of thickness were fabricated, by double action pressing, using tetragonal zirconia polycrystals commercial powder (TZ-3YSB-E, Tosoh, Japan) in a stainless-steel die (Ø18 mm) under 200 MPa of pressure. After pressing, samples were subsequently sintered in air, at 1500 ºC for 2h using a heating rate of 8 ºC/min. Sintered zirconia samples are hereafter referred as 3Y-TZP, Table 10.

Laser patterning was performed in sintered samples, using different processing approaches, to obtain three different textures. In this step, a Nd:YAG laser (OEM Plus) with 1064 nm of wavelength, 3 µm spot size and 6 W of power was employed to irradiate the surface of zirconia discs. The repetition rate and pulse duration were 20 kHz and 35 ns, respectively. In the first approach (LI), a laser fluence of 212.2 J/cm2 was used to scan the whole sample surface using a scan velocity of 50 mm/s, in which two scans in the same direction were performed. In the second approach (LII), 254.7 J/cm2 of laser fluence, a scan velocity of 50 mm/s and four scan of laser beam were used on the surface. The third approach (LIII), a laser fluence of 424.5 J/cm2 was used with a scan velocity of 15 mm/s and one scan on the surface.

In order to evaluate the influence of thermal stresses in laser textured samples, ten discs of each condition were submitted to a thermal treatment in a furnace, in air, at 1200 ºC, for 1 hour, using a heating rate of 5 ºC/min for thermal stresses relaxation. In addition to this treatment, ten LII discs were thermal treated at 500 ºC, following the same conditions as the previous treatments. These two different temperatures were investigated due to different stresses relieves promoted by each one. Moreover, temperatures above 1200 ºC are able to recovery monoclinic transformed grains, while 500 ºC is not. The second temperature was chosen because of the possible benefits, in mechanical strength, to maintain a monoclinic compressive layer.

Considered the gold standard of zirconia surface treatment for adhesion purposes, the SLA treatment was also performed in sintered samples to serve as the control group. For blasting process, 100 µm alumina particles was used, in a constant pressure of 6 bar, at 10 mm from the blasting nozzle and with an

impact angle of 90° for 30s. Afterwards, the samples were immersed in hydrofluoric acid (48%) for 30 minutes at 20 ºC.

Table 10 - Coatings suspensions according to the material and solid content.

Sample name	Description	Objective
3Y-TZP	Sample as sintered	Material's mechanical properties standard value
LI	Laser texture with 212.2 J/cm²	Verify the influence of laser irradiation on zirconia mechanical properties
LII	Laser texture with 254.7 J/cm²	
LIII	Laser texture with 424.45 J/cm²	
SLA	Commercial surface modification using sand blasting followed by acid etching	Commercial treatment mechanical properties standard value
500LII	Thermal treatment at 500 ºC after laser treatment with 254.7 J/cm²	Recovery of the material oxygen content without tetragonal recovery and stress relaxation after laser irradiation
1200LI	Thermal treatment at 500 ºC after laser treatment with 212.2 J/cm²	Recovery of the tetragonal phase, oxygen content and stress relaxation after laser irradiation
1200LII	Thermal treatment at 1200 ºC after laser treatment with 254.7 J/cm²	
1200LIII	Thermal treatment at 1200 ºC after laser treatment with 424.45 J/cm²	

Figure 41 shows a schematic of samples processing steps.

Figure 41 – Fabrication of SLA, laser textured and thermal treated textured samples.

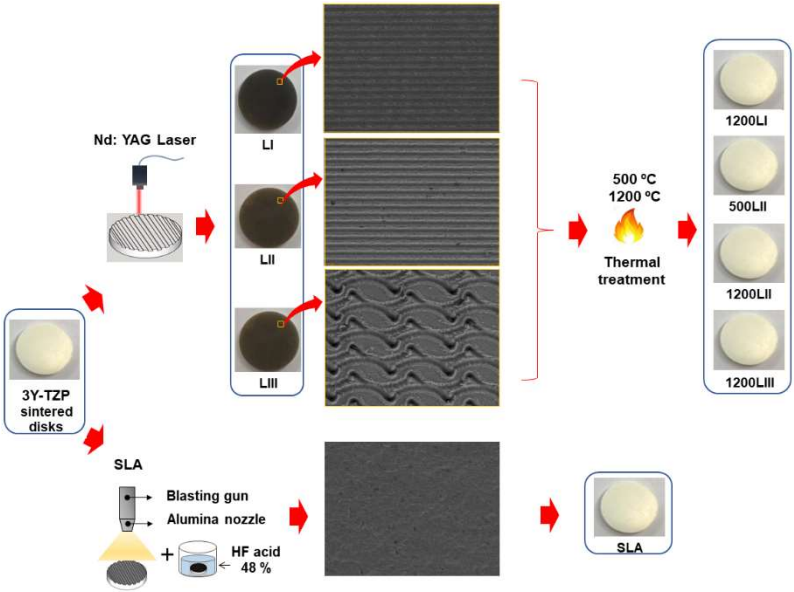

7.3.2 - Characterization

Roughness was measured using a contact profilometer (Mitutoyo SJ-210), three measurements per sample in three discs, resulting in nine measurements for each condition. Typical roughness parameters (Ra, Rt and Rq) were measured, besides Rsk and Rku. These two last parameters were plotted together, creating a chart called morphological space, which describes the nature of machining processes in terms of peaks and valleys relative quantities and shapes [112]. An example of surface feature in this kind of chart is showed in Figure 42.

Figure 42 - Surface appearance in a morphological space chart.

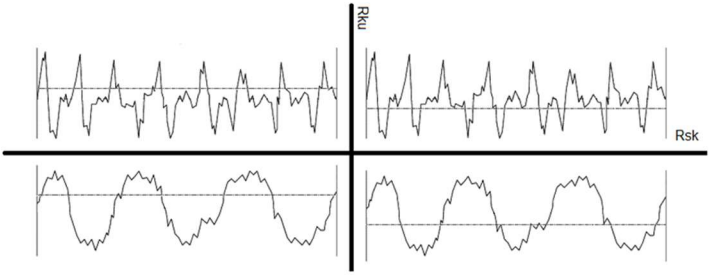

Surface stress level was qualitatively analyzed by instrumented indentation, using a Berkovich indenter, with 0.4 Newtons of maximum load and 30 as loading holding time.

Vickers hardness was also measured by means of indentation measurement method. Three samples of each condition (3Y-TZP, LI, LII, LIII, 1200LI, 1200LII, 1200LII, 500LI and SLA) were indented three times each, using loads of 15, 30 and 45 N and 30 s as the loading holding time.

Biaxial flexural tests were performed in a ball on three balls apparatus, with a Ø5 mm indenter, and a load rate of 0.1 mm/s. Ten samples of each condition (polished and unpolished 3Y-TZP, LI, LII, LIII, 1200LI, 1200LII, 1200LII, 500LI and SLA) were tested.

Wettability tests were performed in a goniometer (Dataphysics, OCA 15 plus) using distilled water and glycerol, in order to obtain polar and dispersive measurements of surface energy for each sample. Five contact angle measurements were obtained for each sample. Conversion from contact angle to surface energy was made by plotting Owens-Wendt equation [153].

$$\sqrt{\gamma_{sv}^{D}} + \sqrt{\gamma_{sv}^{P}}\sqrt{\frac{\gamma_{lv}^{P}}{\gamma_{lv}^{D}}} = \frac{\gamma_{lv}(1+cos\theta)}{2\sqrt{\gamma_{lv}^{D}}} \quad (7)$$

where, γ_{sv} is the dispersive energy of solid-vapor (air), γ_{lv} the energy of liquid-vapor and θ is the contact angle. The subscribed indexes, P or D, are related to polar or dispersive component of surface energy.

7.4 - RESULTS AND DISCUSSION

7.4.1 - Roughness

This work aims to develop study and develop zirconia surfaces with enhanced osseointegration properties and adequate mechanical strength. In this sense, roughness is one of the most important features to be evaluated as mechanical resistance has been demonstrated to be negatively affected when roughness increases. However, as laser causes thermal stresses and phase transformation, the relationship between roughness and strength may follow a different pattern.

Using different approaches, described in materials and methods, it was possible to create different textures as depicted in Figure 43, where is possible to observe surface roughness derived from zirconia solidification after laser irradiation, also reported in previous studies. In this figure, the difference between laser patterning and SLA treatments is clear, since in the former case it is possible to design the surface, while in the second the surface is composed by a randomly distributed roughness.

The differences observed between LI and LII treatments cannot be identified in the analyses of SEM micrographs. However, roughness measurements displayed in Table 11, show an increase in average roughness values of LII specimens arising from valleys formation, i.e. Rsk decrease. This behavior is somehow expected once from LI to LII, laser fluence and number of scans were increased. LIII design follows the same trend, once laser fluence was also increased and scanning configuration creates holes in the samples, instead of scratch-only surfaces, as happened in LI and LII groups.

SLA in turn, doesn’t show a clear trend to create valleys or peaks, as can be evaluated in Rsk values of Table 11. Instead, the random nature of the process seems to create a homogeneous surface.

Table 11 - Roughness parameters after surfaces treatments.

		Ra	Rq	Rz	Rsk	Rku
LI	Mean	2.04	2.28	8.65	0.09	2.14
	SD	0.54	0.63	2.23	0.28	1.37
LII	Mean	3.25	3.67	13.08	-0.26	1.70
	SD	0.65	0.75	2.36	0.10	0.07
LIII	Mean	3.89	5.10	26.49	-0.63	3.55
	SD	0.89	1.10	5.91	0.39	0.79
SLA	Mean	1.22	1.48	7.48	-0.01	2.72
	SD	0.13	0.15	0.69	0.14	0.18

Figure 43 - Surface appearance of laser textured samples and SLA in 500x and 4000x of magnification: A) LI, B) LII, C) LIII and D) SLA.

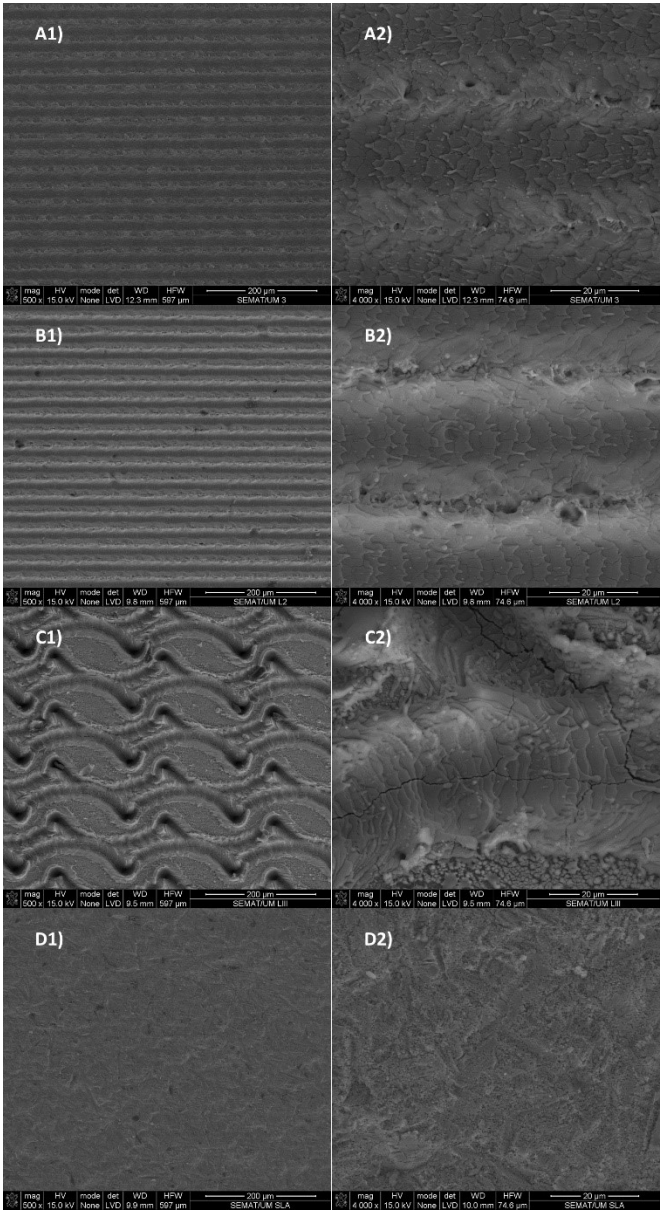

By plotting Rku x Rsk, the machining process is better described. As showed in Figure 42, as higher is the Rku number, the thinner will be the asperities and as lower is the Rsk, more valleys will be formed instead of peeks. Figure 44 shows this relation, and textures obtained for each process used.

For LI and LII, Rku<3, distribution is called patykurtoic and surface is composed by few high peaks and low valleys. SLA and LIII show Rku values close or higher than 3, having a leptokurtoic distribution, where the presence of more deep valleys are observed comparing to LI and LII [154]. Rsk shows a trend in the samples to have more valleys than peaks, except LI, which has the opposite behavior.

Summarizing, it is possible to conclude that LII creates a surface composed mainly by few low (and thick) valleys. LI texturing is formed mainly by few high (and thick) peaks. SLA, in turn, has a weak predominance of valleys instead of peaks, while the thickness of valleys is lower than those observed in laser treated samples. LIII shows a more defined behavior, with a clear predominance of thinner valleys.

The position in negative quadrant of skewness (Rsk) is observed in processes as honing, polishing and grinding, which are processes where peaks are removed instead of valleys filling [112]. However, the current laser processes are more characterized by valleys creation, since ablation creates scratches in the material.

Figure 44 - Morphological space (Rku x Rsk) of modified surfaces.

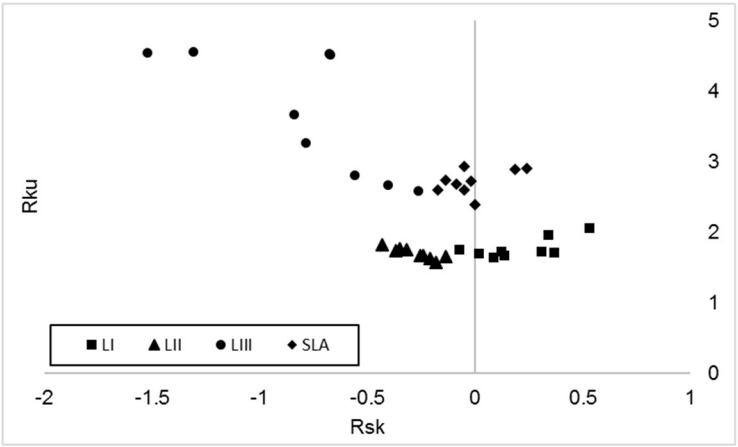

7.4.2 - Wettability

As reported by researchers, laser treatments may make zirconia dark [65]. The cause of this behavior has been shown to be a zirconium dioxide reduction. Because of that, wettability was tested, since surface chemical changes can be related to free surface energy alterations, leading to a complete changing in this behavior. Moreover, roughness is also related to wettability changes [148]. Based on these two parameters (roughness and chemical modification), tests were performed considering that after furnace treatments, surface chemical composition return to the former state (ZrO_2), being thus possible to compare the effects of roughness and chemical modification separately. Figure 45 shows contact angles for water and glycerol measured for all treated surfaces.

These results show that laser treated samples seem to be more hydrophobic than thermal treated ones. In other words, thermal treatments decrease contact angle, which means that chemical changes performed, in this work, by laser treatments increased the hydrophobicity. Moreover, these chemical changes seem to play a more significant role than roughness, once laser textured-only samples shows similar water-contact behaviors.

For glycerol contact angles, the behaviors show an opposite trend, with values increasing for thermal treated textured samples. One exception, however, is seen for 500LII, which has an apparent decrease in contact angle comparing to no thermal treated sample.

Figure 45 - Contact angles measured in different medias to calculate surface energies.

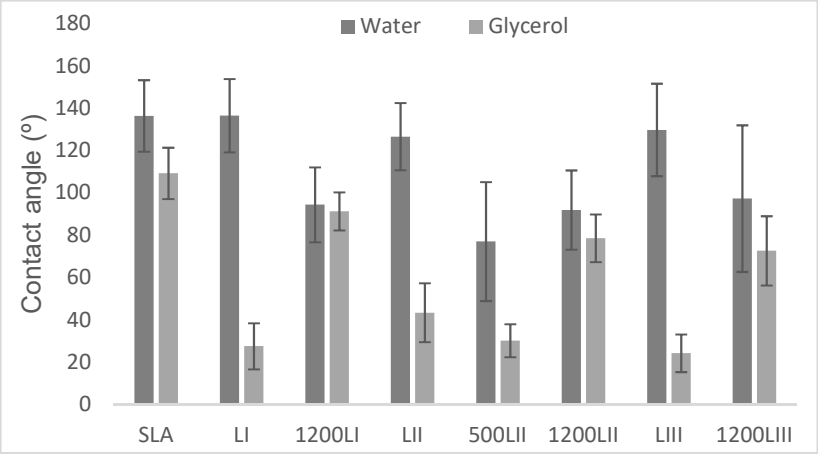

Although chemical featuring seems to be more important than roughness, it is possible to say that all thermal treated samples decrease hydrophobicity when compared to SLA. The same trend is observed for glycerol contact angles. In this sense, XPS results, Figure 38, provide evidences that zircon suboxides are created during laser ablation process. This kind of modification changes the surfaces' free energy, which is responsible for the wettability. The relationship between chemical modifications and texturization in hydrophilicity is reported by Noro [155], which shows that surface physiochemistry plays a more significant role than topography. In addition, his work also highlights the benefit of SLA treatment in the hydrophilicity enhancement.

The wettability behavior of some oxides (ZnO, TiO_2, SnO_2) can be affected by oxygen vacancies creation [156,157]. During this phenomenon hydroxyl groups fill the vacancies, increasing surface hydrophilicity. This phenomenon is based on the oxides reduction, as suggested in the present work and showed by XPS.

As the surface energy of these liquids has different polar and dispersive components, surface energy was calculated, dividing each component, Table 12.

Table 12 - Surface energy of samples.

Treatment	γ_{sl}	γ_{sl}^{D}	γ_{sl}^{P}
SLA	64.6	47.7	16.9
LI	1120.0	710.9	409.8
1200LI	15.6	6.7	8.8
LII	745.0	492.6	252.3
500LII	172.8	160.0	12.8
1200LII	31.6	31.0	0.6
LIII	1032.2	667.5	364.7
1200LIII	77.4	72.8	4.7

Thermal treatment decreases the total surface energy of laser treated samples. SLA, in turn, shows higher values of surface energy when compared to thermal treated samples, except for the case of 1200LIII samples, which shows similar values. Literature about correlation between this data and osseointegration is not clear and, apparently, roughness plays a more significant role in comparison to surface energy [155,158,159]. These results show that is possible to change the wettability of zirconia surfaces by using laser treatments to changing materials' roughness.

7.4.3 - XRD

Based on calculations found elsewhere [30], incident angle of 2 degrees corresponds to a depth analyses of less than 0.5 μm, while 35 degrees evaluates structures up 4 μm of thickness. Figure 46 compares monoclinic content for these two incident angles and shows that the modifications on zirconia structure promoted by both treatments (laser and SLA) were only visible at the outmost layer of the specimens.

Figure 46 - Monoclinic content in different penetration depth

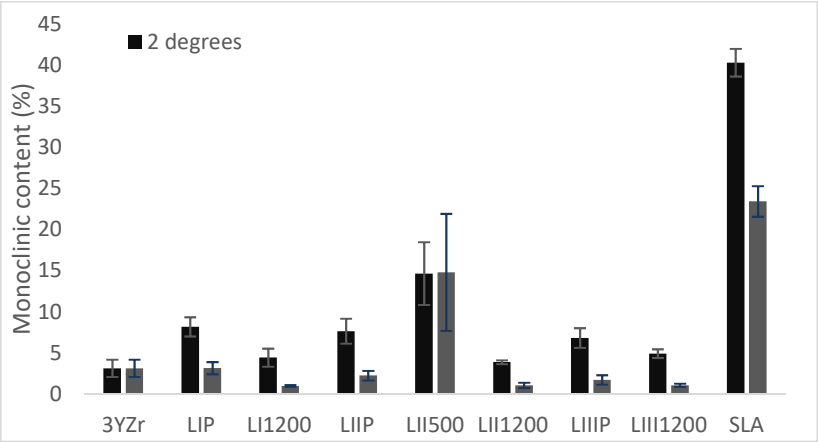

Despite of laser high residual stresses generated from fast material's heating and cooling during laser texturing, SLA samples show high content of monoclinic phase when compared to all laser processed samples. Monoclinic transformations, due to thermal and mechanical stresses, can be deleterious to mechanical properties, depending on cracks nucleation occurrences, i.e. whether tensile stresses are formed in the material for the selected parameters of a specific process [124]. Moreover, blasted surfaces seems to exhibit a more deleterious behavior in aging conditions [150].

Thermal treatments at 1200 ºC, performed after laser texturing, successfully decreased monoclinic content in all samples. However, samples treated at 500 ºC did not produce the same effect, once this temperature increases martensitic transformation depth and monoclinic content.

All laser treated samples revealed similar surface monoclinic content. However, considering a larger depth, 25-35 degrees of X-Ray incidence, samples treated with lower laser fluence seem to have less tetragonal microstructure. This phenomenon, explained in detail elsewhere, is related to the amount of surface incident energy during laser treatment.

7.4.4 - Ball on three balls flexure

In order to measure the influence of surface modifications on the mechanical strength, ball on three balls tests were performed. The roughness is known to affect the ceramics flexural strength, once creates defects on the materials' surface. Because of that, zirconia was tested in two different conditions: polished and as sintered (3Y-TZP) [107]. Moreover, mechanical properties are presented in, Table 13.

Table 13 - Mechanical properties of coated and control groups.

	m	σ_0	Mean	SD
Polished 3Y-TZP	5.7	1602	1481	302
3Y-TZP	5.4	1154	1064	238
LI	8.5	981	926	126
1200LI	7.0	1112	1041	174
LII	5.5	885	818	176
500LII	6.8	1423	1330	225
1200LII	4.5	1267	1157	302
LIII	5.9	579	536	104
1200LIII	10.9	687	657	71
SLA	5.0	1612	1388	513

Flexural resistance results show the influence of surface roughness in the flexural strength. Both Weibull and Gaussian distributions confirm a decrease in the flexural strength of specimens with higher surface roughness, Figure 47. Weibull modulus, in other hand, increases when laser texturing was applied. This behavior is related to flexural resistance reducing, once the creation of larger superficial defects (texture) decreases material resistance. In other hand, the same flaws enhance the reliability of the material, since they are the bigger defects on the surface (Weibull theory).

Thermal treatment conducted at 1200 ºC has shown a positive effect on the improvement of the strength of laser-treated samples. It has been shown elsewhere that this temperature is enough to promote stresses relive [134]. Moreover, monoclinic

content also decreases, as showed in XRD results, and zirconia recovery the oxygen lost during laser process rapid cooling. The Weibull modulus obtained for thermal treated samples shows that thermal treatments conducted at 1200°C have resulted in samples with lower degree of reliability. This behavior can be explained by the stress relieve caused by heat treatments, which enhance flexural resistance and the randomity of maximum residual stresses (caused now by cracks, instead of thermal residual stresses), i.e. after heat treatments, stresses are all caused by crack tips. As LI and LII shows smaller cracks, is reasonable to expect such randomity in the mechanical strength. LIII, in other hand, shows larger cracks, Figure 43-C2, what explains why reliability is enhanced after heat treatments.

The monoclinic content found at the surface of heat treated samples at 500 ºC as well as in the SLA samples seem to enhance zirconia's resistance. In fact, this behavior has been already reported in literature [150] and it can be explained by a compressive layer formed at the surface due to martensitic transformation. Due to this monoclinic layer, Weibull modulus also increases, once compressive stresses are able to suppress residual stresses and crack opening.

Figure 47 - Relationship between flexural strength and roughness of ●: SLA, LI, LII and LIII; ◆: Polished 3Y-TZP and 3Y-TZP as sintered; ■: 500LII; ▲: 1200LI, 1200LII and 1200LIII

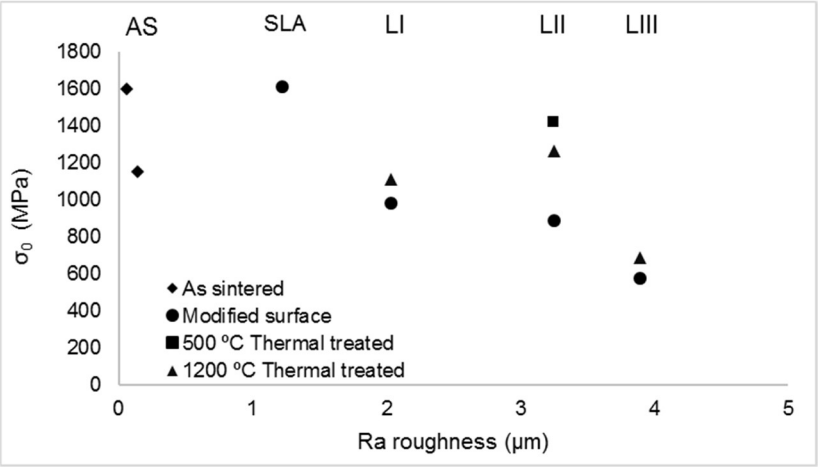

7.4.5 - Surface stress level

To perform a qualitative analysis of surface stress level, we considered that all surface modifications created stresses on the microstructures. In this sense, we admitted that the higher is the stress level developed, the lower will be the penetration depth of an indenter in the sample. Figure 48 was then plotted based on these assumptions.

Comparing SLA results with the remaining samples and crosslinking with B3B results, monoclinic content evaluation and the absence of cracks in microstructure, it is possible to conclude that the expected compressive layer was formed. Moreover, LI and LII show lower penetration depth when compared to all laser textured samples, which may be attributed to surface thermal residual stresses. LIII and 1200LIII samples show high standard deviation, probably because of the higher number of cracks formed on surface during laser treatment. Thermal treatments seem to produce the desired stress relief, once bigger penetration depths were obtained for all thermal treated samples.

Figure 48 - Penetration depth obtained by nanoindentation with 0.4N of load.

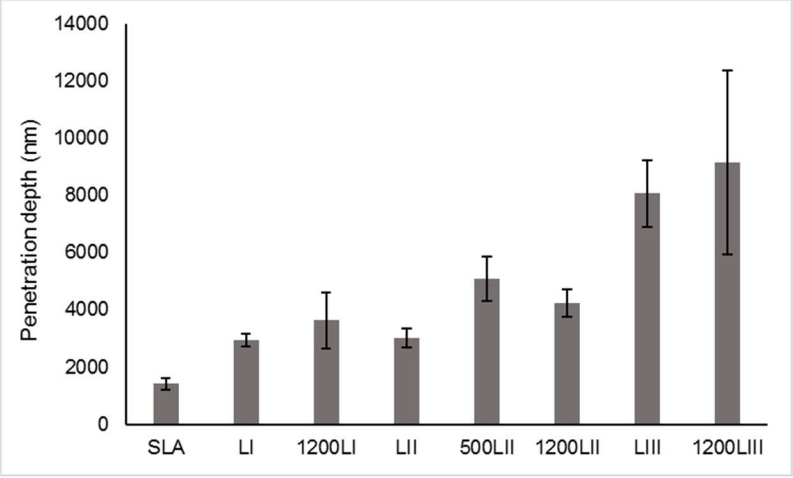

7.4.6 - Texture penetration resistance and crack behavior

In order to evaluate the deformability of textured surfaces, indentation tests were performed, Figure 49. As expected, more deformation is achieved for more textured surfaces. Due to this behavior, despite the procedure is the same as used in hardness test, the property measured was called texture penetration resistance, once the test measures texture deformability instead of material hardness.

Larger differences in hardness were observed for 15 N of normal load. This fact can be explained because of the gradual texture deformation, obtained according to compression induced by load increase. For 15 N, textures were not completely deformed, while for 30 and 45 N the textures assumed a solid behavior. This behavior explains why SLA samples showed the highest stiffness among samples evaluated.

Figure 49 – Texture penetration resistance for all surfaces evaluated.

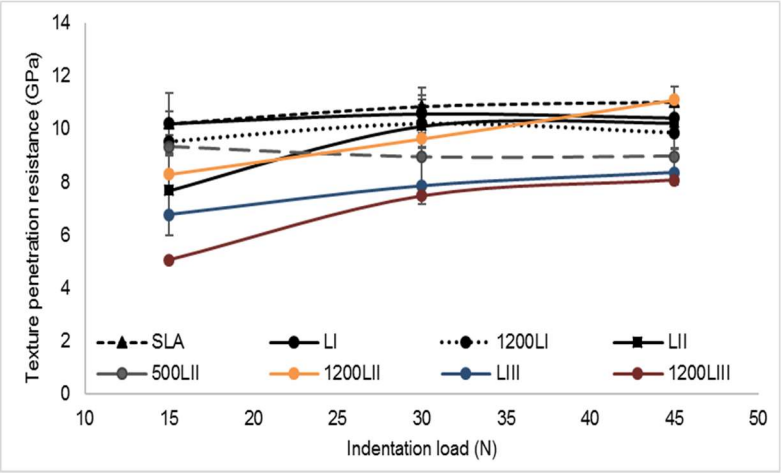

The cracks formed at the edges of indentations were also observed, and qualitatively analyzed, to compare propagation and possible toughening mechanisms in addition to the expected phase transformation (as microcrack shielding) Figure 50.

The presence of cracks was not correlated to any particular group and was considered a random event. It was also observed that crack propagation at the laser-textured surfaces was particularly restrained by the presence of surface asperities. In other zirconia crack reports [117,160], and Figure 50I and J, 3Y-

TZP shows a well-defined crack propagation, with flaws growing from each indent corner. Based on that, is possible to say that other toughening mechanisms were probably also active. SLA in turn, was able to avoid crack nucleation for loads of 15 and 30N. This behavior can be related to the absence of cracks at the monoclinic layer created during the surface modification (as opposed to the laser-textured samples). Notwithstanding, for 45N some samples showed extensive crack propagation, causing a massive microstructure transformation Figure 50G.

Figure 50 - Vickers indentations in 45 N of: A) LI, B) 1200LI, C) LII, D) 1200 LII, E) LIII, F) 1200LIII, G) SLA, H) 500LII and J) 3Y-TZP. Indentation I) was performed using 30 N.

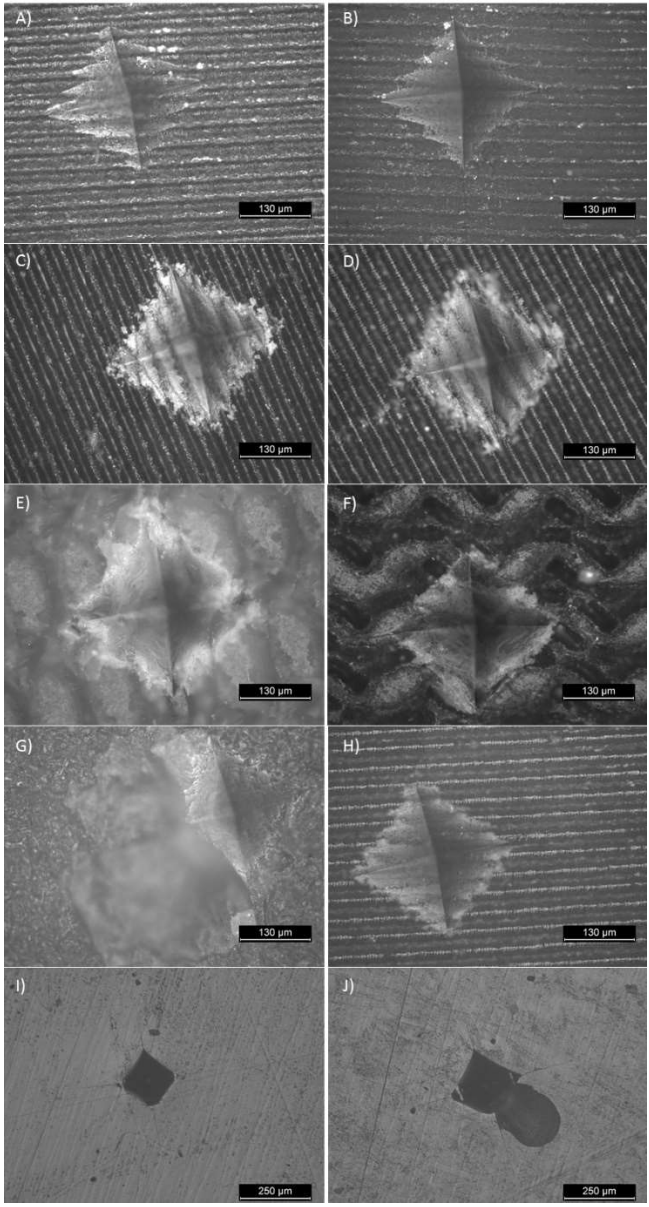

7.5 - CONCLUSIONS

All surface treatments, laser-texturing and SLA, produced an increase in roughness parameters, with the tendency to create more valleys than peaks being observed. The exception was the LI treatment, which creates more peaks instead of valleys.

Surface microcracking was observed in all laser-textured samples, whereas SLA samples did not exhibit such flaws. The surface cracking explained the lower flexural strength displayed by laser-textured samples as compared to the SLA and as-sintered zirconia samples. On the other hand, heat treatments seemed to contribute to the laser-textured samples flexural strength enhancement.

All surface modifications (laser-texturing and SLA) showed to increase the monoclinic content at the surface of zirconia samples, which can be reduced by adequate heat treatments. Moreover, laser textured (LI, LII and LIII) and heat-treated samples (1200LI, 500LII, 1200LII and 1200LIII) exhibited different hydrophobicity behaviors, meaning that laser texturing promotes surface modifications also at the chemical level.

Laser surface texturing produced a slight decrease in the surface hardness of zirconia samples, while SLA treatment showed to result in a quite constant hardness value. Notwithstanding, SLA treatment creates a surface compressive layer, which results in higher flexural strength of the SLA treated zirconia samples.

CHAPTER 8 - GENERAL CONCLUSIONS

- In the framework of this thesis, two different processing approaches were used to decrease 3 mol% yttria stabilized zirconia aging kinetics:
  - Dip coating
  - Laser
- Both processes used were able to accomplish the proposed task. However, each one due to distinct mechanisms and having different challenges.
- During dip coating treatments, surfaces were coated with aging resistant materials: 12 mol% ceria stabilized zirconia and 5 mol% yttria stabilized zirconia. From the point of view of aging avoiding and layer creation, parameters used during dip coating obtained successful results. Coatings seems to be uniform, thin (around 7 μm) and seems to have a good bonding with the bulk. Aging was not observed in accelerated tests until 18h in autoclave, which correspond to 36 years *in vivo*.
- Flexural strength shows a decrease regarding roughness produced during coating process. Using Weibull statistic, flexural resistance was found as 1154 MPa for as sintered samples, 726 MPa for 5Y-PSZ dip coated samples and 673 MPa for 12Ce-TZP dip coated samples. Flexural tests also showed that mechanical resistance is not strongly affected by the material used as coating, but by the surface quality obtained, i.e. roughness.
- During laser irradiation, a thin layer of bulk material was melted, followed by an abrupt solidification, causing recrystallization and grain size decrease. The thermal stress generated during this process, causes phase transformation and crack nucleation.
- Laser processing was followed by a thermal treatment, relieving stresses. After this, aging kinetic was decreased, since samples show recrystallized nanograins.
- As laser treatments promote crack nucleation, flexural resistance was expected to decrease. In this sense, thermal treatment was also investigated, showing a potential to decrease damages caused by laser irradiation. In the less severe approach, in terms of process parameters, the flexural strength of the samples was measured as 981 MPa, increasing to 1112 MPa after

thermal treatments at 1200 ºC. Medium process conditions showed 885 MPa of flexural strength after laser texturing, increasing to 1267 after thermal treatments at 1200 ºC. The most severe condition showed 579 MPa before thermal treatment and 687 MPa after.

- Zirconia blackening after laser treatment was caused by the creation of suboxides. These suboxides were demonstrated by XPS analysis. Moreover, samples wettability was different for black and white textured discs, evidencing a physical-chemical surface changing.
- In an overall view of this work, results can be classified as satisfactory, once all approaches used were able to decrease aging kinetics of 3 mol% yttria stabilized zirconia. Nevertheless, process must be further studied in terms of reliability and surface quality, aiming to increase flexural strength of the samples.

CHAPTER 9 - FUTURE WORKS

The findings of the research presented in this thesis open future perspective on several additional studies, among which can be mentioned:

- Improvement of dip coating parameters to obtain better surface features and flexural strength;
- Control of surface damage produced by laser treatment to increase materials' flexural strength;
- *In-vivo* behaviors assessment for dip coated and lased treated samples;
- Combination of both techniques used: dip coating and laser
- Laser treatment of different zirconia-based materials.

9.1 - FURTHER CONTRIBUTIONS OF THIS THESIS

In addition to the papers contained in this document, complementary and parallel studies and works were developed during doctoral period, as indicated in the following lists.

Papers

- ✓ C. G. Moura, R. S. F. Pereira, A. Lopes, M. Andritschky, J. P. Grilo, F. S. Silva, R. Nascimento. **Effects of laser fluence and liquid media on preparation of small Ag nanoparticles by laser ablation in liquid.** Optics & Laser Technology, 2017; 97: 20-28.
- ✓ C. G. Moura, R. S. F. Pereira, M. Buciumeanu, O. Carvalho, R. Nascimento, F. S. Silva. **Effect of Laser Surface Texturing on Primary Stability and Surface Properties of Zirconia Implants.** Ceramics International, 2017.

Conferences

- ✓ R. S. F. Pereira, C. G. Moura, F. S. Silva, B. Henriques, M. C. Fredel. **Zirconia aging behavior after surface laser treatment**. 15th European Inter-Regional Conference on Ceramics, 5-7 September 2016, Villeurbane, France.
- ✓ R. S. F. Pereira, C. G. Moura, F. S. Silva, B. Henriques, M. C. Fredel. **Protective dip coated layers to zirconia dental**

applications. 7º Congresso Nacional de Biomecânica, 10-11 February 2017, Guimarães, Portugal.

- ✓ C. G. Moura, R. S. F. Pereira, R. M. Nascimento, F. S. Silva. **Surface modification of zirconia by Nd:YAG laser irradiation.** 7º Congresso Nacional de Biomecânica, 10-11 February 2017, Guimarães, Portugal.
- ✓ R. S. F. Pereira, C. G. Moura, B. Henriques, F. S. Silva, M. C. Fredel. **Protective coatings to avoid zirconia aging behavior.** VIII International Symposium on Materials, 9-12 April 2017, Aveiro, Portugal.
- ✓ C. G. Moura, R. S. F. Pereira, R. M. Nascimento, F. S. Silva. **Influence of liquid medium and laser fluence on production of silver nanoparticles by pulsed laser ablation.** VIII International Symposium on Materials, 9-12 April 2017, Aveiro, Portugal.
- ✓ D. Faria, R. Pereira, G. Miranda, J. M. Guimarães, F. S. Silva. **Mechanical properties of zirconia with outer layer of zirconia-hydroxyapatite or zirconia-βTCP composites for biomedical applications.** VIII International Symposium on Materials, 9-12 April 2017, Aveiro, Portugal.
- ✓ R. S. F. Pereira, C. G. Moura, B. Henriques, F. S. Silva, M. C. Fredel. **Mechanical properties of aging resistant coated 3Y-TZP.** 15th Conference & Exhibition of the European Ceramic Society, 9-13 July 2017, Budapest, Hungary.
- ✓ C. G. Moura, M. Buciumeanu, R. S. F. Pereira, O. Carvalho, F. S. Silva, R. M. Nascimento. **Effect of zirconia surface treatment on friction coefficient and surface properties.** 15th Conference & Exhibition of the European Ceramic Society, 9-13 July 2017, Budapest, Hungary.

REFERENCES

[1] GARVIE, R. C.; HANNINK, R. H.; PASCOE, R. T. Ceramic steel? **Nature**, v. 258, p. 703–704, 1975.

[2] PEREIRA, G. K. R. et al. Comparison of different low-temperature aging protocols: Its effects on the mechanical behavior of Y-TZP ceramics. **Journal of the Mechanical Behavior of Biomedical Materials**, v. 60, p. 324–330, 2016.

[3] CAMPOSILVAN, E. et al. Enhanced reliability of yttria-stabilized zirconia for dental applications. **Acta Biomaterialia**, v. 17, p. 36–46, 2015.

[4] RIETH, P. H.; REED, J. S.; NAUMANN, A. W. Fabrication and flexural strength of ultra-fine grained yttria-stabilised zirconia. **American Ceramic Society Bulletin**, v. 55, n. 717, 1976.

[5] BASU, B. Toughening of yttria-stabilised tetragonal zirconia ceramics. **International Materials Reviews**, v. 50, n. 4, p. 239–256, 2005.

[6] PICONI, C.; MACCAURO, G. Zirconia as a ceramic biomaterial. **Biomaterials**, v. 20, p. 1–25, 1999.

[7] CHEVALIER, J.; CALES, B.; DROUIN, J. M. Low-temperature aging of Y-TZP ceramics. **Journal of the American Ceramic Society**, v. 82, n. 8, p. 2150–2154, 1999.

[8] DEVILLE, S. et al. A critical comparison of methods for the determination of the aging sensitivity in biomedical grade yttria-stabilized zirconia. **Journal of Biomedical Materials Research B**, v. 72, n. 2, p. 239–45, 2005.

[9] KOBAYASHI, K. KUWAJIMA, H. AND MASAKI, T. Phase change and mechanical properties of ZrO2-Y203 solide electrolyte after ageing. **Solid State Ionics**, v. 3, n. 4, p. 489–493, 1981.

[10] CHEVALIER, J.; OLAGNON, C.; FANTOZZI, G. Subcritical crack propagation in 3Y-TZP ceramics: static and cyclic fatigue. **Journal of American Ceramic Society**, v. 82, n. 11, p. 3129–3138, 1999.

[11] REVERON, H. et al. Towards long lasting zirconia-based composites for dental implants: transformation induced plasticity and its consequence on ceramic reliability. **Acta Biomaterialia**, v. 48, p. 423–432, 2017.

[12] LUCAS, T. J. et al. Effect of grain size on the monoclinic transformation, hardness, roughness, and modulus of aged partially stabilized zirconia. **Dental Materials**, v. 31, n. 12, p. 1487–1492, 2015.

[13] SANON, C. et al. Low temperature degradation and reliability of one-piece ceramic oral implants with a porous surface. **Dental Materials**, v. 29, p. 389–397, 2013.

[14] CHEVALIER, J. et al. The tetragonal-monoclinic transformation in zirconia: Lessons learned and future trends. **Journal of the American Ceramic Society**, v. 92, n. 9, p. 1901–1920, 2009.

[15] FABRIS, S.; PAXTON, A. T.; FINNIS, M. W. A Stabilization mechanism of zirconia based on oxygen vacancies only. **Acta Materialia**, v. 50, n. 20, p. 5171–5178, 2002.

[16] PALMERO, P. et al. Towards long lasting zirconia-based composites for dental implants . Part I : Innovative synthesis , microstructural characterization and in vitro stability. **Biomaterials**, v. 50, p. 38–46, 2015.

[17] HALLMANN, L. et al. The influence of grain size on low-temperature degradation of dental zirconia. **Journal of Biomedical Materials Research - Part B Applied Biomaterials**, v. 100 B, p. 447–456, 2012.

[18] MATSUI, K. et al. Mechanism of alumina-enhanced sintering of fine zirconia powder: Influence of alumina concentration on the initial stage sintering. **Journal of the American Ceramic Society**, v. 91, n. 6, p. 1888–1897, 2008.

[19] YILBAS, B. S. Laser treatment of zirconia surface for improved surface hydrophobicity. **Journal of Alloys and Compounds**, v. 625, p. 208–215, 2015.

[20] ZANATTA, R.; ESPER, M.; PUCCI, C. Effects of different surface treatments of zirconia on the bond strength of self-adhesive resinous cement. **Journal of Adhesion Science and Technology**, v. 31, n. 1, p. 21–30, 2017.

[21] INGLIS, C. E. Stresses in a plate due to the presence of cracks and sharp corners. **Transactions of the Royal Institution of Naval Architects**, v. 44, p. 15–38, 1913.

[22] BÜTIKOFER, L.; STAWARCZYK, B.; ROOS, M. Two regression methods for estimation of a two-parameter Weibull distribution for

reliability of dental materials. **Dental Materials**, v. 31, n. 2, p. e33–e50, 2015.

[23] WEIBULL, W. A statistical distribution function of wide applicability. **Journal of Applied Mechanics**, p. 293–297, 1951.

[24] GONZAGA, C. C. **Crescimento de trinca subcrítico em cerâmicas odontológicas: Efeito do material (microestrutura) e do método de ensaio**. 2007. 194 f. Tese (Doutorado em Odontologia) - Faculdade de Odontologia, Universidade de São Paulo, São Paulo. 2007.

[25] HANNINK, R. H. J.; KELLY, P. M.; MUDDLE, B. C. Transformation toughening in zirconia-containing ceramics. **Journal of the American Ceramic Society**, v. 83, n. 3, p. 461–487, 2000.

[26] YOSHIDA, K. et al. Large increase in fracture resistance of stishovite with crack extension less than one micrometer. **Nature Scientific Reports**, p. 1–8, 2015.

[27] KYOCERA. **Global Kyocera**. Disponível em: <http://global.kyocera.com/prdct/fc/list/material/silicon_nitride/silicon_nitride.html>. Acesso em: 15 jun. 2017.

[28] ZHAO, Z. **Low temperature environmental degradation of zirconia ceramics**. 2004. 264 f. Tese (PhD em Engenharia de Materiais) - University of Windsor, Windsor, Ontario, Canada. 2004.

[29] OHTAKA, O.; YAMANAKA, T. New high-pressure and temperature phase of ZrO2 above 1000 ^{o}C at 20 GPa. **Physical Review B**, v. 49, n. 14, p. 9295–9298, 1994.

[30] CHEVALIER, J.; GREMILLARD, L.; DEVILLE, S. Low-temperature degradation of zirconia and implications for biomedical implants. **Annual Review of Materials Research**, v. 37, p. 1–32, 2007.

[31] FERNÀNDEZ, R. et al. Fatigue and fracture characteristics of a fine-grained (Mg,Y)–PSZ zirconia ceramic. **Journal of the European Ceramic Society**, v. 19, p. 1705–1715, 1999.

[32] YOSHIMURA, M.; TANI, E.; SOMIYA, S. The confirmation of phase equilibria in the system ZrO2-CeO2 below 1400 ^{o}C. **Solid State Ionics**, v. 3, n. 4, p. 477–481, 1981.

[33] LUGHI, V.; SERGO, V. Low temperature degradation -aging- of zirconia: A critical review of the relevant aspects in dentistry. **Dental Materials**, v. 26, p. 807–820, 2010.

[34] CHEVALIER, J.; GREMILLARD, L. Zirconia as a biomaterial. **Comprehensive Biomaterials II**, v. 1, p. 122–144, 2017.

[35] ZHANG, F. et al. Strength, toughness and aging stability of highly-translucent Y-TZP ceramics for dental restorations. **Dental Materials**, v. 32, n. 12, p. e327–e337, 2016.

[36] TURON-VINAS, M. et al. Mechanical properties of 12Ce-ZrO2/3Y-ZrO2 composites. **Ceramics International**, v. 41, p. 14988–14997, 2015.

[37] BRAVO-LEON, A. et al. Fracture toughness of nanocrystallien tetragonal zirconia with low ytttia content. **Acta Materialia**, v. 50, p. 4555–4562, 2002.

[38] CHRISTEL, P. et al. Biomechanical compatibility and design of ceramic implants for orthopedic surgery. **Annals of the New York Academy of Sciences**, v. 523, p. 234–256, 1988.

[39] ZARONE, F.; RUSSO, S.; SORRENTINO, R. From porcelain-fused-to-metal to zirconia: Clinical and experimental considerations. **Dental Materials**, v. 27, p. 83–96, 2011.

[40] ARDLIN, B. I. Transformation-toughened zirconia for dental inlays, crowns and bridges: Chemical stability and effect of low-temperature aging on flexural strength and surface structure. **Dental Materials**, v. 18, p. 590–595, 2002.

[41] ANDREIUOLO, R.; GONÇALVES, S. A.; DIAS, K. R. H. C. A zircônia na odontologia restauradora. **Revista Brasileira de Odontologia**, v. 68, n. 1, p. 49–53, 2011.

[42] QIAN, D. et al. Impact of thermal shock cycles on mechanical properties and microstructure of lithium disilicate dental glass-ceramic. **Ceramics International**, n. July, p. 0–1, 2017.

[43] POINERN, G. E. J.; BRUNDAVANAM, R. K.; FAWCETT, D. Nanometre scale hydroxyapatite ceramics for bone tissue engineering. **American Journal of Biomedical Engineering**, v. 3, n. 6, p. 148–168, 2013.

[44] TANAKA, M. et al. Finite element analysis of the possible mechanism of cervical lesion formation by occlusal force. **Journal of Oral rehabilitation**, v. 30, p. 60–67, 2003.

[45] MAGALHÃES, M. F. DE et al. Measurement of thermophysical properties of human dentin: Effect of open porosity. **Journal of Dentistry**, v. 36, n. 8, p. 588–594, 2008.

[46] BLODGETT, D. W.; BALDWIN, K. C. **Laser ultrasonic techniques for assessment of tooth structure**. SPIE proceedings: Laser-Tissue Interaction Xi: Photochemical, Photothermal, and Photomechanical, 2000, San Francisco. **Anais**...2000

[47] CHEVALIER, J. What future for zirconia as a biomaterial? **Biomaterials**, v. 27, p. 535–543, 2006.

[48] SATO, T.; SHIMADA, M. Control of the tetragonal-to-monoclinic phase transformation of yttria partially stabilized zirconia in hot water. **Journal of Materials Science**, v. 20, p. 3988–3992, 1985.

[49] SATO, T.; SHIMADA, M. Transformation of yttria-doped tetragonal ZrO2 polycrystals by annealing in water. **Journal of American Ceramic Society**, v. 68, n. 6, p. 356–359, 1985.

[50] YOSHIMURA, M. et al. Role of H2O on the degradation process of Y-TZP. **Journal of Materials Science Letters**, v. 6, p. 465–467, 1987.

[51] LAWSON, S. Environmental degradation of zirconia ceramics. **Journal of the European Ceramic Society**, v. 15, p. 485–502, 1995.

[52] SCHUBERT, H.; FREY, F. Stability of Y-TZP during hydrothermal treatment: Neutron experiments and stability considerations. **Journal of the European Ceramic Society**, v. 25, p. 1597–1602, 2005.

[53] SANON, C. et al. A new testing protocol for zirconia dental implants. **Dental Materials**, v. 31, p. 15–25, 2015.

[54] DEVILLE, S.; CHEVALIER, J.; GREMILLARD, L. Influence of surface finish and residual stresses on the ageing sensitivity of biomedical grade zirconia. **Biomaterials**, v. 27, p. 2186–2192, 2006.

[55] TSUBAKINO, H.; HAMAMOTO, M.; NOZATO, R. Tetragonal-to-monoclinic phase transformation during thermal cycling and isothermal ageing in yttria-partially stabilized zirconia. **Journal of Materials Science**, v. 26, p. 5521–5526, 1991.

[56] INTERNATIONAL STANDARD. **ISO 13356: Implants for surgery - Ceramic materials based on yttria-stabilized tetragonal zirconia (Y-TZP).**Geneva, Switzerland, 2008.

[57] ARAÚJO, M. et al. Glass coatings on zirconia with enhanced bioactivity. **Journal of the European Ceramic Society**, v. 36, n. 13, p. 3201–3210, 2016.

[58] STADLINGER, B. et al. Comparison of zirconia and titanium implants after a short healing period. A pilot study in minipigs. **International Journal of Oral and Maxillofacial Surgery**, v. 39, p. 585–592, 2010.

[59] SOON, G. et al. Review of zirconia-based bioceramic: Surface modification and cellular response. **Ceramics International**, v. 42, p. 12543–12555, 2016.

[60] CURTIS, A.; WILKINSON, C. Topographical control of cells. **Biomaterials**, v. 18, n. 24, p. 1573–1583, 1997.

[61] PARK, S.; PARK, K.; CHO, S. Comparison of removal torques of SLActive ® implant and blasted , laser-treated titanium implant in rabbit tibia bone healed with concentrated growth factor application. **Journal of Advanced Prosthodont**, v. 8, p. 110–115, 2016.

[62] DANTAS, T. A. et al. Bioactive materials driven primary stability on titanium biocomposites. **Materials Science and Engineering C**, v. 77, p. 1104–1110, 2017.

[63] BAN, S. et al. Effect of sintering condition, sandblasting and heat treatment on biaxial flexural strenght of Zirconia. **Key Engineering Materials**, v. 361, p. 779–782, 2008.

[64] KOSMAČ, T.; OBLAK, Č.; MARION, L. The effects of dental grinding and sandblasting on ageing and fatigue behavior of dental zirconia (Y-TZP) ceramics. **Journal of the European Ceramic Society**, v. 28, p. 1085–1090, 2008.

[65] NODA, M. et al. Surface damages of zirconia by Nd:YAG dental laser irradiation. **Dental Materials**, v. 29, n. 5, p. 536–541, 2010.

[66] OLIVEIRA, U. O. B. DE. **Laser treatment of alloys: Processing, microstructure and structural properties**. 2007. 132 f. Tese (Doutorado em Matemática e Ciências Naturais) - University of Groningen, Groningen, Netherlands. 2007.

[67] ALMEIDA, A.; GUPTA, D.; VILAR, R. **Laser-assisted development of titanium alloys: the search for new biomedical materials**. SPIE proceedings: International Conference on Lasers, Applications, and Technologies, 2010, San Francisco. **Anais**...San Francisco, California: SPIE, 2011

[68] NEVES, P. et al. KrF excimer laser dry and steam cleaning of silicon surfaces with metallic particulate contaminants. **Applied Physics A: Materials Science and Processing**, v. 74, p. 191–199,

2002.

[69] CANGUEIRO, L. T. et al. Femtosecond laser ablation of bovine cortical bone. **Journal of Biomedical Optics**, v. 17, n. 12, p. 1250051–12500510, 2012.

[70] MIRHOSSEINI, N. et al. Laser surface micro-texturing of Ti-6Al-4V substrates for improved cell integration. **Applied Surface Science**, v. 253, p. 7738–7743, 2007.

[71] STEEN, W. M. **Laser Material Processing**. London: Springer-Verlag London, 1998.

[72] RENK, K. F. **Basic of laser physics**. Heidelberg: Springer, 2011.

[73] ZHANG, G. et al. Reactive hot pressing of ZrB2-SiC composites. **Journal of the American Ceramic Society**, v. 83, n. 9, p. 2330–2332, 2000.

[74] MADEIRA, S. et al. Effect of sintering pressure on microstructure and mechanical properties of hot-pressed Ti6Al4V-ZrO2 materials. **Materials and Design**, v. 120, p. 394–403, 2017.

[75] COOPER, A. R.; EATON, L. E. Compaction behavior of several ceramic powders. **Journal of the American Ceramic Society**, v. 45, n. 3, p. 97–101, 1962.

[76] ROMAGNOLI, M. et al. A non-destructive method to assess delamination of ceramic tiles. **Journal of the European Ceramic Society**, v. 27, p. 1631–1636, 2007.

[77] ZHOU, W. et al. Dielectric properties of BN modified carbon fibers by dip-coating. **Ceramics International**, v. 39, p. 6569–6576, 2013.

[78] NANDI, B. K.; UPPALURI, R.; PURKAIT, M. K. Effects of dip coating parameters on the morphology and transport properties of cellulose acetate – ceramic composite membranes. **Journal of Membrane Science**, v. 330, p. 246–258, 2009.

[79] GROSSO, D.; MARIE, P. How to exploit the full potential of the dip-coating process to better control film formation. **Journal of Materials Chemistry**, v. 21, p. 17033–17038, 2011.

[80] RASHID, A. et al. Fabrication of porcelain foam substrates coated with SiC , Ni , and Cr using the dip-coating technique. **Ceramics International**, v. 41, p. 2940–2947, 2015.

[81] GU, Y.; MENG, G. A model for ceramic membrane formation by dip-coating. **Journal of the European Ceramic Society**, v. 19, p. 1961–1966, 1999.

[82] RASHID, A. et al. Physical , mechanical , and thermal properties improvement of porous alumina substrate through dip-coating and re-sintering procedures. **Ceramics International**, v. 42, p. 7717–7729, 2016.

[83] CONCEIÇAO, S. I.; VELHO, J. L.; FERREIRA, J. M. F. Influence of deagglomeration and carboxymethyl cellulose binders on rheological behaviour of kaolin suspensions. **Applied Clay Science**, v. 23, p. 257–264, 2003.

[84] RAO, S. P.; TRIPATHY, S. S.; RAICHUR, A. M. Dispersion studies of sub-micron zirconia using Dolapix CE 64. **Colloids and Surfaces A: Physicochemical and Engineering Aspects**, v. 302, p. 553–558, 2007.

[85] PATTERSON, I.; KAMAL, M. R. Shear deagglomeration of solid aggregates suspended in viscous liquids. **The Canadian Journal of Chemical Engineering**, v. 52, p. 306–315, 1974.

[86] FERREIRA, M. F.; OLIVEIRA, M. I. L. L.; CHEN, K. Influence of the deagglomeration procedure on aqueous dispersion, slip casting and sintering of Si3N4-based ceramics. **Journal of the European Ceramic Society**, v. 22, p. 1601–1607, 2002.

[87] MIYAZAKI, T. et al. Current status of zirconia restoration. **Journal of Prosthodontic Research**, v. 57, n. 4, p. 236–261, 2013.

[88] FORNABAIO, M. et al. Zirconia-based composites for biomedical applications: Role of second phases on composition, microstructure and zirconia transformability. **Journal of the European Ceramic Society**, v. 35, n. 0, p. 4039–4049, 2015.

[89] DENRY, I.; KELLY, J. R. Emerging ceramic-based materials for dentistry. **Journal of Dental Research**, v. 93, n. 12, p. 1235–42, 2014.

[90] TEBALDO, V.; GAUTIER, G. Influences of evaluation methods and testing load on microhardness and Young's modulus of ZTA and ATZ ceramics. **Ceramics International**, v. 39, p. 2683–2693, 2013.

[91] PERRICHON, A. et al. A testing protocol combining shocks, hydrothermal ageing and friction, applied to Zirconia Toughened Alumina (ZTA) hip implants. **Journal of the Mechanical Behavior**

of Biomedical Materials, v. 65, n. July 2016, p. 600–608, 2016.

[92] NEVAREZ-RASCON, A. et al. On the wide range of mechanical properties of ZTA and ATZ based dental ceramic composites by varying the Al2O3 and ZrO2 content. **International Journal of Refractory Metals and Hard Materials**, v. 27, p. 962–970, 2009.

[93] MARRO, F. G. et al. Surface modification of 3Y-TZP with cerium oxide. **Journal of the European Ceramic Society**, v. 31, p. 331–338, 2011.

[94] STAWARCZYK, B. et al. Comparison of four monolithic zirconia materials with conventional ones: Contrast ratio, grain size, four-point flexural strength and two-body wear. **Journal of the Mechanical Behavior of Biomedical Materials**, v. 59, p. 128–138, 2016.

[95] TOUAIHER, I. et al. Effect of loading configuration on strength values in a highly transformable zirconia-based composite. **Dental Materials**, v. 32, p. e211–e219, 2016.

[96] ZHANG, Y. Making yttria-stabilized tetragonal zirconia translucent. **Dental Materials**, v. 30, p. 1195–1203, 2014.

[97] KRISHNAMURTHY, R. et al. Oxygen diffusion in yttria-stabilized zirconia: A new simulation model. **Journal of American ceramic society**, v. 1830, n. 87, p. 1821–1830, 2004.

[98] STRICKLER, W.; CARLSON, W. G. Ionic conductivity of cubic solid solutions in the system CaO-Y2O3-ZrO2. **Journal of the American Ceramic Society**, v. 47, n. 3, p. 122–127, 1964.

[99] CALVIÉ, E. et al. A global investigation into in situ nanoindentation experiments on zirconia: From the sample geometry optimization to the stress nanolocalization using convergent beam electron diffraction. **Journal of Microscopy**, v. 249, n. 2, p. 99–110, 2013.

[100] CASELLAS, D. et al. Fracture toughness and mechanical strength of Y-TZP / PSZ ceramics. **Scripta Materialia**, v. 45, p. 213–220, 2001.

[101] CHEVALIER, J. et al. Critical effect of cubic phase on aging in 3 mol% yttria-stabilized zirconia ceramics for hip replacement prosthesis. **Biomaterials**, v. 25, n. 24, p. 5539–5545, 2004.

[102] FISCHER, J.; STAWARCZYK, B. Compatibility of machined Ce-TZP/Al2O3 nanocomposite and a veneering ceramic. **Dental Materials**, v. 23, p. 1500–1505, 2007.

[103] GAILLARD, Y. et al. Quantification of hydrothermal degradation in zirconia by nanoindentation. **Acta Materialia**, v. 56, p. 4206–4216, 2008.

[104] LIMA, J. M. C. et al. Effect of thickness, processing technique and cooling rate protocol on the flexural strength of a bilayer ceramic system. **Dental Materials**, v. 29, p. 1063–1072, 2013.

[105] LI, L. et al. Mechanical behavior of ceramic-metal joint under quasi-static and dynamic four point bending: Microstructures, damage and mechanisms. **Ceramics International**, v. 43, p. 6684–6692, 2017.

[106] GRUBER, M. et al. Effect of metallization on the strength and fracture behaviour of functional co-fired multilayer ceramics. **Journal of the European Ceramic Society**, v. 37, n. 14, p. 4389–4396, 2016.

[107] TOMLINSON, W. J.; FARRELL, J. Fracture strength, surface roughness and corrosion of ceramics. **Ceramics International**, v. 18, p. 355–357, 1992.

[108] SHEN, Z. et al. Fractography of self-glazed zirconia with improved reliability. **Journal of the European Ceramic Society**, v. 37, n. 14, p. 4339–4345, 2017.

[109] QUINN, G. D.; BRADT, R. C. On the vickers indentation fracture toughness Test. **Journal of the American Ceramic Society**, v. 90, n. 3, p. 673–680, 2007.

[110] MARSHALL, D. B. et al. The compelling case for indentation as a functional exploratory and characterization tool. **Journal of the American Ceramic Society**, v. 98, n. 9, p. 2671–2680, 2015.

[111] WANG, H.; ABOUSHELIB, M. N.; FEILZER, A. J. Strength influencing variables on CAD/CAM zirconia frameworks. **Dental Materials**, v. 24, n. 5, p. 633–638, 2008.

[112] MEZARI, R. A. et al. Wear mechanism and morphologic space in ceramic honing process. **Wear**, v. 362–363, p. 33–38, 2016.

[113] ZOGHEIB, L. V.; BONA, A. DELLA. Effect of hydrofluoric acid etching duration on the roughness and flexural strength of a lithium disilicate-based glass ceramic. **Brazilian Dental Journal**, v. 22, n. 1, p. 45–50, 2011.

[114] LOHBAUER, U.; MÜLLER, F. A; PETSCHELT, A. Influence of surface roughness on mechanical strength of resin composite versus

glass ceramic materials. **Dental Materials**, v. 24, n. 2, p. 250–256, 2008.

[115] FLURY, S.; PEUTZFELDT, A.; LUSSI, A. Influence of surface roughness on mechanical properties of two computer-aided design/computer-aided manufacturing (CAD/CAM) ceramic materials. **Operative Dentistry**, v. 37, n. 6, p. 617–24, 2012.

[116] SAKHAROVA, N. A. et al. Comparison between Berkovich, Vickers and conical indentation tests: A three-dimensional numerical simulation study. **International Journal of Solids and Structures**, v. 46, n. 5, p. 1095–1104, 2009.

[117] HARADA, K. et al. Effect of loading conditions on the fracture toughness of zirconia. **Journal of Prosthodontic Research**, v. 57, n. 2, p. 82–87, 2013.

[118] PETIT, F.; VANDENEEDE, V.; CAMBIER, F. Relevance of instrumented micro-indentation for the assessment of hardness and Young's modulus of brittle materials. **Materials Science and Engineering A**, v. 456, p. 252–260, 2007.

[119] NIIHARA, K.; MORENA, R.; METALS, O. Evaluation of KIc of brittle solids by the indentation method with low crack-to-indent ratios. **Jornal of Material Science Letters**, v. 1, p. 13–16, 1982.

[120] HAO, L.; LAWRENCE, J.; CHIAN, K. S. Osteoblast cell adhesion on a laser modified zirconia based bioceramic. **Journal of Materials Science: Materials in Medicine**, v. 16, n. 8, p. 719–726, 2005.

[121] ROITERO, E. et al. A parametric study of laser interference surface patterning of dental zirconia: Effects of laser parameters on topography and surface quality. **Dental Materials**, v. 33, n. 1, p. e28–e38, 2016.

[122] VAN DRIEL, H. M.; SIPE, J. E.; YOUNG, J. F. Laser-induced periodic surface structure on solids: A universal phenomenon. **Physical Review Letters**, v. 49, n. 26, p. 1955–1958, 1982.

[123] YASUNO, K. et al. Zirconia implants with laser surface treatment : Peri-implant bone response and enhancement of osseointegration. **Journal of Hard Tissue Biology**, v. 23, n. 1, p. 93–100, 2014.

[124] STÜBINGER, S. et al. Effect of Er:YAG, CO2 and diode laser irradiation on surface properties of zirconia endosseous dental

implants. **Lasers in Surgery and Medicine**, v. 40, n. 3, p. 223–228, 2008.

[125] TRIANTAFYLLIDIS, D.; LI, L.; STOTT, F. H. Crack-free densification of ceramics by laser surface treatment. **Surface and Coatings Technology**, v. 201, n. 6, p. 3163–3173, 2006.

[126] MIRANDA, P. V. et al. Surface alterations of zirconia and titanium substrates after Er,Cr:YSGG irradiation. **Lasers in Medical Science**, v. 30, n. 1, p. 43–48, 2015.

[127] LIU, L. et al. Effect of Nd:YAG laser irradiation on surface properties and bond strength of zirconia ceramics. **Lasers in Medical Science**, v. 30, n. 2, p. 627–634, 2015.

[128] MAHMOODI, N. et al. Effect of sandblasting, silica coating, and laser treatment on the microtensile bond strength of a dental zirconia ceramic to resin cements. **Lasers in Medical Science**, v. 31, n. 2, p. 205–211, 2016.

[129] SINHAMAHAPATRA, A. et al. Oxygen-deficient zirconia (ZrO2−x): A new material for solar light absorption. **Nature Scientific Reports**, v. 6, n. 27218, p. 1–8, 2016.

[130] BESPALOV, I. et al. Initial stages of oxide formation on the Zr surface at low oxygen pressure: An in situ FIM and XPS study. **Ultramicroscopy**, v. 159, p. 147–151, 2015.

[131] MELK, L. et al. The influence of unshielded small cracks in the fracture toughness of yttria and of ceria stabilised zirconia. **Journal of the European Ceramic Society**, v. 36, n. 1, p. 147–153, 2016.

[132] KIM, H.-T. et al. The effect of low temperature aging on the mechanical property & phase stability of Y-TZP ceramics. **The Journal of Advanced Prosthodontics**, v. 1, p. 113–117, 2009.

[133] KUSHIMA, A.; YILDIZ, B. Oxygen ion diffusivity in strained yttria stabilized zirconia: where is the fastest strain? **Journal of Materials Chemistry**, v. 20, p. 4809–4819, 2010.

[134] CHEVALIER, J.; OLAGNON, C.; FANTOZZI, G. Study of the residual stress field around Vickers indentations in a 3Y-TZP. **Journal of Materials Science**, v. 31, n. 10, p. 2711–2717, 1996.

[135] TORAYA, H.; SOMIYA, M.; YOSHIMURA, S. Calibration curve for quantitative analysis of the monoclinic-tetragonal ZrO2 system by X-ray diffraction. **Journal of the American Ceramic Society**, v. 67, n. 6, p. C-119-C-121, 1984.

[136] GARVIE, R. C.; NICHOLSON, P. S. Phase analysis in zirconia systems. **Journal of the American Ceramic Society**, v. 55, n. 6, p. 303–305, 1972.

[137] SPOHR, A. M. et al. Surface modification of In-Ceram zirconia ceramic by Nd:YAG laser, Rocatec system, or aluminum oxide sandblasting and its bond strength to a resin cement. **Photomedicine and Laser Surgery**, v. 26, n. 3, p. 203–208, 2008.

[138] EOM, T. G. et al. Experimental study of bone response to hydroxyapatite coating implants: Bone-implant contact and removal torque test. **Oral and Maxillofacial Surgery**, v. 114, n. 4, p. 411–418, 2012.

[139] ELIAS, C. N.; MEIRELLES, L. Improving osseointegration of dental implants. **Expert Review of Medical Devices**, v. 7, n. 2, p. 241–256, 2010.

[140] ROSA, M. B. et al. The influence of surface treatment on the implant roughness pattern. **Journal of Applied Oral Science**, v. 20, n. 5, p. 550–5, 2012.

[141] WENNERBERG, A.; ALBREKTSSON, T. Effects of titanium surface topography on bone integration: A systematic review. **Clinical Oral Implants Research**, v. 20, n. SUPPL. 4, p. 172–184, 2009.

[142] KAZAMA-KOIDE, M. et al. A new method for fabricating zirconia copings using a Nd:YVO4 nanosecond laser. **Dental Materials**, v. 33, n. 3, p. 422–429, 2014.

[143] SOON, G. et al. Review of zirconia-based bioceramic : Surface modification and cellular response. **Ceramics International**, v. 42, p. 12543–12555, 2016.

[144] WEBSTER, T. J.; SIEGEL, R. W.; BIZIOS, R. Osteoblast adhesion on nanophase ceramics. **Biomaterials**, v. 20, n. 13, p. 1221–1227, 1999.

[145] NAKONIECZNY, D. S. et al. Trends and perspectives in modification of zirconium oxide for a dental prosthetic applications - A review. **Biocybernetics and Biomedical Engineering**, v. 37, n. 1, p. 229–245, 2017.

[146] LIU, X. et al. Influence of substratum surface chemistry/energy and topography on the human fetal osteoblastic cell line hFOB 1.19: Phenotypic and genotypic responses observed in vitro.

Biomaterials, v. 28, n. 31, p. 4535–4550, 2007.

[147] GAGGL, A. et al. Scanning electron microscopical analysis of laser-treated titanium implant surfaces: A comparative study. **Biomaterials**, v. 21, p. 1067–1073, 2000.

[148] HAO, L.; LAWRENCE, J. CO2 Laser modification of the wettability characteristics of a magnesia partially stabilized zirconia bioceramic. **Journal of Physics D: Applied Physics**, v. 36, n. 11, p. 1292–1299, 2003.

[149] HEIROTH, S. et al. Laser ablation characteristics of yttria-doped zirconia in the nanosecond and femtosecond regimes. **Journal of Applied Physics**, v. 107, n. 1, p. 0149081–01490810, 2010.

[150] COTIČ, J.; JEVNIKAR, P.; KOCJAN, A. Ageing kinetics and strength of airborne-particle abraded 3Y-TZP ceramics. **Dental Materials**, v. 33, n. 7, p. 847–856, 2017.

[151] LAWRENCE, J.; LI, L. On the mechanisms of wetting characteristics modification for selected metallic materials by means of high power laser radiation. **Journal of Laser Applications**, v. 14, n. 2, p. 107–113, 2002.

[152] ALEISA, K. I. et al. Effect of types of luting agent on push-out bond strength of zirconium oxide posts. **Journal of Dentistry**, v. 41, n. 4, p. 377–383, 2013.

[153] ANNAMALAI, M. et al. Surface energy and wettability of van der Waals. **Eletronic Suplementary Material for Nanoescale**, p. 1–7, 2016.

[154] GADELMAWLA, E. S. et al. Roughness parameters. **Journal of Materials Processing Technology**, v. 123, p. 133–145, 2002.

[155] NORO, A. et al. Influence of surface topography and surface physicochemistry on wettability of zirconia (tetragonal zirconia polycrystal). **Journal of Biomedical Materials Research B**, v. 101 B, n. 2, p. 355–363, 2013.

[156] MRABET, C. et al. Effects of surface oxygen vacancies content on wettability of zinc oxide nanorods doped with lanthanum. **Journal of Alloys and Compounds**, v. 688, p. 122–132, 2016.

[157] JOTHI PRAKASH, C. G.; CLEMENT RAJ, C.; PRASANTH, R. Fabrication of zero contact angle ultra-super hydrophilic surfaces. **Journal of Colloid and Interface Science**, v. 496, p. 300–310,

2017.

[158] SARTORETTO, S. C. et al. Early osseointegration driven by the surface chemistry and wettability of dental implants. **Journal of applied oral science**, v. 23, n. 3, p. 279–87, 2015.

[159] HAO, L.; LAWRENCE, J. Effects of Nd:YAG laser treatment on the wettability characteristics of a zirconia-based bioceramic. **Optics and Lasers in Engineering**, v. 44, n. 8, p. 803–814, 2006.

[160] NASTIC, A. et al. Instrumented and vickers indentation for the characterization of stiffness, hardness and toughness of zirconia toughened Al2O3 and SiC armor. **Journal of Materials Science and Technology**, v. 31, n. 8, p. 773–783, 2015.